Geological characterisation of a proposed carbon sequestration site in Govan Mbeki Municipality, Mpumalanga, South Africa

T. Dhansay

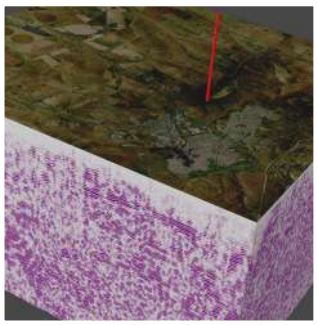
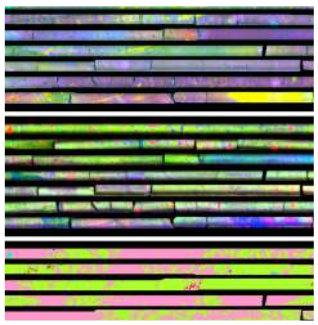
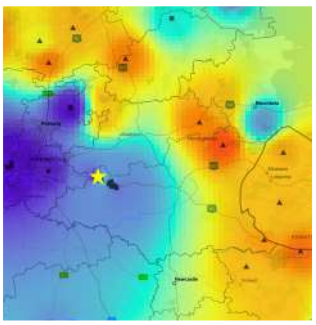

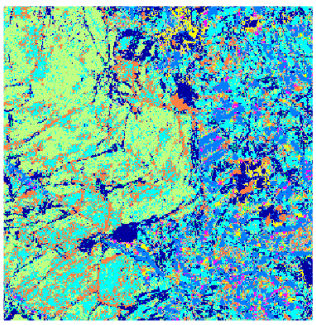

SPECIAL PUBLICATION I 23

Minerals and Energy Division

Council for Geoscience

COUNCIL FOR GEOSCIENCE
SOUTH AFRICA

GEOLOGICAL CHARACTERISATION OF A PROPOSED CARBON SEQUESTRATION SITE IN GOVAN MBEKI MUNICIPALITY, MPUMALANGA, SOUTH AFRICA

compiled by

Taufeeq Dhansay

SPECIAL PUBLICATION NO. 23

MINERALS AND ENERGY DIVISION

2023

COUNCIL FOR GEOSCIENCE
SOUTH AFRICA

Project leader	**Ngqondi Nxokwana**
Task leader	Taufeeq Dhansay
Author	Taufeeq Dhansay

Contributors

Mashudu Baloyi
Dawn Black
Sifiso Bucibo
Janet Bunk
Wahiebah Daniels
Mpumelelo Dube
Nangamso Dunga
Marinda Havenga
Nigel Hicks
Noel Kamrajh
Mbuso Khwela
Maphuti Kwata
Sechaba Lenong
Mmeli Luzipo
Brassnavy Manzunzu
Thulani Maupa
Vunganai Midzi
Tshiamo Moleele
Thabo Mosia
Themba Mothupi
Ponani Mthembi
Thomas Muedi
Portia Munyangane
Mawande Ncume
Clement Ndou
Vhuhwavhohau Nengovhela
Mbuyiseni Ngcobo
Douglas Phakula
Ashley Philander
Keshree Pillay
Musarrat Safi
Simon Sebothoma
Zamampondo Sibewu
Tshilidzi Tsotetsi

Linguistic editing and layout
Z.E. Nel

Published in September 2023

ISBN: 978-1-990942-24-2

Cover: Regional overview of the proposed study area, including various integrated and fundamental geoscience datasets considered in this study.

Obtainable from the Council for Geoscience, 280 Pretoria Street, Silverton, Pretoria, or by mail from the Publications Shop, Council for Geoscience, Private Bag, X112, Pretoria, 0001; Tel: (012) 841-1017.

Internet Home Page address: http://www.geoscience.org.za.

TABLE OF CONTENTS

LIST OF FIGURES

LIST OF TABLES

GEOLOGICAL CHARACTERISATION OF A PROPOSED CARBON SEQUESTRATION SITE IN GOVAN MBEKI MUNICIPALITY, MPUMALANGA, SOUTH AFRICA

by

Taufeeq Dhansay

Executive summary

1. *South Africa produces the highest reported anthropogenic carbon dioxide (CO_2) emissions on the African continent and is a significant emitter of anthropogenic CO_2 worldwide, accounting for approximately 500 million tonnes of anthropogenic CO_2 per annum. Approximately half of these emissions are attributed to coal-fired energy generation. The remaining emissions are from transportation and manufacturing.*

2. *The South African government has committed to reducing anthropogenic CO_2 emissions by at least 40% within the next decade. Furthermore, Government has committed to doing so within a Just Transition framework.*

3. *South Africa's socio-economic development relies heavily on coal. The coal industry is one of the largest producers of raw materials and a key employer in South Africa. Owing to its reliance on extensive coal reserves, the country will need to create resilient strategies to achieve its climate change mitigation targets, while avoiding negative impacts on socio-economic development.*

4. *Carbon capture, utilisation and storage (CCUS) is a technology that meets this requirement. CCUS aims to capture anthropogenic CO_2 at its source and to store it safely and permanently in suitable underground reservoirs. The utilisation aspect aims to incorporate some of the captured CO_2 in suitable industrial applications, such as petrochemical and manufacturing processes. The technology will therefore enable the coal industry to continue, while at the same time contributing to the mitigation of anthropogenic CO_2 emissions.*

5. *A number of South African reservoirs are suited to the storage of anthropogenic CO_2. These include deep saline storage reservoirs, benign offshore hydrocarbon reservoirs and subeconomic coal seams. However, additional storage reservoirs are needed, especially proximal to large emission sites, in order to meet South Africa's CO_2 reduction targets.*

6. *Basalt sequences provide an extremely promising storage reservoir. This is because these sequences contain minerals that are potentially highly reactive with anthropogenic CO_2. These reactions occur rapidly and ensure that anthropogenic CO_2 is converted/incorporated into geological sequences where it is permanently stored.*

7. *This report presents the findings of a geological characterisation study into the suitability of the lower Ventersdorp Supergroup volcanic sequences in sequestering anthropogenic CO_2.*

8. *Geographically, these sequences are suitable because they span volumetrically extensive horizons below South Africa's largest point-source CO_2 emitters. Moreover, at suitable depths of approximately 1 000 m below key emission sources, these strata constitute potentially extensive reservoirs.*

9. *These sequences are also suitable from a geological perspective. Mineralogy and petrographic investigations have highlighted the presence of potentially reactive minerals having undergone minimal hydrothermal alteration and natural carbonation. Geophysical and borehole data shows that many of these potentially reactive sequences are at least 100 m thick. Hyperspectral scanning of these boreholes indicates the presence of intermittent cycles of potentially reactive and non-reactive sequences, which can mitigate the undue migration of sequestered CO_2.*

10. *The structural geology and tectonic setting suggest that this region overlies the relatively stable Kaapvaal Craton. In addition, the seismic hazard assessment of the area highlights minimal natural seismicity. Low-magnitude seismicity towards the northern outskirts of the area is attributed to ongoing gold and coal mining activity.*

11. *Environmental and hydrogeological investigations have provided critical information on the natural baseline conditions of the proposed region. While these studies reveal that the region is characterised by reasonably fresh surface and groundwater sources, they have also identified key acidic and alkaline pollutant sources. These pollutants are generally linked to nearby mining activities. Environmental baseline assessments have also provided information on the natural conditions, which will support active monitoring during any potential development.*

12. *Socio-economic indicators report that the economy of this region is defined by mining, agriculture and industrial processes. The population has moderate access to education and the unemployment rate is approximately 25–30%. Crucially, the economy of the area is inextricably linked to coal mining and industries associated with*

the coal and hydrocarbon sectors.

13. *The findings of this study suggest that the basaltic sequences of the Ventersdorp Supergroup can serve as a viable reservoir for the sequestration of anthropogenic CO_2. This potential should be taken into account in further planning and the economic assessment of South Africa's coal-linked industries, especially in light of the country's recently adopted carbon tax regime and revised energy strategy.*

14. *There are technical challenges. These include the significantly large depth range and relatively nonporous and impermeable nature of the proposed reservoir sequences. These challenges can be overcome, for example, by artificially increasing permeability. Such an intervention will require additional geological and structural modelling.*

15. *This study should be followed by an engineering and design phase, complemented by an active monitoring programme. The purpose of this follow-up work should include the development of appropriate guiding policies and procedures and to determine the potential commercial viability of CCUS in South Africa's future socio-economic and energy development sectors.*

16. *Finally, the underlying and highly fractured siliciclastic sequences of the lowermost Witwatersrand Supergroup represent an additional potential storage reservoir. These sequences may constitute a possible deep saline anthropogenic CO_2 storage reservoir. This prospect should be further investigated and factored into an assessment of South Africa's true CCUS storage potential.*

Table 1. Report summary table.

Summary table		
Objectives and conclusions	The results of this study suggest that the basaltic sequences of the Ventersdorp Supergroup may be capable of mineral carbonation and permanent storage of anthropogenic CO_2.	Results have been achieved by combining mineralogy, petrology and integrated geological modelling using borehole core data and collected samples.
	The results of this study support the proposition that CCUS technologies should be considered in South Africa's future energy development plans.	Achieved by establishing a potential geological reservoir with a volumetric extent capable of supporting the sequestration of several million tonnes of CO_2.
Innovation	This is the first study to show that the mineralogy of ancient (3 000 million year old) volcanic sequences has the potential to react with injected anthropogenic CO_2.	These results were achieved through an innovative integrated geoscience approach. The integration of multiple geoscience datasets has aided and supported the required level of confidence. The methodology should also be applied to research with comparable goals and in geologically similar areas.
Limitations	The findings of this study suggest that the proposed reactive sequences are characterised by relatively low porosity and permeability. Additional technical investigations are required.	These findings have been achieved through various porosity and permeability analyses, for example water/mercury intrusion porosimetry, helium pycrometry and Hoek cell permeability analyses.
Recommendations	Additional studies and modelling exercises should be undertaken to establish the likely permeability and flow paths of injected anthropogenic CO_2.	Computational modelling of the reservoir should be undertaken, supported by drilling and simulation studies.
	These findings should be considered in the context of South Africa's Just Transition. The results of the study should find expression in South Africa's coal strategy and national Integrated Resource Plan (IRP).	Economic assessments should be conducted in the framework of the hydrocarbon and carbon trading scenarios, especially in view of the concept of potentially mitigating anthropogenic CO_2.

GLOSSARY OF TERMS

Term	Definition/description
Amygdale	Cavity/void in extrusive volcanic rocks. The amygdale may or may not be filled with fluids, gases or secondary minerals.
Anthropogenic	Any process, phenomenon, or environmental impact caused by human activity.
Archaean	Geological eon approximately 4 to 2.5 billion years ago.
Basalt	Globally abundant volcanic rock comprised predominantly of silicate minerals.
Capture	Process of capturing anthropogenic CO_2 at source with the intention of transporting it to a proposed injection/utilisation site.
Carbonation	Conversion of silicate minerals to carbonate-bearing mineral phases.
Carbon dioxide	Anthropogenic greenhouse gas produced by burning hydrocarbon-bearing fossil fuels.
Coal	Combustible sedimentary rock primarily composed of carbon, hydrogen and other, lesser, quantities of metals.
Council for Geoscience	The mandated custodian for all geoscience data and information in the Republic of South Africa, as inscribed in the Geoscience Act (no. 100 of 1993), as amended.
Craton	Extensive, thick and ancient section of continental crust. Generally extends more than 100 km below the ground surface.
Electromagnetic	Reaction of a geological sequence or horizon to the earth's natural magnetic field.
Geochronology	Calculated age of a geological sequence, obtained through various techniques, for example, isotope geochemistry.
Geothermal	Latent heat present in the earth's crust and that increases with depth.
Hyperspectral	Type of imaging or sensing technology that captures a wide range of spectral bands or wavelengths across the electromagnetic spectrum. Unlike traditional multispectral imaging, which captures a limited number of discrete spectral bands, hyperspectral imaging captures a much more detailed and continuous range of spectral information.
Just Transition	Principle of transitioning towards a low-carbon economy without disrupting or negatively affecting socio-economic linkages to the hydrocarbon industry.
Mineralogy	Mineral constituents in a specific geological sequence.
Permeability	Property of a material or rock that determines the ease with which fluids, such as water, oil or gas can flow through it. Permeability measures the interconnectedness and openness of the pore spaces within the material, which influence the movement and transmission of fluids.
Petrology	Characterisation of specific geological sequences. Includes the chemistry, constituent mineralogy, texture and similar properties.
Porosity	Measure of empty spaces or voids within a material or rock. Porosity is a property that describes the amount of pore space relative to the total volume of the material.
Porphyritic	Texture commonly observed in igneous rocks comprising two distinct grain sizes. The larger crystals, known as *phenocrysts*, are embedded in a finer-grained matrix called the *groundmass*.
Proterozoic	Geological eon approximately 2.5 billion years to 541 million years ago.
Pseudotachylite	Rock or rock-like material that forms as a result of extreme frictional heating during seismic events, such as earthquakes or meteorite impacts.
Radiometric	Radioactive decay response of geological sequences or horizons.
Reflection seismics	Geophysical method used to study and map subsurface structures and layers in the earth's crust. The method involves the generation and recording of seismic waves reflected and refracted at interfaces between different rock formations.
Reservoir	Suitable underground zone or horizon that supports the storage of anthropogenic material.
Saline	High dissolved salt content in water, making it unsuitable for human consumption.
Seismicity	Occurrence, distribution and frequency of earthquakes in a specific region or globally.
Silicate minerals	Refers to a group of common rock-forming minerals that primarily consist of silicon, oxygen and metals such as aluminum, calcium, iron and magnesium.

Term	Definition/description
Siliciclastic	Sediments or sedimentary rocks primarily composed of silicate minerals, such as quartz, feldspar, clay minerals and lithic fragments.
Socio-economic	Social and economic factors or characteristics that influence the living conditions of individuals, communities and societies.
Stress	Natural pressure on and below the earth's surface, particularly including compressive and extensive pressures.
Ultramafic	Rocks or minerals that are composed primarily of mafic minerals rich in magnesium and iron, with low amounts of silica.
Utilisation	Ability to use captured anthropogenic CO_2 in various industrial and manufacturing industries.
Ventersdorp	Ventersdorp Supergroup volcanic lavas emplaced approximately 3 100 million years ago across a very large surface area.
World Bank	International financial institution that provides loans, grants and expertise to support global developmental projects. The primary goal of the World Bank is to reduce poverty and promote economic growth by offering financial and technical assistance to member countries.

LIST OF ABBREVIATIONS

2D/3D	Two/three-dimensional
CCUS	Carbon capture, utilisation and storage
CGS	Council for Geoscience
CO_2	Carbon dioxide
DEM	Digital elevation model
DSHA	Deterministic seismic hazard assessment
EC	Electrical conductivity
Ga	Billion years ago
GDP	Gross domestic product
ICP-MS	Inductively coupled plasma mass spectrometer
IDTIMS	Isotope dilution thermal ionisation mass spectrometer
IRP	Integrated Resource Plan
KLIP	Karoo Large Igneous Province
km	Kilometre
kPa	Kilopascal
Ma	Million years ago
mD	Millidarcy
mg/L	Milligrams per litre
Ma	Million years
Mmax	Maximum magnitude
MPa	Megapascal
PGA	Peak ground acceleration
PPL	Plane-polarised light
PSHA	Probabilistic seismic hazard assessment
REE	Rare earth element
RGB	Red, green and blue
SANS	South African National Standard
SEM	Scanning electron microscope
SHRIMP	Sensitive high-resolution ion microprobe
SRTM	Shuttle radar topographic mission
TAS	Total alkali-silica
TDS	Total dissolved solids
µm	Micrometre
XCT	X-ray computed tomography
XPL	Cross-polarised light
XRD	X-ray diffraction
VCR	Ventersdorp Contact Reef

1 INTRODUCTION

South Africa produces the highest reported anthropogenic CO_2 emissions on the African continent (Abu-Goodman *et al.*, 2023). South Africa emits around 500 million tonnes of anthropogenic CO_2 annually. At least half of these emissions are associated with the country's rich coal deposits being used for energy generation (Eskom, 2022). South Africa burns approximately 100 million tonnes of coal for energy production per annum. The coal industry accounts for more than 80% of South Africa's energy generation and is one of the largest producers of raw materials and employers in the country. The South African government has committed to reducing the country's anthropogenic CO_2 emissions by at least 40% within the next decade. It has reiterated this commitment by ratifying various United Nations Framework Convention on Climate Change accords and developing revised energy generation strategies (Kruger, 2018). South Africa's national development strategy is closely aligned to international Sustainable Development Goals (Figure 1).

According to the current guiding framework, South Africa intends to reduce anthropogenic CO_2 emissions by reducing its reliance on coal as the primary source of energy. The country has developed an IRP that outlines the national energy generation ambitions over the next decade (Department of Mineral Resources and Energy, 2019). Within this framework, there are plans to significantly reduce coal-fired energy generation, while meeting energy demands through the accelerated development of renewable energy sources. The speed with which this transition can be implemented is a significant challenge. South Africa's socio-economic reliance on coal, its impact on national development plans and the slow uptake of renewable technologies, among other factors, suggest that this transition cannot be immediate, but should instead follow a Just Transition. In other words, the country's shift to a low-carbon economy should be implemented without negatively impacting socio-economic development linked to high-carbon industries.

Meeting climate change mitigation scenarios while continuing to rely on coal requires the development of innovative technologies. CCUS offers one such innovative solution (Metz *et al.*, 2005; Szulczewski *et al.*, 2012; Scott *et al.*, 2013). The technology proposes capturing anthropogenic CO_2 at source, utilising some of the trapped carbon for various industrial and manufacturing applications and storing the remainder permanently in suitable underground geological reservoirs (Boot-Handford *et al.*). CCUS technologies therefore aim to curb the emission of CO_2 specifically, without specifically targeting the various sources of these emissions.

Previous investigations have shown that South Africa has at least 1 500 million tonnes of anthropogenic CO_2 storage potential (Cloete, 2010). The bulk of this potential storage capacity resides in deep saline reservoirs along South Africa's near- and offshore regions (Figure 2). Geologically, these reservoirs are located in often highly porous and permeable Mesozoic volcanosedimentary sequences. Investigations have also demonstrated additional storage

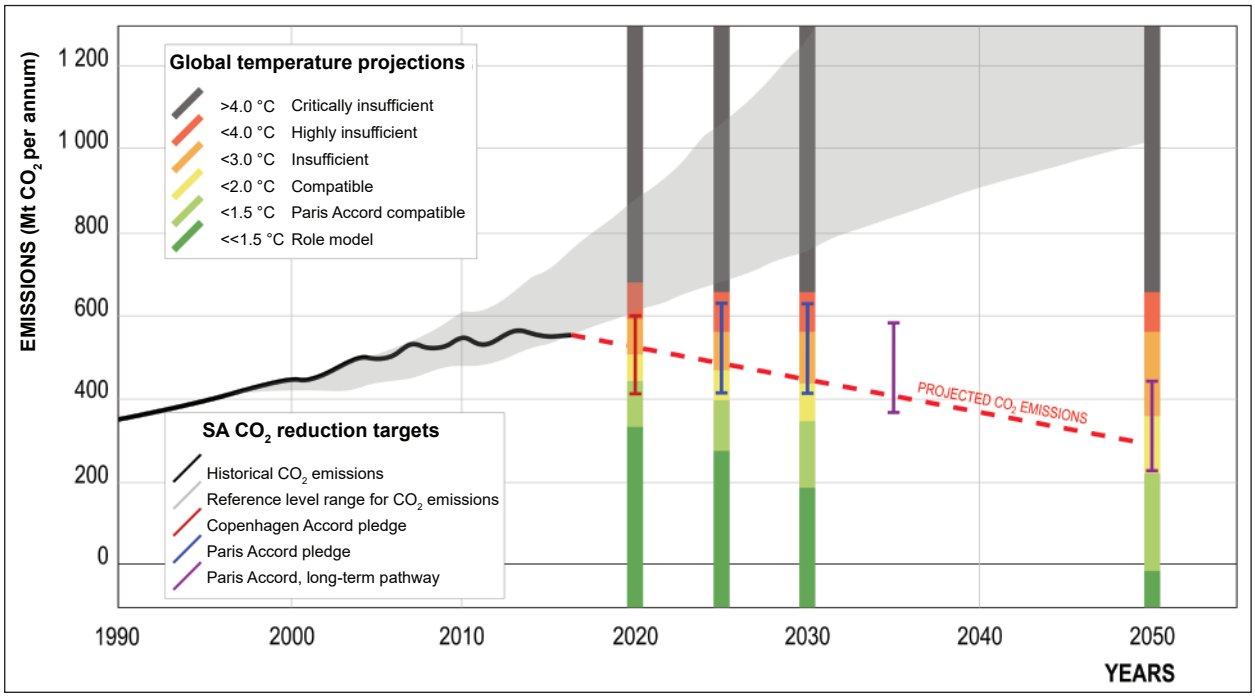

Figure 1. Overview of South Africa's projected CO_2 emissions relative to estimated global temperature rise (Friedlingstein *et al.*, 2020).

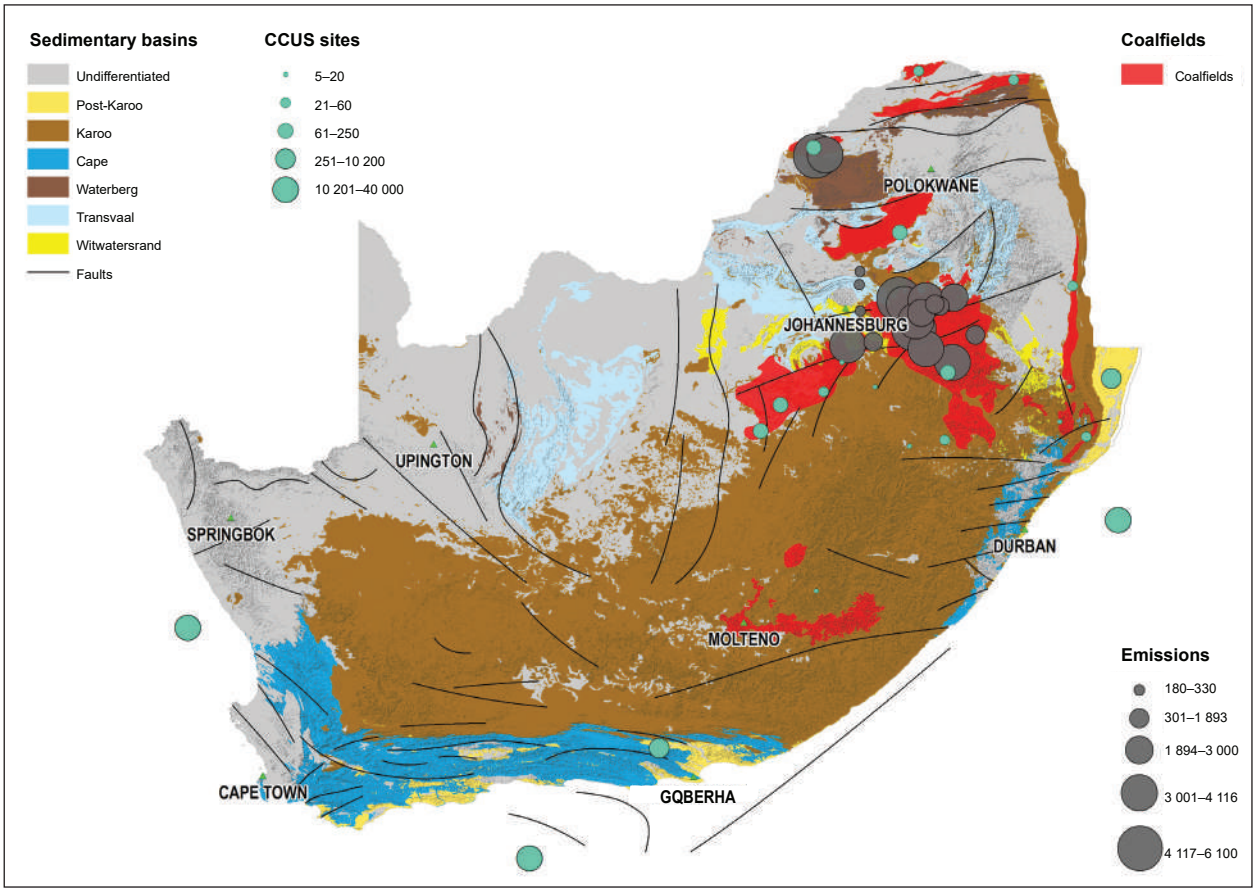

Figure 2. Overview of South Africa's energy generation relative to major CO_2 point-source emitters. Major sedimentary basins and associated coalfields as well as proposed carbon sequestration sites are depicted. Data from https://maps.geoscience.org.za.

capacity in abandoned offshore hydrocarbon reservoirs and deep, generally uneconomic, coal seams. A major challenge relating to developing and implementing CCUS technologies within these reservoirs relates to their remote location relative to the main point-source anthropogenic CO_2 emitters. Their use for CCUS would necessitate significant reliance on transport and associated infrastructure. Moreover, technology advances may yet make some of these abandoned offshore hydrocarbon reservoirs and deep coal seams economically viable. Successful implementation of CCUS technologies will require the discovery of additional storage reservoirs.

Basaltic sequences constitute an additional promising storage reservoir for anthropogenic CO_2 (Gislason and Oelkers, 2014). The promising nature of these reservoirs relates to their mineralogical characteristics. Basaltic sequences are rich in silicate minerals which make them highly reactive to anthropogenic CO_2. Mineral reactivity is arguably the most ideal characteristic of a potential reservoir. This is because reactions between the anthropogenic CO_2 and the silicate minerals promote carbonation. That is the process through which the injected anthropogenic CO_2 is incorporated into carbonate-bearing minerals and therefore rendered permanently immobile. Basalts, which are among the most abundant geological sequences on earth (Bryan and Ernst, 2008), can potentially store approximately 0.5–1.2 metric tonnes of CO_2 per tonne of basalt (Gislason and Oelkers, 2014; Matter *et al.*, 2016).

This report presents the findings of an investigation into the suitability of basaltic sequences of the Ventersdorp Supergroup as a potential storage reservoir for anthropogenic CO_2. The study is part of an ongoing research and development programme to investigate and implement South Africa's first pilot-scale CCUS plant (Dhansay *et al.*, 2022). The programme is funded by the World Bank (grant number TF0A3137), and the implementing agencies of the project are the Council for Geoscience and (previously) the South African National Energy Development Institution.

The methodology employed in this study follows the principles of the Council for Geoscience's Integrated Geoscience Mapping Programme. In particular, the programme aims to integrate several geoscience datasets towards achieving the research objectives of the CCUS project. These datasets include, among others, 1:50 000-scale geological and structural maps, bore-

hole modelling of legacy boreholes, petrology, mineralogy, reservoir modelling, geochemistry, aerial and ground geophysics, hydrogeology, environmental geology, engineering geology, seismic hazard modelling and socio-economic analysis. The results presented were considerably supported and enabled by an extensive stakeholder and communication programme. The outcomes of the study are the foundation for the necessary research and development defining the geological characterisation component of the Council for Geoscience's CCUS programme. The completion of this work prepares the way for the next key components comprising the front-end engineering and the design and construction phases.

2. GEOGRAPHY

The proposed CCUS pilot research site is located on the southernmost portion of the Goedehoop 308 farm near the town of Leandra, Govan Mbeki Local Municipality, in Mpumalanga Province, South Africa. This farm is designated as a research site in support of the proposed CCUS implementation and development project. The Govan Mbeki Local Municipality is one of seven local municipalities under the jurisdiction of the Gert Sibande District Municipality (Figure 3). According to the District Development Model, Govan Mbeki Municipality is designated as a potentially growing petrochemical hub in the larger district municipality (Table 2). Economic data for the Govan Mbeki Municipality is provided by the Govan Mbeki Municipality (Govan Mbeki Municipality, 2022).

The gross domestic product (GDP) of the municipality is approximately R 25 to 30 billion. The economy of the area is the most diverse within the Gert Sibande District. Mining is the key contributor to GDP, accounting for approximately 40% of total GDP. Manufacturing contributes approximately 25%, trade approximately 15% and the remaining notable contributors are support industries such as transportation, agriculture and construction (Figure 4). Gold and coal are the predominant mining commodities in the municipality. The Sasol coal-to-liquid and synthetic fuel industry is the key manufacturing contributor. The Sasol synthetic fuel industry, commissioned in 1979 and Eskom's Matla power station, commissioned in 1984, are the two largest energy producers in the municipality. These add up to a total potential generation capacity of approximately 4 200 MW. In addition, Eskom's Kriel and Tutuka power stations are located within 50 km of the town of Leandra. These power stations, commissioned in 1982 and 1986, respectively, have a combined total potential energy generation capacity of approximately 6 500 MW (Eskom, 2022).

Table 2. Key economic clusters across the Gert Sibande District Municipality.

Municipality	Innovation clusters
Govan Mbeki	Petrochemicals
eMalahleni	Mining and metals
Steve Tshwete	Metals manufacturing
City of Mbombela	Agriculture, technology and fresh produce market
Thaba Chweu	Potential forestry and fresh produce market
Nkomazi	Potential agro-processing

With approximately 400 000 residents, Govan Mbeki Local Municipality is the most populous in the Gert Sibande District Municipality. Of the approximately 90 000 households, approximately 70% are housed in

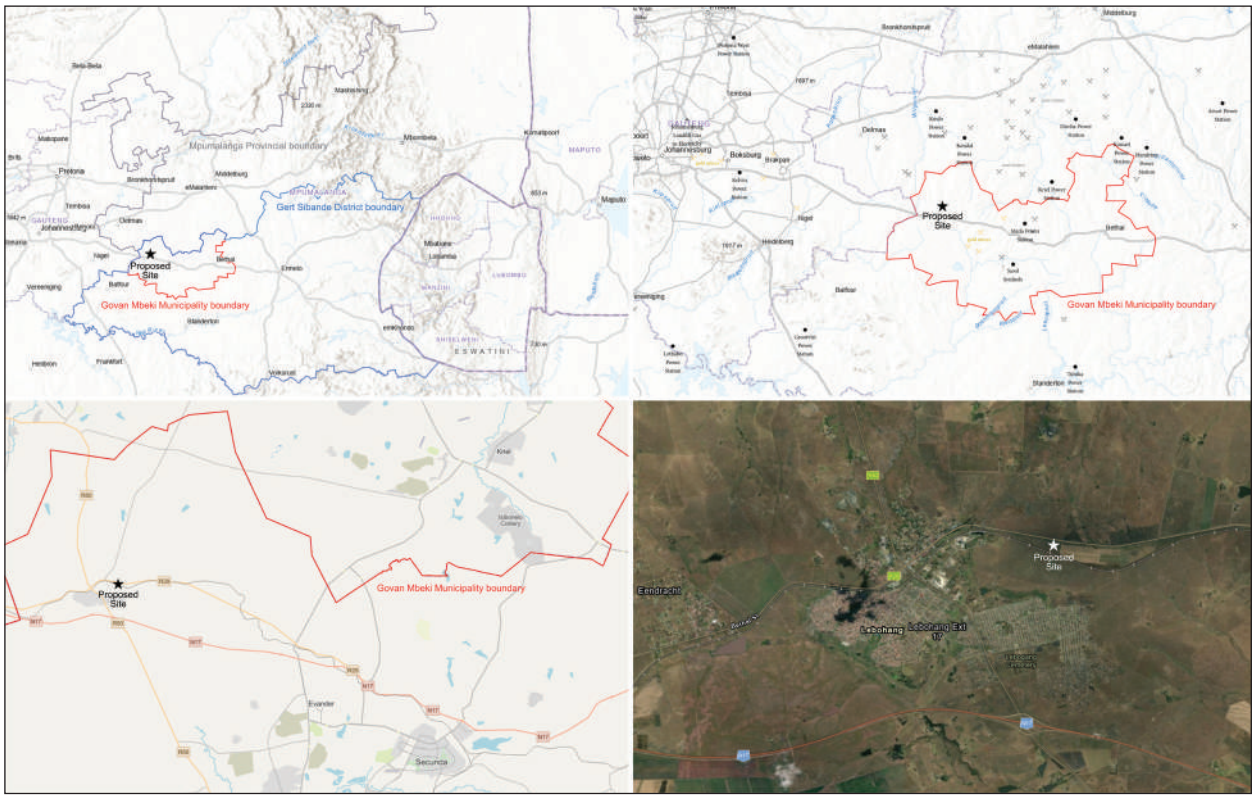

Figure 3. Overview of the proposed injection site, relative to the provincial boundary (top left), the district boundary (top right), the municipal boundary (bottom left) and the perimeter of the town of Leandra (bottom right).

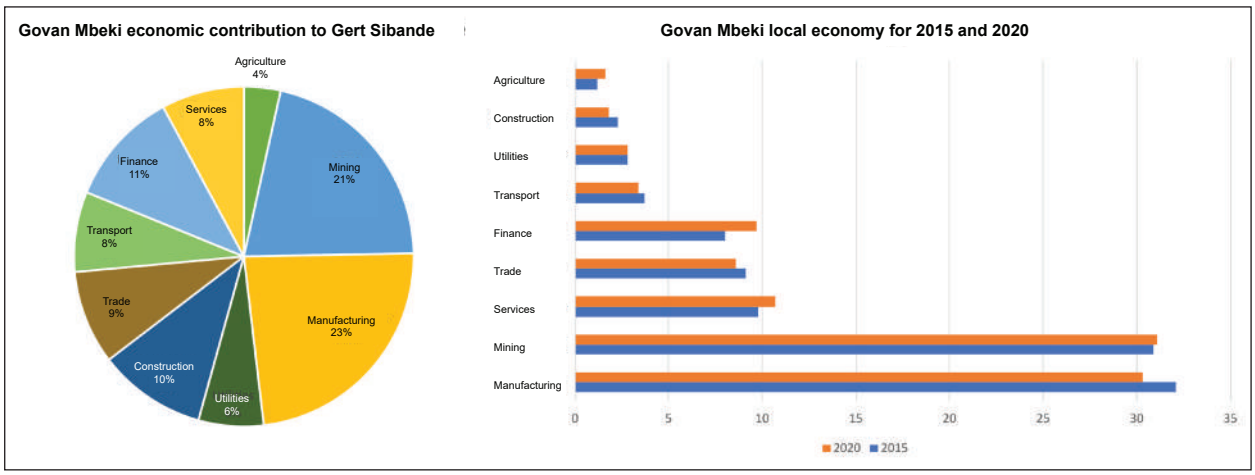

Figure 4. Key economic indicators for Govan Mbeki Municipality. Contribution to the economic growth of the district (left) and economic growth within the municipality (right).

formal dwellings. At least 90% of the formal dwellings have access to electricity, which is predominantly used for lighting. Recently, the municipality has seen a population growth rate of 3–5% annually, making it the second fastest-growing municipality in Mpumalanga Province. Moreover, the population is expected to increase beyond 500 000 residents within the next decade. The municipality has a male to female ratio of 52:48.

Approximately 50–60% of the population lives below the poverty line, earning a monthly income equivalent to or less than R 3 200.00. The unemployment rate is approximately 25% with a youth unemployment rate of approximately 25–30%. Approximately 8% of the population in Govan Mbeki Municipality has no formal education. Approximately 31% has attained a senior certificate and approximately 13% has some level of higher education. Mining, manufacturing and trade, especially in the hydrocarbon development and application industry, are the key employment sectors in the municipality. Additionally, the listing of these industries in relation to the municipality's projected innovation sectors in Table 2 underscores their significance to the region's socio-economic development goals.

Govan Mbeki Local Municipality is characterised by a relatively flat-lying landscape comprised of plains and hills, ranging in altitude from 1 700–1 400 m above sea level (Figure 5). The region is part of the larger Highveld ecoregion, defined by a moderate to low relief with varied grassland vegetation. The vegetation is characterised by medium-dense to very dense tufted grasses. The climate is subtropical with the lowest average temperatures recorded around June. The windiest months are generally recorded around September/October. The highest rainfall generally occurs around December, and July is generally the driest month. Mean annual precipitation is generally around 662 mm.

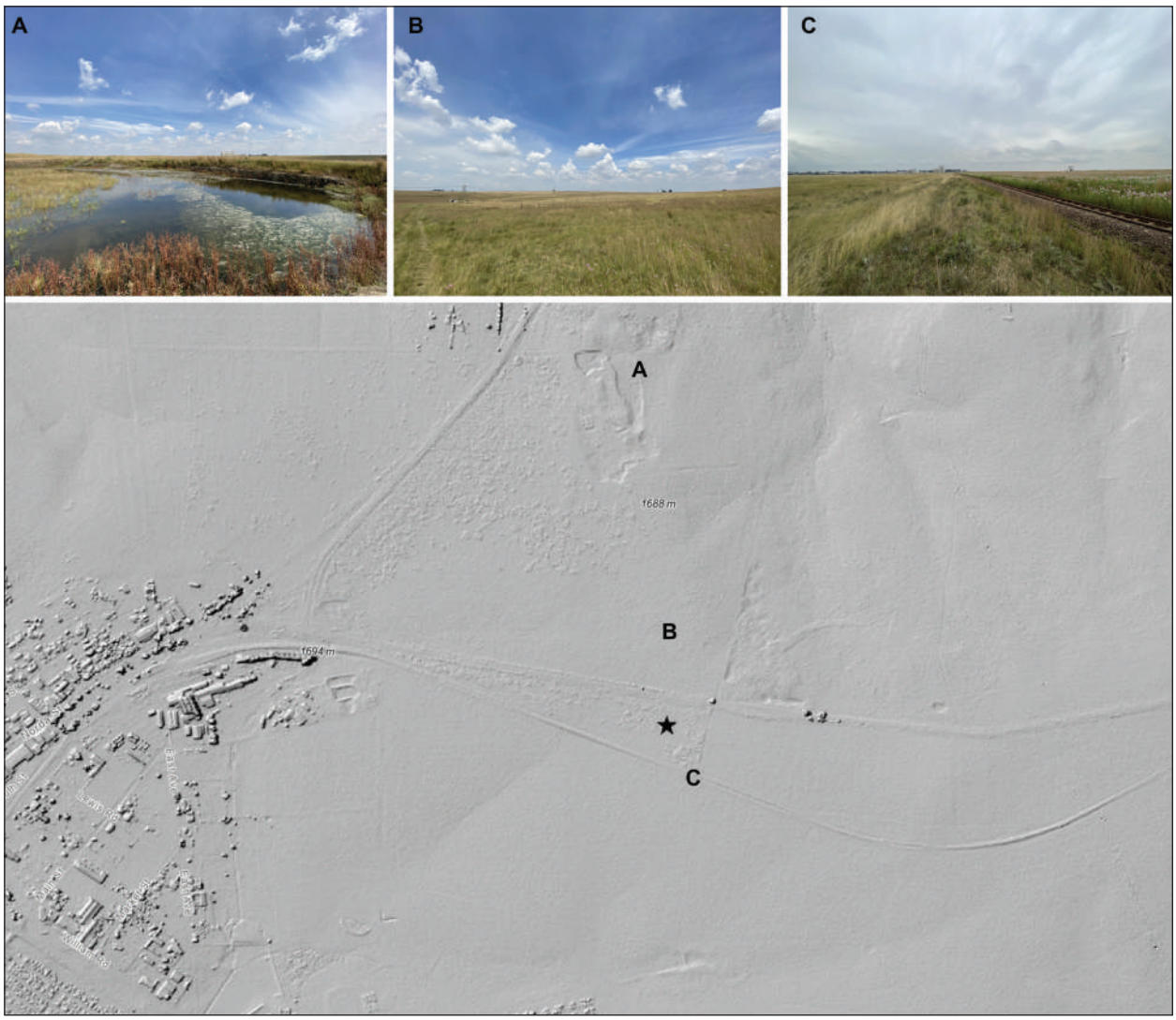

Figure 5. Photos of sites A–C (photos at the top) on the high-resolution (2 m) digital elevation image (bottom) around the proposed injection site (black star).

3. GEOLOGY

3.1 GEOLOGICAL BACKGROUND

The proposed CCUS pilot site is situated at the eastern extent of the Kaapvaal Craton. The craton is an ancient remnant of the earth's earliest continental crust that formed during the Archaean. The craton is characterised by a highly dense and thick subcontinental lithospheric mantle keel extending to approximately 250 km below the surface (Evans *et al.*, 2011). The Kaapvaal Craton itself can be subdivided into several smaller cratonic blocks, namely the Polokwane, Witwatersrand, Kimberley, Mbombela and Eswatini blocks. These blocks are sutured together by deep crustal discontinuities that would have been consolidated by continental-scale tectonic processes (Dhansay, 2021). The proposed CCUS pilot site is located on the Witwatersrand Block near the contact zone with the Mbombela Block (Dhansay *et al.*, 2022).

The lowermost and oldest sequence below the proposed CCUS pilot site is the ca 3 200 Ma Witwatersrand Supergroup (Cornell *et al.*, 2021). The sequence mainly comprises quartzite with interspersed conglomerate and volcanic layers. The quartzites are generally composed entirely of quartz with very minor mica and feldspar. These also appear to have been extensively recrystallised. The conglomerates are noteworthy for their high proportion of gold-bearing sulfides. Generally, these horizons are no more than 1–10 m thick. Figure 6 presents a simplified geological map of the immediate surrounds of the proposed injection site (Pretorius *et al.*, 1986). The map is restricted to the Witwatersrand Supergroup as the key basement structure and architecture critical to the project objectives. Figure 7 presents a detailed stratigraphic profile of the geology underlying the proposed injection site (Dhansay *et al.*, 2022).

The ca 2 700 Ma Ventersdorp Supergroup overlies the Witwatersrand Supergroup. The contact zone is defined by the Ventersdorp Contact Reef and is characterised by a highly deformed and altered mélange with significant pseudotachylite occurrences. The Ventersdorp Supergroup is subdivided into several groups representing various phases of volcanic emplacement and evolution. The Klipriviersberg Group comprises the lowermost part of the Ventersdorp Supergroup. The group is characterised by a wide range of volcanic assemblages, including mafic to ultramafic basaltic rocks, agglomeratic sequences and vesicular porphyritic lavas. The Platberg Group of interlayered siliciclastic and mafic to ultramafic volcanic rocks overlie the Klipriviersberg Group. The uppermost part of the Ventersdorp Supergroup comprises mostly siliciclastic and generally felsic volcanic rocks of the Pniel Group (Gumsley *et al.*, 2020).

A wide variety of chemical and siliclastic sequences of the ca 2 500 Ma Transvaal Supergroup overlie the

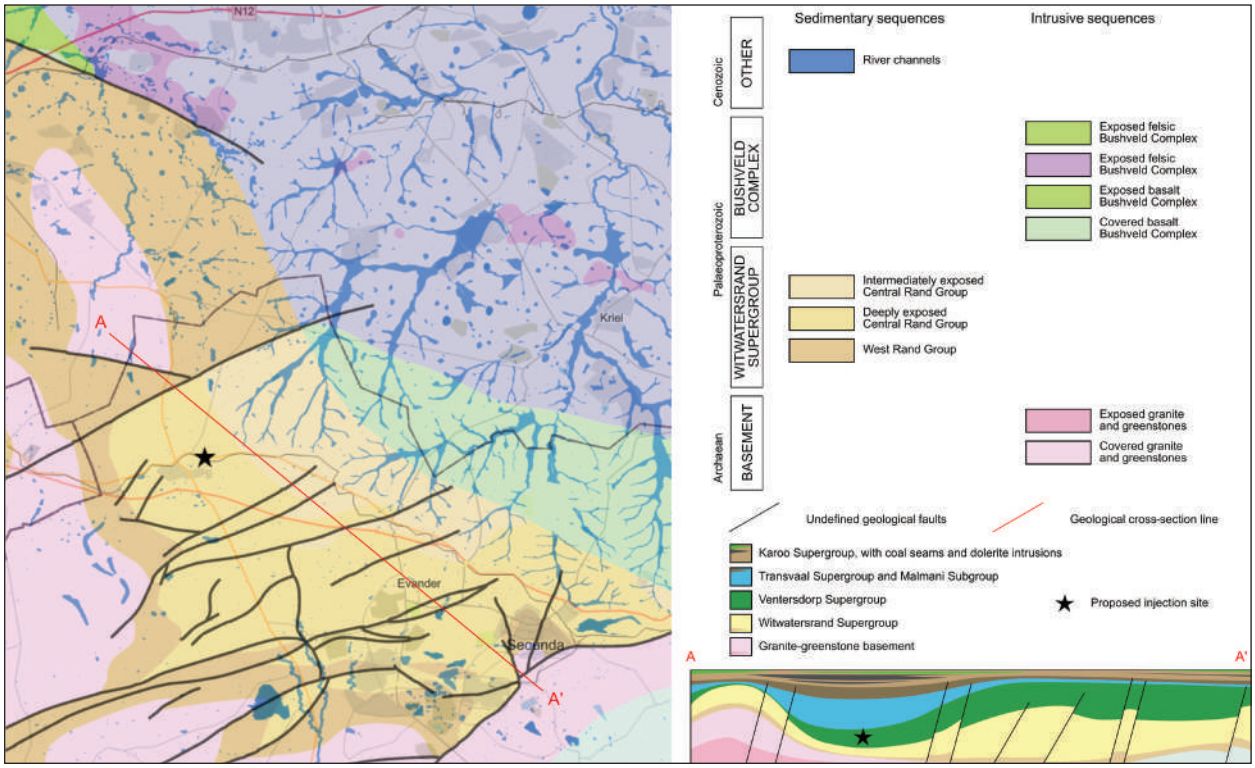

Figure 6. Simplified geological map of the area around the proposed injection site. Geological map restricted to the Witwatersrand Supergroup basement (Pretorius *et al.*, 1986).

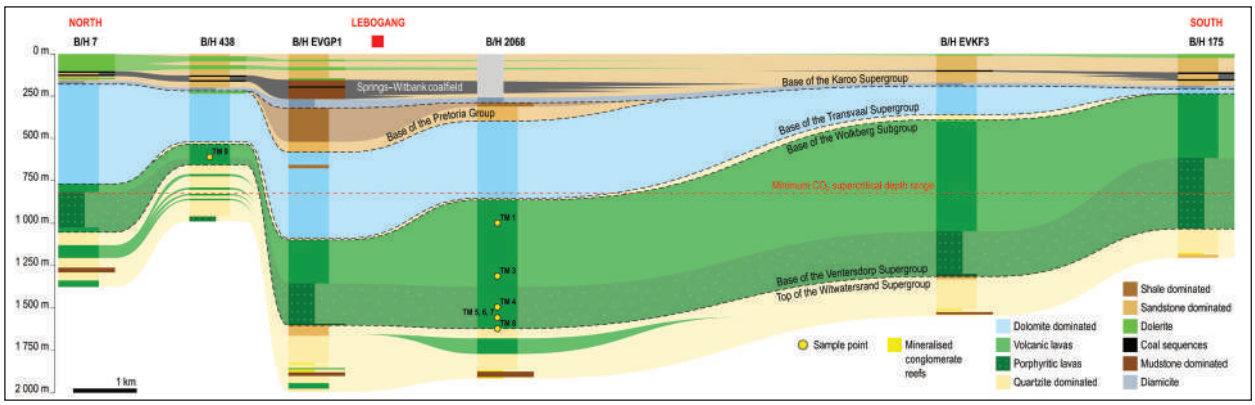

Figure 7. Schematic geological profile across the study area. Figure 8 depicts the locations of boreholes used in the construction of the geological profile and Figure 14 features photomicrographs of samples noted in the profile (Dhansay *et al.*, 2022).

Ventersdorp Supergroup (Zeh *et al.*, 2020). The contact region is defined by highly recrystallised quartzite of the Wolkberg Group followed by massive dolomitic sequences of the Malmani Subgroup. The Malmani Subgroup is further characterised by interlayered chert and cemented in-fill brecciated sequences. The upper part of the Transvaal Supergroup is defined by the mostly siliciclastic and interlayered volcanic sequences of the Pretoria Group.

The ca 330–180 Ma sequences of the Karoo Supergroup overlie the Transvaal Supergroup (Johnson *et al.*, 1996). The lowermost portion of the Karoo Supergroup is defined by massive glacial tillite and diamictite of the Dwyka Group. Chemical sedimentary sequences of the Ecca Group, characterised by carbonaceous shale with interlayered coal horizons, overlie the Dwyka Group. While the mostly fluvial sequences of the Beaufort Group overlie the Ecca Group, these sequences are not well developed and preserved in the study area. The uppermost part of the Karoo Supergroup is defined by the ca 180 Ma Karoo Large Igneous Province (Muedi *et al.*, 2022) including massive flood basalt sequences occurring throughout the study area as cross-cutting dykes and sills.

The youngest sequences exposed on the surface of the study area and generally overlying the Karoo Supergroup comprise a range of Quaternary (less than ca 2.5 Ma) soils and sediments including clays and reworked material of the underlying sequences.

3.2 CHARACTERISATION OF THE VENTERSDORP SUPERGROUP

3.2.1 Borehole information

The proposed CCUS pilot site aims to target the lower part of the Ventersdorp Supergroup, specifically the Klipriviersberg Group, as a potential anthropogenic CO_2 storage reservoir. The characterisation of the Klipriviersberg Group below the proposed CCUS pilot site is aided by legacy borehole data available at the Council for Geoscience's National Core Library. At least 22 physical boreholes were logged and used in this investigation together with more than 1 500 digital borehole logs across Mpumalanga Province (Figure 8). Figure 9 presents the ca 1 500 m depth range of one of the selected boreholes located near the proposed injection site, featuring various mineral spectral signatures.

The Klipriviersberg Group itself can be subdivided into several distinct formations (Gumsley *et al.*, 2020; Dhansay *et al.*, 2022). The lowermost part comprises the Westonaria Formation composed of ultramafic komatiitic lavas. The Alberton Formation overlies the Westonaria Formation and is characterised by the development of large plagioclase phenocrysts. The Orkney Formation follows and is characterised by relatively homogeneous ultramafic lavas with interlayered tuff horizons. The Jeanette Formation overlies the Orkney Formation and is, in turn, characterised by the occurrence of agglomeratic layers. The overlying Loraine Formation is characterised by a transition of fine-grained mafic to ultramafic lavas and the presence of spherule beds. The uppermost sequence of the Klipriviersberg Group is characterised by amygdaloidal lavas of the Edenville Formation.

The available borehole information suggests that only the Westonaria, Alberton and Orkney Formations are developed below the proposed CCUS pilot site. According to the borehole information, the combined thickness of these units is approximately 750 m. The lowermost Westonaria Formation is approximately 10–15 m thick, while the remaining units are characterised by massive flood basalts and porphyritic and vesicular lava flows. The Ventersdorp Supergroup sequences exhibit a significant thinning towards the northern extent of the study area. This shallowing is linked to the presence of Archaean granites of the Devon Dome (Coward *et al.*, 1995).

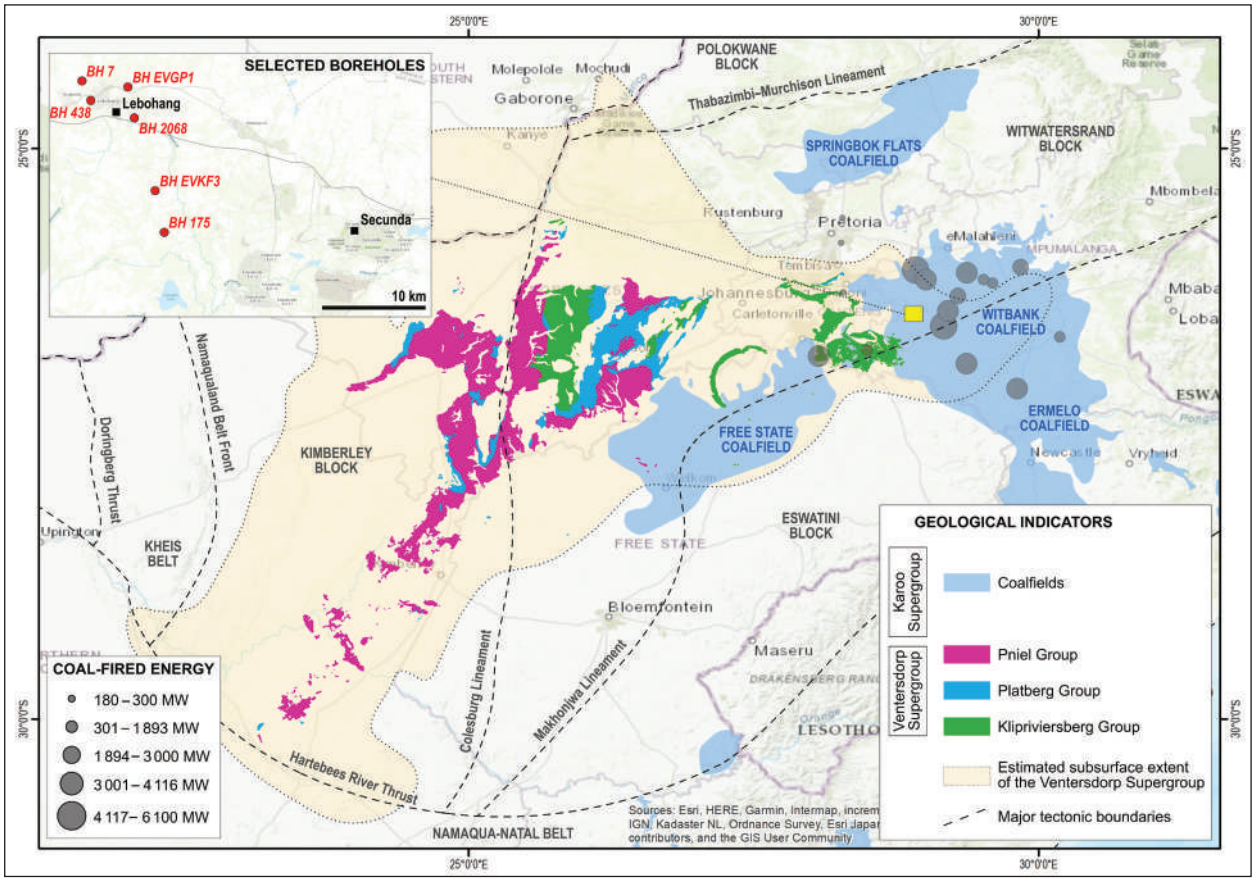

Figure 8. Overview of the extent of the Ventersdorp Supergroup. Included are the positions of the major point-source CO_2 emitters and their associated coalfields. The inset map shows the locations of geological boreholes used in this study (Dhansay *et al.*, 2022).

3.2.2 Hyperspectral scanning

Further characterisation of the Klipriviersberg Group is undertaken through applications of hyperspectral core scanning (Figure 9). Available boreholes were scanned using the *Sisu* hyperspectral core scanner at the Council for Geoscience's National Core Library. Hyperspectral scanning enables the collection of high-resolution mineral spectral information through reflectance spectroscopy undertaken across different spectral regions including the visible near-infrared, short-wave infrared and long-wave infrared spectrum — 0–12 µm wavelength range. The various minerals can be identified and their related textural relationships established using their spectrum absorption properties (De la Rosa *et al.*, 2022). The properties allow for the rapid and precise characterisation of multiple geological boreholes with a view to identifying key mineral sequences relevant to CO_2 reactivity.

The results of the hyperspectral borehole scanning were used to delineate key horizons with distinctive mineral spectral signatures (Figure 11). This included identifying interlayered zones characterised by predominantly mafic and less mafic mineral compositions. This information is critical to establishing the potential degree of mineral carbonation. Zones exhibiting higher mafic compositions, for example a higher concentration of silicate minerals, are more likely to undergo mineral carbonation more rapidly than zones characterised by lower mafic compositions. Hyperspectral data provides key information on the occurrence and degree of alteration. This is crucial because the occurrence of mineral alteration products may have a bearing on the readiness and degree of anticipated mineral carbonation. However, hyperspectral suggests that the prevalence of mineral alteration is relatively low and restricted to specific horizons in the sequence, for example where high-permeability zones facilitate greater fluid-induced mineral alteration.

3.2.3 Borehole sampling

Borehole logging, supported by hyperspectral core scanning, enabled the identification of key horizons deemed to be crucial as both reactive and non-reactive zones, i.e. zones hosting high and low concentrations of reactive minerals. Several analytical techniques further clarified the characteristics of these zones as potentially efficient reactive and non-reactive zones. Analyses of selected samples from available borehole core at the Council for Geoscience's National Borehole Repository were conducted. Table 3 presents an overview of the samples

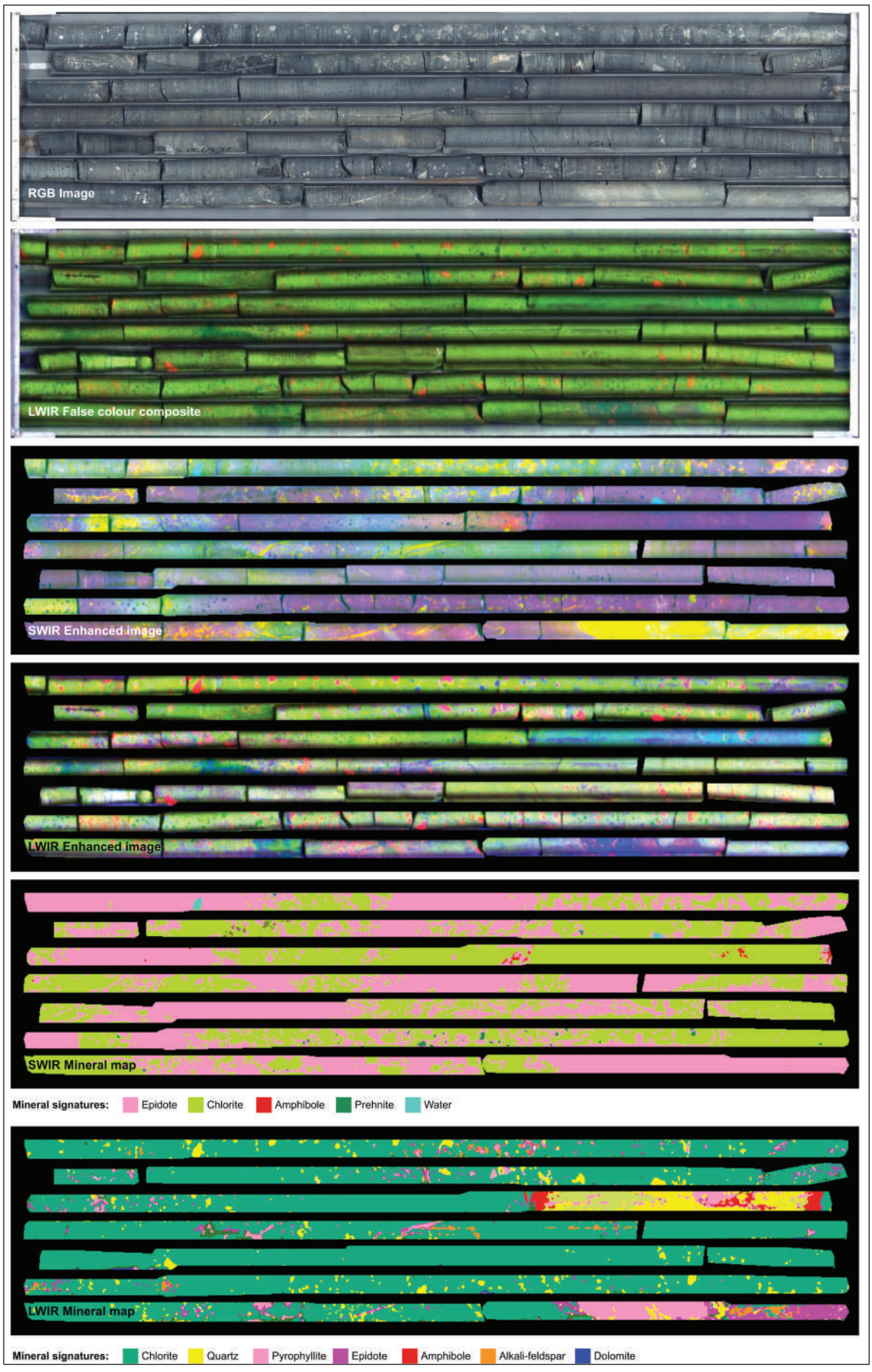

Figure 9. Overview of the ca 1 500 m depth range of borehole 2068. Illustrating RGB, short-wave and long-wave infrared spectra, including dominant mineral maps.

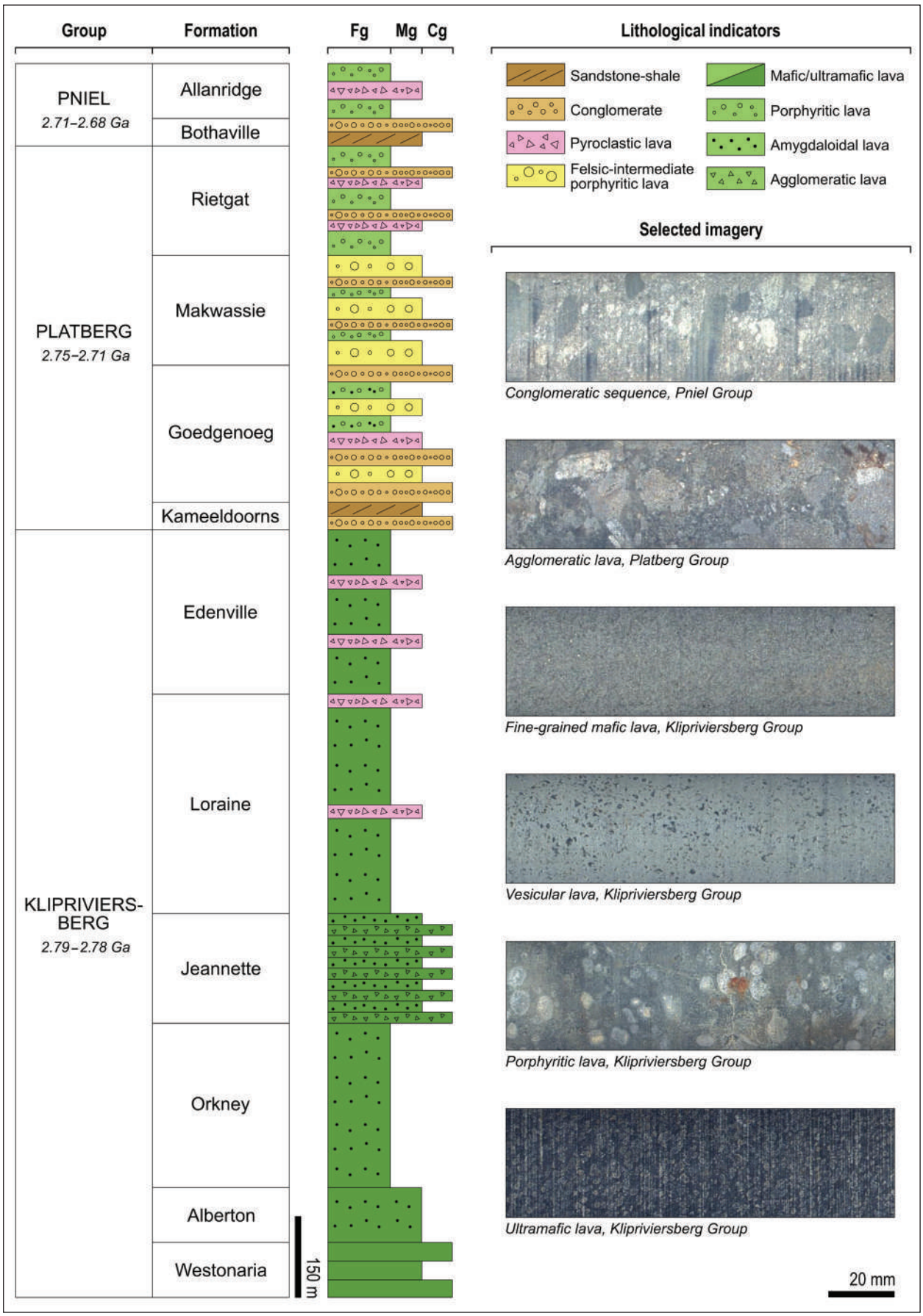

Figure 10. Simplified stratigraphic column of the Ventersdorp Supergroup (Dhansay *et al.*, 2022). Core images from the Council for Geoscience National Borehole Repository (https://maps.geoscience.org.za).

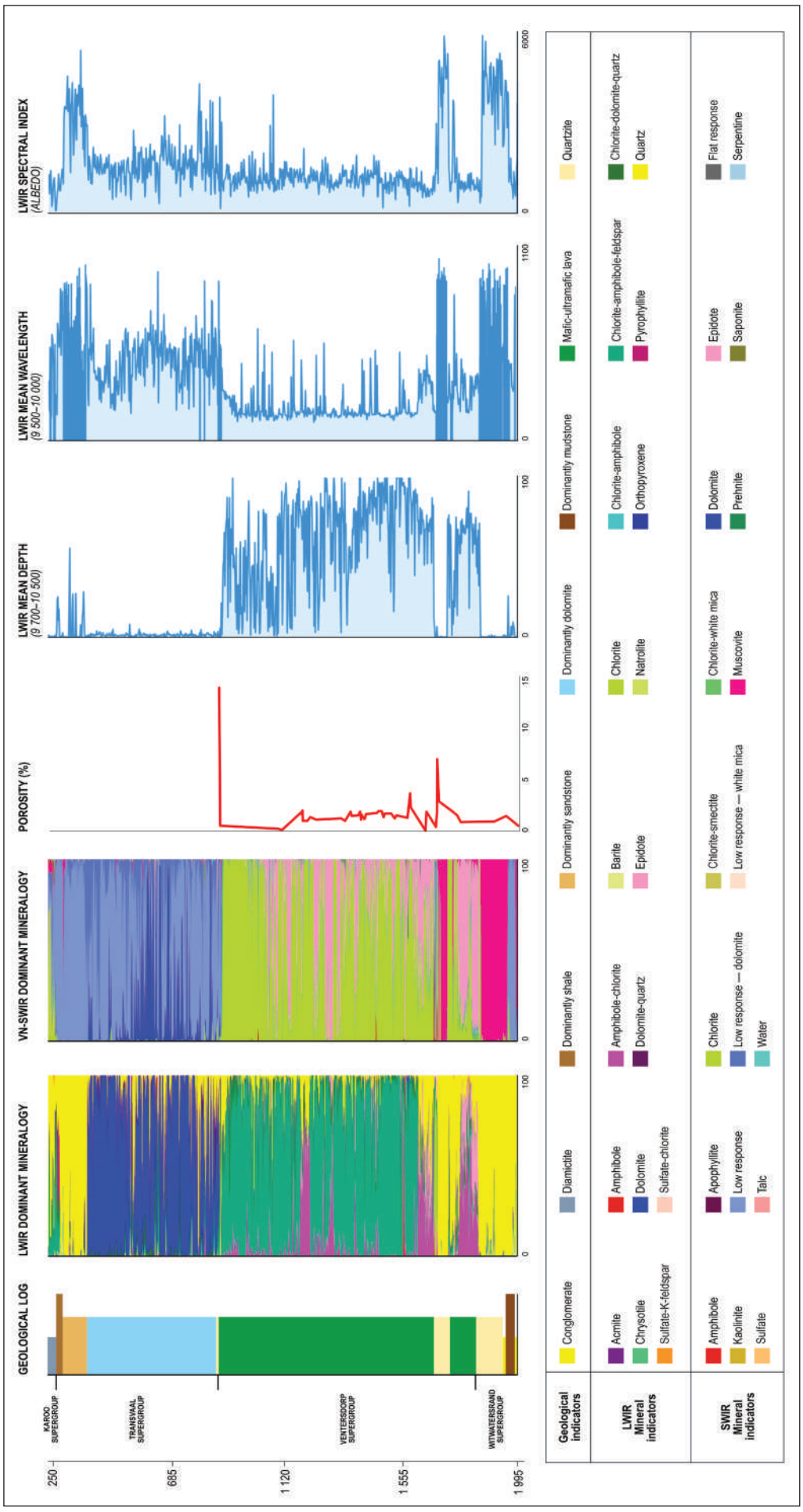

Figure 11. Overview of hyperspectral data acquired on borehole BH 2068. The figure depicts a simplified geological log, the dominant mineral map ranging from the visible near-infrared to long-wave infrared, the long-wave infrared mean depth ranges, wavelength and spectral index (Dhansay *et al.*, 2022).

Table 3. Overview of selected borehole samples and general descriptions.

No.	ID	Borehole	Depth (m)	Type	Lithology
1	TM9	438	700	Reactive	Ultramafic flow
2	DBS009	687	745	Non-reactive	Porphyritic flow
3	PM015	687	750	Reactive	Ultramafic flow
4	TM1	2 068	1 000	Reactive	Massive flow
5	DBS010	2 068	1 001	Non-reactive	Massive flow
6	TM2	2 068	1 005	Reactive	Amygdaloidal flow
7	DBS011	2 068	1 017	Non-reactive	Massive flow
8	DBS012	2 068	1 167	Non-reactive	Massive flow
9	DBS013	2 068	1 275	Non-reactive	Massive flow
10	PM016	2 068	1 292	Reactive	Vesicular flow
11	TM3	2 068	1 300	Reactive	Massive flow
12	DBS014	2 068	1 348	Non-reactive	Massive flow
13	PM017	2 068	1 356	Reactive	Highly amygdaloidal flow
14	PM018	2 068	1 361	Reactive	Amygdaloidal/vesicular flow
15	DBS015	2 068	1 378	Non-reactive	Massive flow
16	PM019	2 068	1 383	Reactive	Agglomerate
17	DBS016	2 068	1 437	Non-reactive	Massive flow
18	PM020	2 068	1 443	Reactive	Highly amygdaloidal flow
19	DBS017	2 068	1 451	Non-reactive	Massive flow
20	PM025	2 068	1 465	Reactive	Agglomerate
21	TM4	2 068	1 500	Reactive	Massive flow
22	TM5	2 068	1 510	Reactive	Massive flow
23	TM6	2 068	1 515	Reactive	Massive flow
24	TM7	2 068	1 520	Reactive	Massive flow
25	DBS018	2 068	1 562	Non-reactive	Massive flow
26	PM022	2 068	1 574	Reactive	Amygdaloidal flow
27	PM023	2 068	1 576	Reactive	Highly amygdaloidal flow
28	TM8	2 068	1 600	Reactive	Amygdaloidal flow
29	DBS019	2 068	1 686	Non-reactive	Massive flow
30	DBS020	2 068	1 691	Non-reactive and reactive	Massive flow
31	PM024	2 068	1 693	Reactive	Ultramafic flow
32	PM021	2 068	1 699	Reactive	Massive flow
33	MN21-007	2 188	1 043	Reactive	Amygdaloidal/vesicular flow
34	MN21-006	2 188	1 053	Reactive	Amygdaloidal/vesicular flow
35	MN21-005	2 188	1 065	Reactive	Vesicular/brecciated flow
36	MN21-004	2 188	1 090	Reactive	Vesicular flow
37	DBS001	2 188	1 102	Non-reactive	Massive flow
38	PM001	2 188	1 106	Reactive	Amygdaloidal lava
39	PM002	2 188	1 107	Reactive	Amygdaloidal lava
40	PM003	2 188	1 108	Reactive	Amygdaloidal/massive flow
41	DBS002	2 188	1 128	Non-reactive	Massive flow
42	PM004	2 188	1 138	Reactive	Amygdaloidal/vesicular flow
43	PM005	2 188	1141	Reactive	Amygdaloidal/vesicular flow
44	MN21-002	2 188	1 151	Reactive	Amygdaloidal/vesicular flow
45	MN21-001	2 188	1 162	Non-reactive	Massive flow
46	DBS003	2 188	1 315	Non-reactive	Massive flow
47	PM006	2 188	1 321	Reactive	Agglomerate
48	DBS004	2 188	1 364	Non-reactive	Massive flow
49	PM007	2 188	1 367	Reactive	Highly amygdaloidal flow
50	PM008	2 188	1 368	Reactive	Highly amygdaloidal flow
51	PM009	2 188	1 375	Reactive	Highly amygdaloidal flow
52	DBS005	2 188	1 431	Non-reactive	Massive flow
53	PM010	2 188	1 459	Reactive	Highly amygdaloidal flow
54	DBS006	2 188	1 492	Non-reactive	Massive flow
55	PM011	2 188	1 508	Reactive	Highly amygdaloidal flow
56	DBS007	2 188	1 514	Non-reactive and reactive	Amygdaloidal/massive flow
57	DBS008	2 188	1 640	Non-reactive	Massive flow
58	PM012	2 188	1 645	Reactive	Highly amygdaloidal flow
59	PM013	2 188	1 755	Reactive	Porphyritic flow
60	PM014	2 188	1 779	Reactive	Ultramafic flow
61	LP001	2 188	1 794	Reactive	Medium-grained quartzite
62	LP002	2 188	1 939	Reactive	Coarse-grained quartzite
63	LP003	2 188	1 991	Reactive	Fine-grained quartzite
64	LP004	2 188	2 043	Reactive	Medium-grained quartzite

collected and used for various mineralogical and petrographic characterisations. In general, 5–30 cm quarter core fraction samples were collected from four different boreholes (Figure 12). Figure 7 shows the locations of selected samples and their various depth intervals.

3.2.4 Mineralogy

The critical horizons delineated by means of hyperspectral scanning were further characterised through detailed mineralogical assessments (Figures 16 and 17). Mineral characterisation to establish the presence of potentially reactive minerals and the volumetric occurrence of alteration minerals that may diminish potential reactivity, is crucial. Therefore, mineral characterisation, including X-ray diffraction (XRD) and scanning electron microscopy (SEM), was carried out (Figure 13). Existing borehole material was used to analyse selected characteristic zones (Table 3) with the results corroborating the findings of the hyperspectral analyses. The dominant mineralogy throughout the Klipriviersberg Group comprises plagioclase, pyroxene, chlorite, epidote and quartz. The main alteration products, chlorite and epidote, indicate that the Klipriviersberg Group underwent greenschist facies metamorphic alteration. Tables 14 and 15 present detailed mineralogical results for the selected samples.

3.2.5 Petrography

The mineralogical assessments were further supported by a petrographic characterisation of the selected samples (Figure 14). Petrographic characterisation is an important adjunct to mineralogical studies. This makes it possible to carry out detailed assessments of the nature of observed minerals, including their textural relationships and reactive features. The observations obtained from the mineralogical assessments were corroborated by the petrographic analysis. The petrographic analysis further confirmed the characterisation of key textural relationships. The analysis entailed describing the type of alteration and potential availability of reactive silicate minerals such as pyroxenes and feldspars. Moreover, the analysed phenocrysts comprise plagioclase and smaller amounts of quartz.

In general, the petrographic analyses delineate an increase in the concentration of carbonate and other alteration minerals towards the base of the Ventersdorp Supergroup, i.e. towards the Ventersdorp Contact Reef

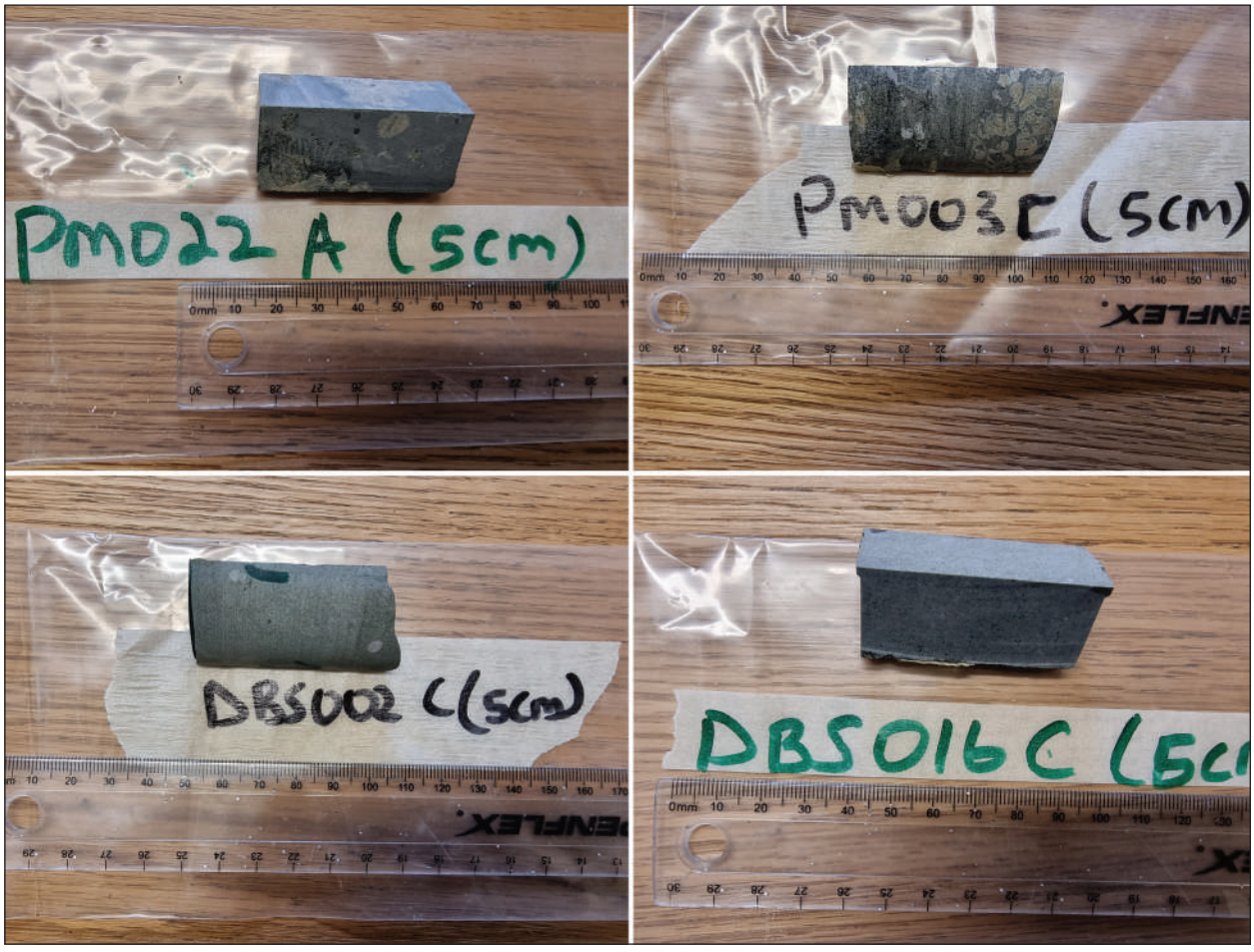

Figure 12. Examples of quarter core fraction samples collected from representative boreholes.

Figure 13. Results of automated SEM analyses of the selected samples from available boreholes.

NOTABLE SAMPLE CHARACTERISTICS	
Sample	TM 1
Lithology	Ferroaxinite vein
Dominant mineralogy	Ferroaxinite (70%); Quartz (20%); Clinopyroxene (5%)
Texture	Fine grained
Pore space (%)	ca 5%
Alteration	<1%
Carbonation	<1%
Sample	TM 2
Lithology	Amygdaloidal basalt
Dominant mineralogy	Plagioclase (30%); Clinopyroxene (15%); Chlorite (15%)
Texture	Fine to medium grained
Pore space (%)	ca 13%
Alteration	ca 20%
Carbonation	< 1%
Sample	TM 3
Lithology	Basalt
Dominant mineralogy	Quartz (50%); Epidote (45%); Calcite (1%)
Texture	Medium grained
Pore space (%)	ca 2%
Alteration	ca 45%
Carbonation	<1%
Sample	TM 4
Lithology	Basalt
Dominant mineralogy	Clinopyroxene (20%); Plagioclase (20%); Chlorite (15%)
Texture	Fine grained
Pore space (%)	ca 12%
Alteration	ca 20%
Carbonation	<1%
Sample	TM 5
Lithology	Basalt
Dominant mineralogy	Clinopyroxene (25%); Plagioclase (15%); Chlorite (20%)
Texture	Medium to coarse grained
Pore space (%)	ca 14%
Alteration	ca 20%
Carbonation	<1%
Sample	TM 6
Lithology	Basalt
Dominant mineralogy	Clinopyroxene (20%); Chlorite (20%); Epidote (20%)
Texture	Coarse grained
Pore space (%)	ca 13%
Alteration	ca 40%
Carbonation	<1%
Sample	TM 7
Lithology	Amygdaloidal basalt
Dominant mineralogy	Clinopyroxene (50%); Chlorite (20%); Epidote (15%)
Texture	Fine to medium grained
Pore space (%)	ca 10%
Alteration	ca 35%
Carbonation	ca 10%
Sample	TM 8
Lithology	Ultramafic basalt
Dominant mineralogy	Talc (50%); Epidote (30%); Haematite (10%)
Texture	Coarse grained
Pore space (%)	ca 5%
Alteration	ca 80%
Carbonation	ca 50%
Sample	TM 9
Lithology	Porphyritic basalt
Dominant mineralogy	Calcite (50%); Chlorite (25%); Quartz (15%)
Texture	Coarse grained
Pore space (%)	ca 10%
Alteration	ca 75%
Carbonation	ca 50%

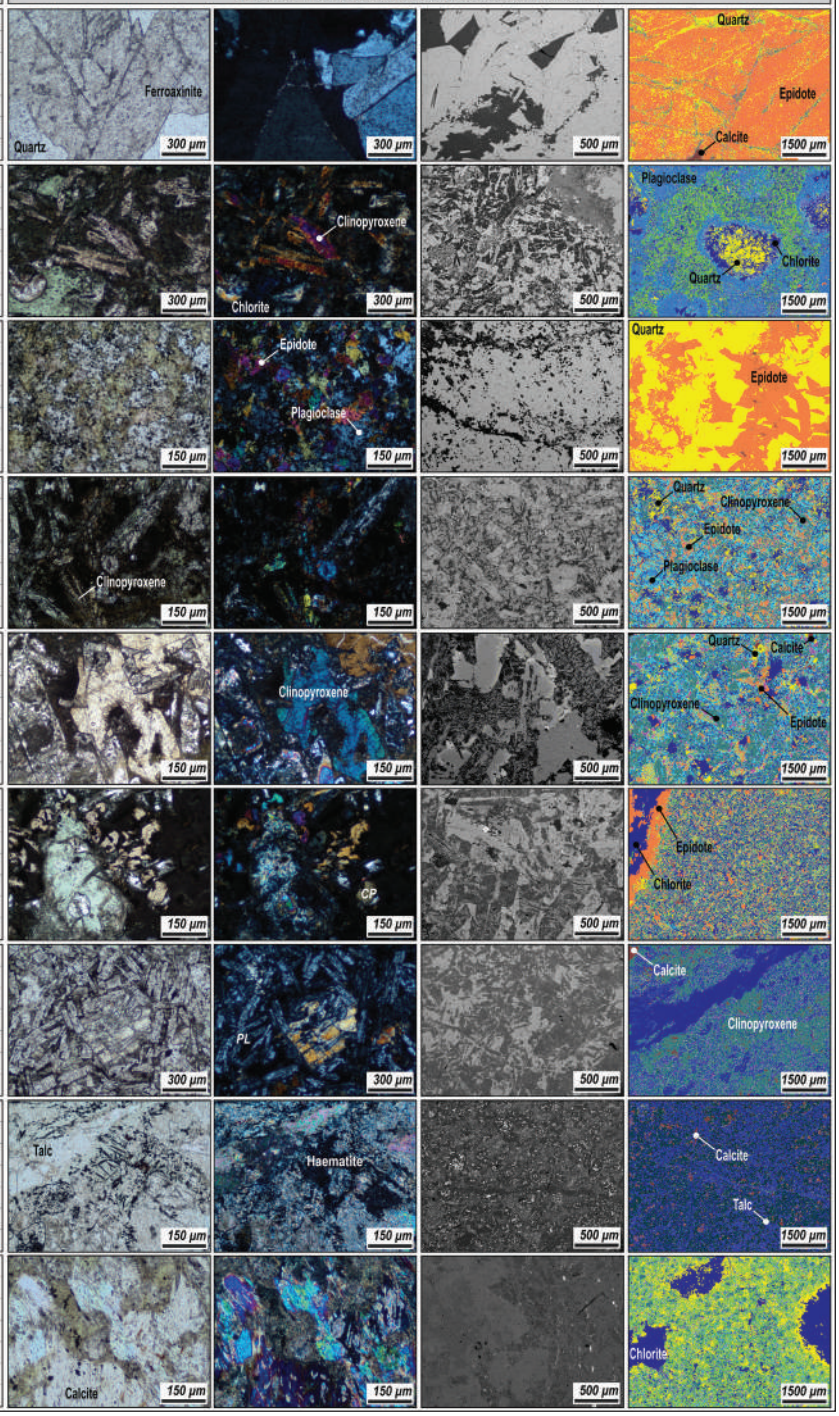

Figure 14. Overview of petrographic analyses and photomicrographs of samples of the Ventersdorp Supergroup sequences. Photomicrographs include optical microscopy in plane-polarised light (PPL), cross-polarised light (XPL) and automated SEM. Characteristic features are also described (Dhansay *et al.*, 2022).

with the Witwatersrand Supergroup. This zone is a significant permeable horizon that probably promoted the alteration of silicate minerals. Moreover, the higher sequences exhibit limited alteration with a better preservation of silicate minerals.

3.2.6 Porosity and permeability

The porosity and permeability of any proposed geological reservoir are key to determining its viability and the mechanisms involved in its development. The porosity of a geological reservoir refers to the number of void spaces present and the number and distribution of pore spaces which may be filled with fluids or gases. A larger volume of pore space would suggest greater capacity to store anthropogenic substances. The permeability of a geological reservoir refers to its ability to transmit fluids or gases between the inherent pore spaces under a specific pressure gradient, i.e. the concentration of pore interconnections. Higher permeability suggests that fluids or gases are more easily transmitted across pore spaces.

Porosity and permeability analyses were carried out on samples collected across the Klipriviersbrg Group (Figures 16 and 17). Permeability analyses were conducted at Rocklab (South Africa) using water circulation within a Hoek cell on rock samples ca 20–50 mm in length. A water circulation pressure of 3 500 KPa was applied during the test. The results suggest that the lithologies are impermeable at the pressures applied. Helium pycrometry porosity analyses were conducted at the Particle Physics Laboratory (USA). The results for the porosity and permeability analyses for the selected samples are presented in Tables 16 and 17. The results suggest that the samples have relatively low porosities, with the highest recorded porosity at approximately 5%. The characteristics of the basaltic samples suggest that porosity, permeability and interconnectivity may be limited to a microscopic scale.

Mico X-ray computed tomography (XCT) scanning was undertaken at Necsa (South Africa) to further investigate potential microscopic void space interconnectivity. Scanning was undertaken at a scale of 10 microns with the results indicating that, on a microscale, porosities may be as high as 30%. Calculated permeabilities of ca 1 000 mD were determined (Figure 15). The variation of results obtained by the largely macroscale (Hoek cell and pycrometry) and microscale (XCT) analyses suggests that porosity and permeability are limited only to the microscale. Furthermore, increasing permeability to enable potential anthropogenic CO_2 injection will require artificially increasing permeability, for example by exceeding the prevailing *in situ* pore fluid pressures.

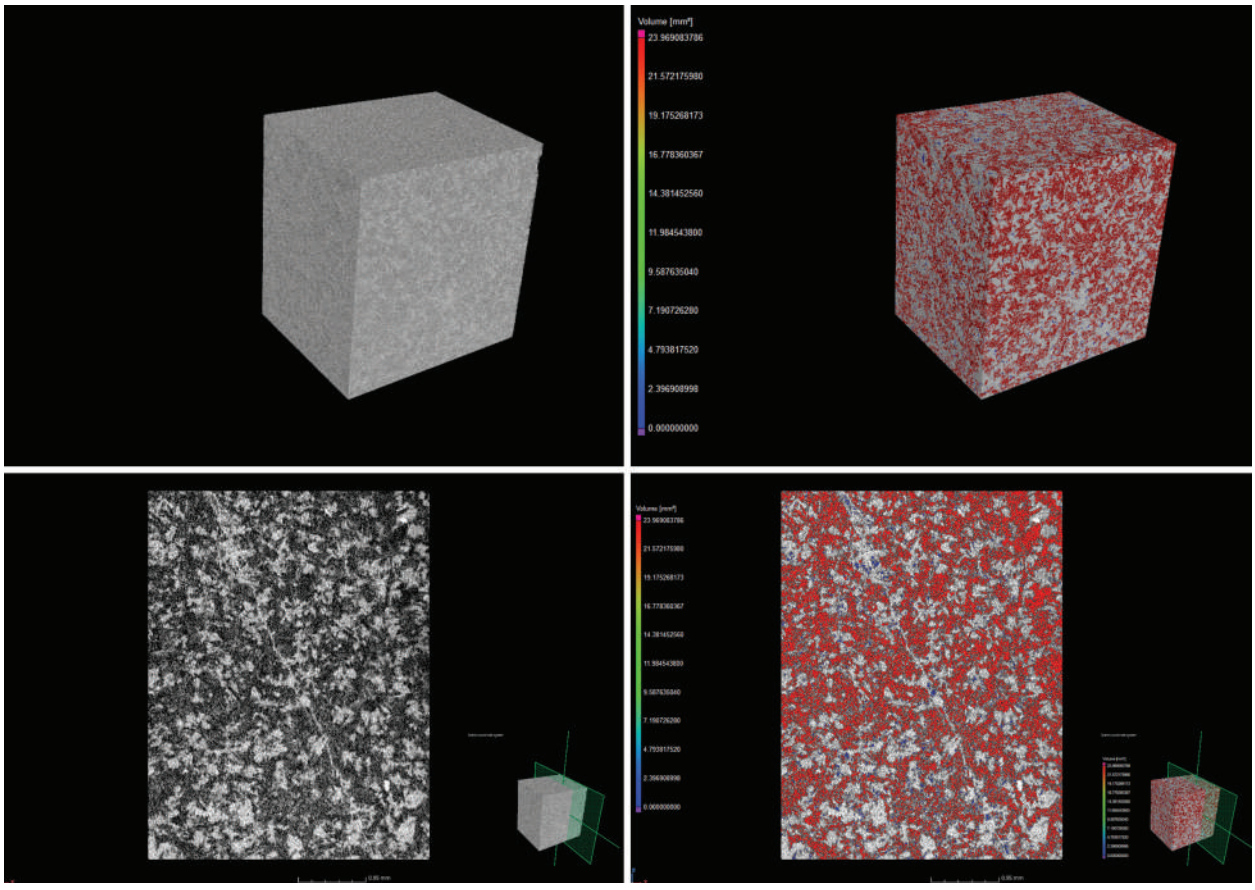

Figure 15. 3D visualisation of micro XCT scanning of a selected sample.

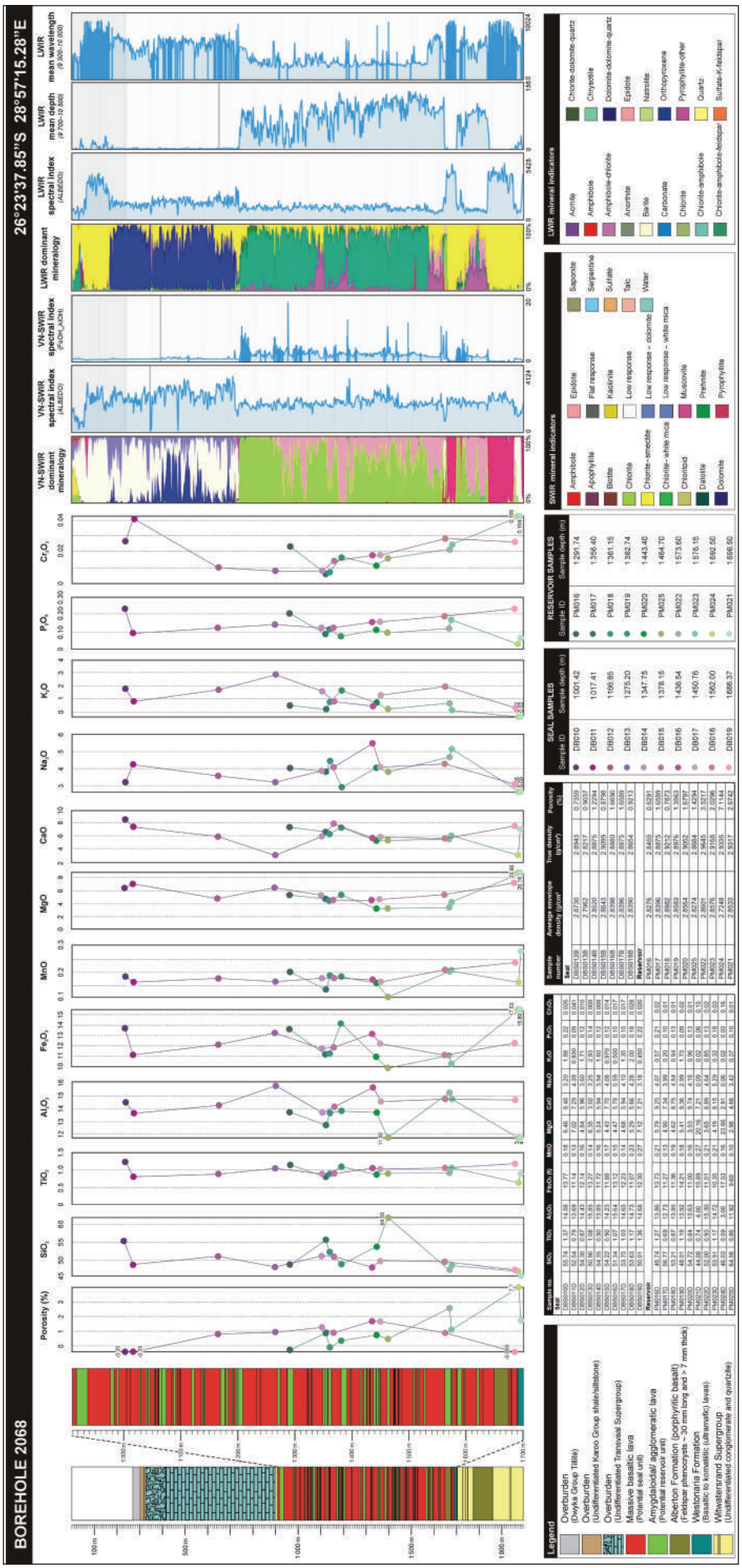

Figure 16. Overview of mineralogy and key reservoir characteristics of selected reactive and non-reactive sequences of the Klipriviersberg Group, obtained from borehole 2068 (Dhansay *et al.*, 2022).

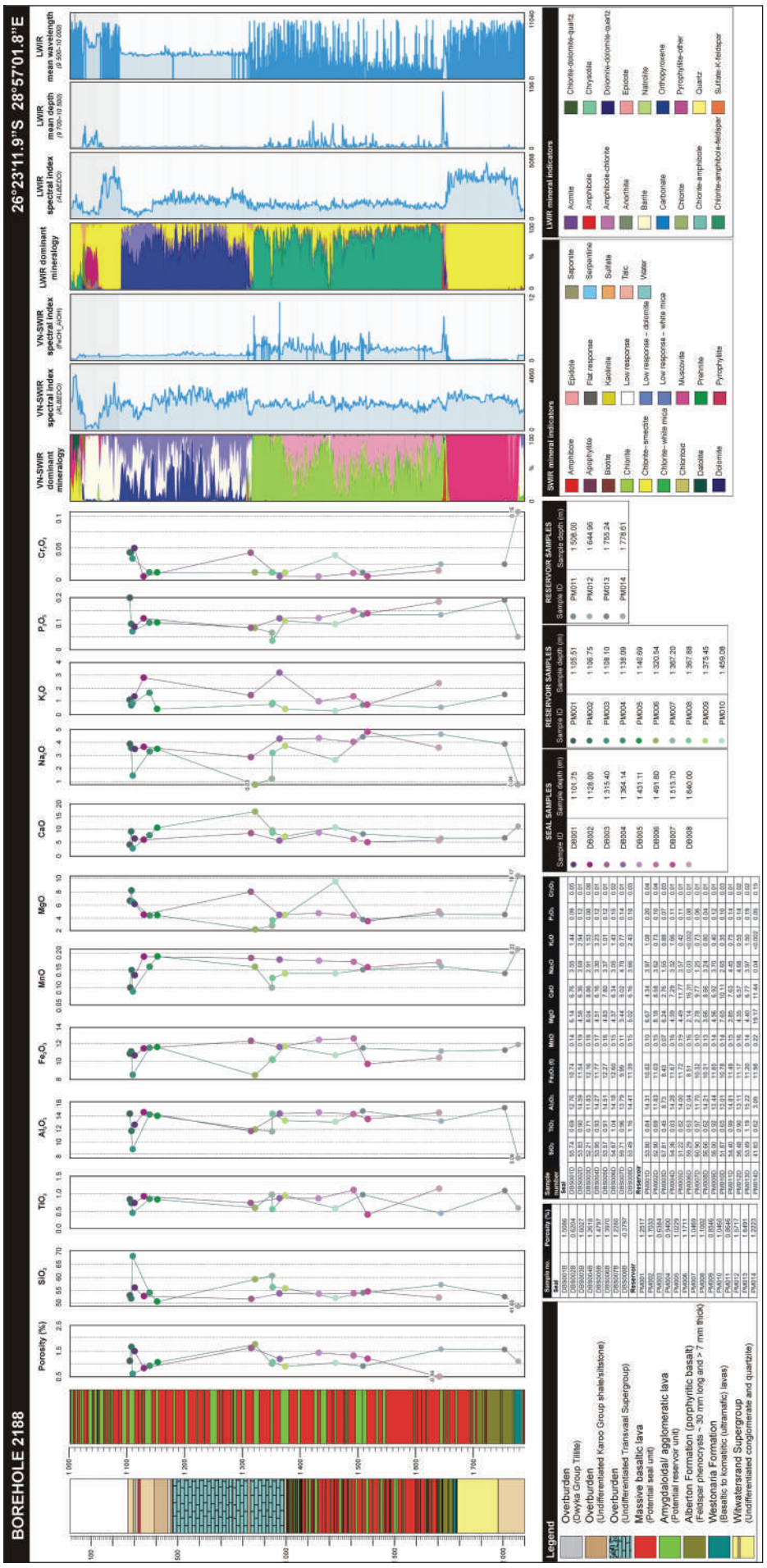

Figure 17. Overview of mineralogy and key reservoir characteristics of selected reactive and non-reactive sequences of the Klipriviersberg Group, obtained from borehole 2188 (Dhansay *et al.*, 2022).

3.2.7 Geochemistry

Geochemical investigations of bulk and trace elements allow for the description and delineation of the evolution of distinct geological sequences. Moreover, this information is crucial to determining how any proposed geological reservoir may react to anthropogenic CO_2. Tables 18 and 19 present whole rock and trace element analyses of selected samples of the Ventersdorp Supergroup. The data presented in these tables was obtained from samples collected during the project and additional sources referenced in the tables. The data is presented in bulk and trace element geochemical discrimination diagrams in Figures 18 and 19, respectively.

Figure 18 highlights various bulk rock geochemical classification diagrams. Figure 18 (A, B, C and D) presents discrimination diagrams after De la Roche *et al.*, 1980, Middlemost, 1994, Pearce, 1996 and Winchester and Floyd, 1977, respectively. These plots suggest that Klipriviersberg Group samples collected from boreholes near the proposed injection site are classified within the andesite-basalt range. These sequences display relatively low concentrations of SiO_2, Zr/Ti, Nb/Y and Zr/TiO_2 ratios. For reference, samples from the Platberg and Pniel Groups that generally highlight more felsic signatures and range from dacite to rhyolite, respectively, are presented. Geodynamic evolution plots (after Pearce, 2008 (Figure 18E) and Hollocher *et al.*, 2012) (Figure 18F) are also presented. These plots suggest that sequences of the Klipriviersberg Group display lower concentrations and ratios of Nb/Yb and La/Yb. The results are correlated with well-known evolutionary models of the Ventersdorp Supergroup and suggest emplacement within a continental arc setting (Crow and Condie, 1988).

Figure 19 displays trace element spider diagrams. These include chondrite normalised rare earth element plots (Figure 19A) and normalised to primitive mantle plots (Figure 19B, C and D). In general, sequences of the Klipriviersberg Group are less enriched than samples from the Platberg and Pniel Groups. The Klipriviersberg Group samples exhibit greater enrichment of light rare earth elements than heavy rare earth elements. Although no significant anomalies are present, some Klipriviersberg Group samples exhibit tantalum enrichment. This enrichment is likely attributable to crustal contamination or the assimilation of a magma that had previously been metasomatised (Gumsley *et al.*, 2020).

3.2.8 Geochronology

Isotope geochronology is an important tool for allowing the detailed subdivision of various geological sequences and the characterisation of key tectono-metamorphic events. Moreover, detailed geochronological information is important in characterising the evolution and emplacement of large igneous provinces, with a view to understanding the temporal constraints of various lava flows that may constitute ideal geological reservoirs for the storage of anthropogenic CO_2. Table 4 presents available geochronology data for selected geological sequences near the proposed injection site. Specific geological sequences and the isotopic techniques employed are also presented. The data suggests that volcanic sequences of the Ventersdorp Supergroup were emplaced between ca 2 729 and 2 714 Ma and that they were defined by alternating cycles of volcanic outpourings, often interspersed with siliciclastic sequences

3.3 GEOPHYSICS

A variety of geophysical applications were used to create a geological characterisation of the subsurface. These applications measure the properties of subsurface geological sequences based on physical properties, such as density, magnetic susceptibility, electrical conductivity

Table 4. Summary of geochronological data for selected sequences around the proposed injection site. Data after Muedi *et al.* (2022) (A); Dankert and Hein (2010) (B); Zeh *et al.* (2020) (C); Poujol and Anhaeusser (2001) (D).

Supergroup	Group	Formation	Age	Technique
Karoo	KLIP	N/A	185 ± 0.25 Ma	U-Pb ID-TIMS[A]
Transvaal	Pretoria	Hekpoort	2 224 ± 21 Ma	Rb-Sr whole rock[B]
	Chuniespoort	Oaktree	2 583 ± 5 Ma	U-Pb SHRIMP[B]
	Black Reef	N/A	2 618 ± 11 Ma	U-Pb LA-ICP-MS[C]
	Wolkberg	N/A	2 769 ± 8 Ma	U-Pb LA-ICP-MS[C]
Ventersdorp	Platberg	Makwassie	2 643 ± 80 Ma	U-Pb ID-TIMS[B]
		Goedgenoeg	2 709 ± 4 Ma	U-Pb SHRIMP[B]
	Klipriviersberg	Alberton	2 714 ± 8 Ma	U-Pb SHRIMP[B]
		VCR	2 729 ± 19 Ma	U-Pb SHRIMP[B]
Witwatersrand	Central Rand	Booysens	2 894 ± 7 Ma	U-Pb SHRIMP[B]
		Blyvooruitzicht	2 902 ± 13 Ma	U-Pb SHRIMP[B]
	West Rand	Crown	2 914 ± 8 Ma	U-Pb SHRIMP[B]
		Rietkuil	2 931 ± 8 Ma	U-Pb SHRIMP[B]
		Promise	2 991 ± 15 Ma	U-Pb SHRIMP[B]
Johannesburg Dome	N/A	N/A	3 340 ± 3 Ma	U-Pb ID-TIMS[D]

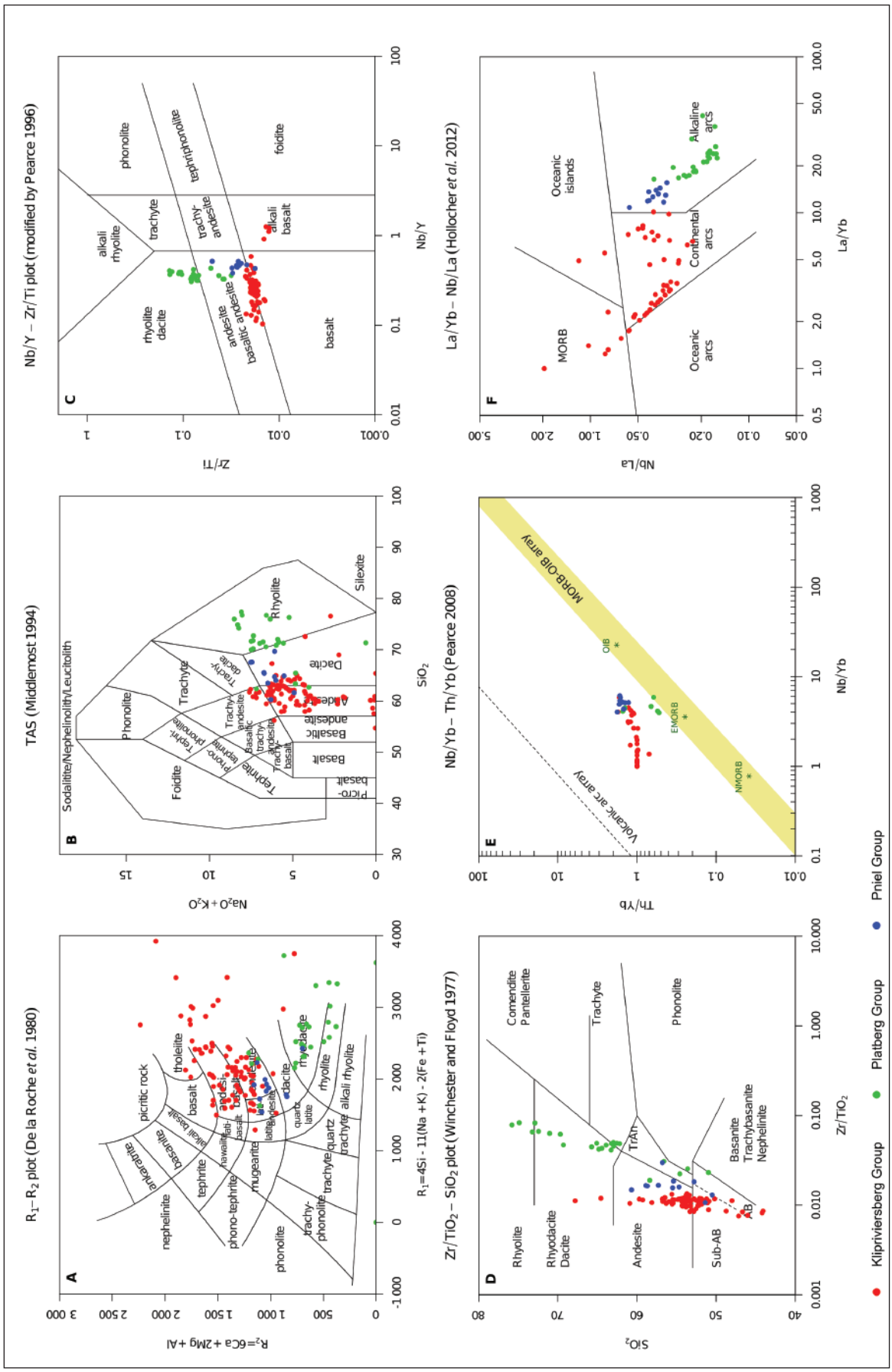

Figure 18. Various geochemical characterisation plots of Ventersdorp Supergroup samples. In particular, the R1-R2 (De la Roche *et al.*, 1980) (A), total alkali-silica (TAS) (Middlemost, 1994) (B), Nb/Y-Zr/Ti (Pearce, 1996) (C), Zr/TiO_2-SiO_2 (Winchester and Floyd, 1977) (D), Nb/Yb-Th/Yb (Pearce, 2008) (E) and Lz/Yb-Nb/La (Hollocher *et al.*, 2012) (F) plots are shown.

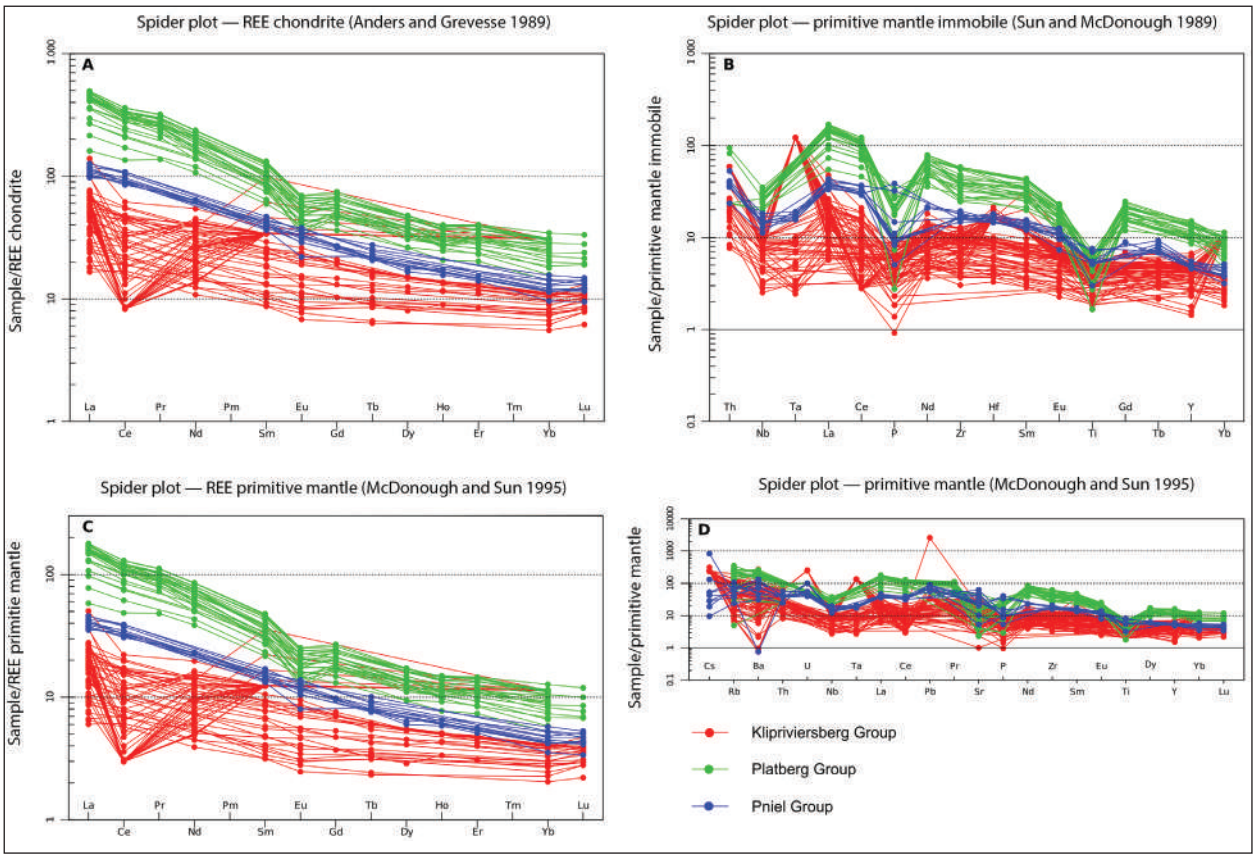

Figure 19. Trace element spider geochemical characterisation plots of Ventersdorp Supergroup samples. These include rare earth element characterisation plots normalised to chondrite (Anders and Grevesse, 1989) (A), primitive mantle (Sun and McDonough, 1989) (B), rare earth element primitive mantle (McDonough and Sun, 1995) (C) and primitive mantle plots (McDonough and Sun, 1995) (D).

and radioactivity. Variations of these physical properties across a particular area may be used to describe various natural processes. This data is used in mineral exploration, groundwater movement delineation, and to understand how the underlying strata may behave during potential anthropogenic processes. Geophysical data was collected using various geophysical systems, including electromagnetics, spectrometry and magnetics. The data was integrated to support the geological characterisation of the subsurface and the area surrounding the proposed injection site. The survey was undertaken with a helicopter-mounted (AS350B3 ZS-RWB) time domain system. Line spacings of 500 and 100 m, a flight direction of 45° and a tie-line flight direction of 135° were used.

3.3.1 Electromagnetic data

Electromagnetic data is used to characterise the surface and subsurface strata by measuring variations in electrical conductivity, or resistivity, of these strata (Palacky, 1993). An electromagnetic field is generated which interacts with the underlying geological sequences. Depending on the characteristics of the geological sequences, secondary electromagnetic responses are generated and measured by a receiver (Telford *et al.*, 1990). Geological sequences that are more conductive will generate a higher electromagnetic response that will be picked up across a larger number of response channels (Kearey *et al.*, 2002). The conductivity of geological sequences is generally influenced by several variables. For example, increased electrical conductivity is associated with increased moisture content, high concentrations of dissolved electrolytes, increased porosity and the presence of certain mineral sequences.

Figure 20 presents several conductivity depth slices generated from 0–200 m below the surface and in the area surrounding the proposed injection site. Regions presented in blue represent sequences with relatively low conductivity signatures, while those in red indicate sequences with relatively higher conductivity signatures. In general, the shallower conductivity slices correspond to specific shallow geological and surface features. These are likely influenced by the surface exposure of the Karoo Supergroup strata and surrounding farming and anthropogenic activities. Moreover, the lower-conductivity areas are likely related to shallow to moderately deep geological features, such as dolerite from the Karoo Large Igneous Province. The intermediate to deeper conductivity depth slices exhibit the onset of distinct geological features including a prominent northwest-trending magnetic lineament. This feature is likely

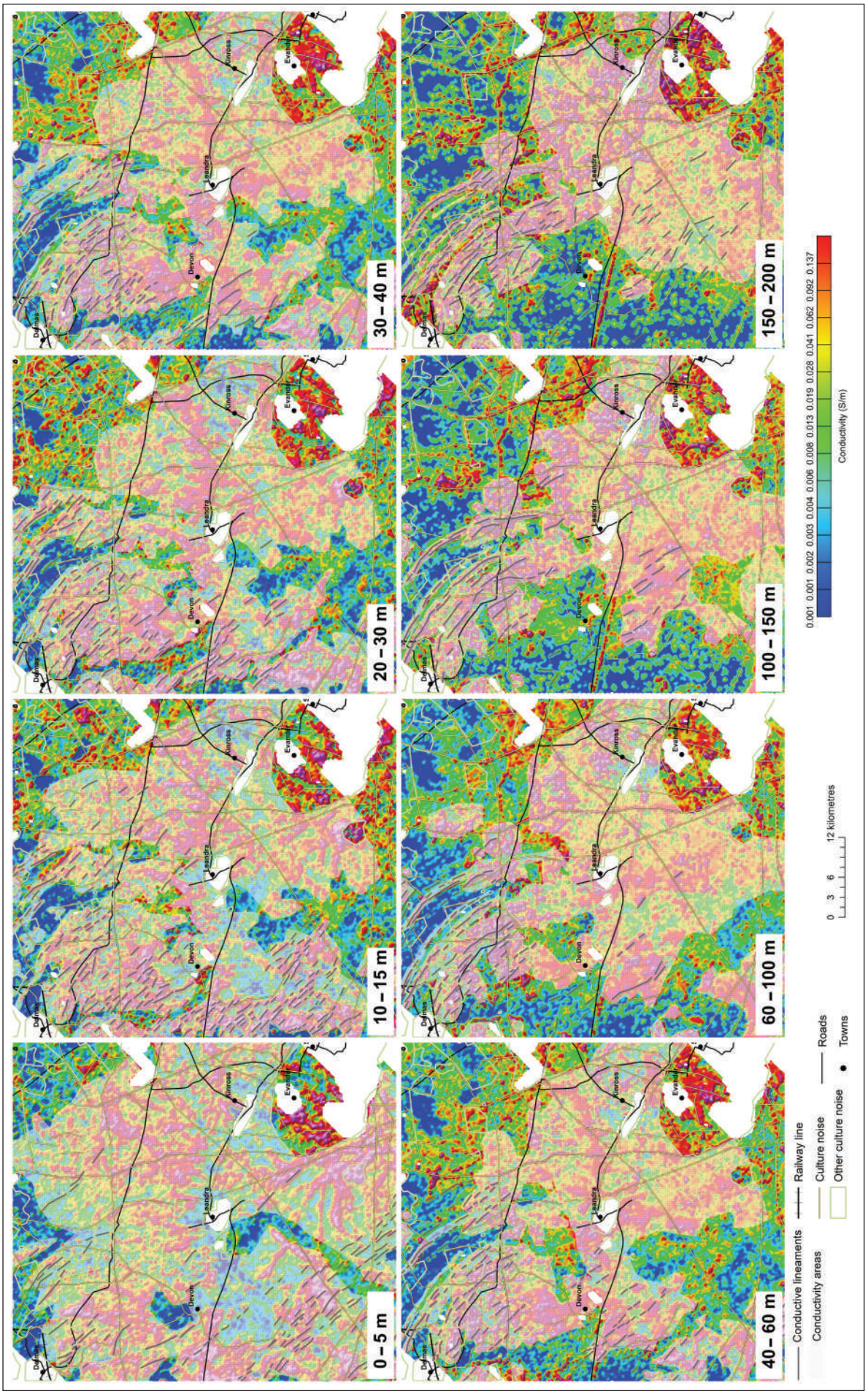

Figure 20. Electromagnetic conductivity response around the proposed injection site for various depth slices (0–200 m).

related to additional intrusive magmatic rocks emplaced along existing basement structures.

3.3.2 Magnetic data

The magnetic method is used to characterise the subsurface and related strata by measuring variations in the earth's magnetic field. The magnetic field is subject to localised variations associated with changes in the magnetic properties of the underlying geological sequences. These properties may include the composition of the geology, containing magnetic minerals such as magnetite. Moreover, changes in the texture and structural variation of the geological sequences can also influence magnetic responses, for example how the textural characteristics affect the orientation and polarisation of magnetic minerals.

Subsurface features with relatively high magnetic signatures are apparent in the vicinity of the proposed injection site. In particular there is an array of northwest-trending features and other distinct linear features. These lineaments likely represent the edges of intrusive bodies and structural features. Figure 21 presents an overview of all the linear features interpreted around the proposed injection site, including their total magnetic intensity signatures. In addition, an overview of known faults, especially those mapped within the Witwatersrand Supergroup basement, is presented.

The magnetic data makes it possible to develop an anticipated 3D subsurface model displaying the expected subsurface aerial extent of the Ventersdorp Supergroup (Figure 22). This model corroborates geological models derived from the available borehole data and suggests that the proposed injection site is predominantly surrounded by the Ventersdorp Supergroup. The model further depicts at least 284 km^3 of Ventersdorp lavas surrounding the proposed injection site.

3.3.3 Radiometric data

The radiometric method is generally used to characterise the topmost geological and surface layer by measuring the radiometric responses of the surface sequences. These responses are generally associated with

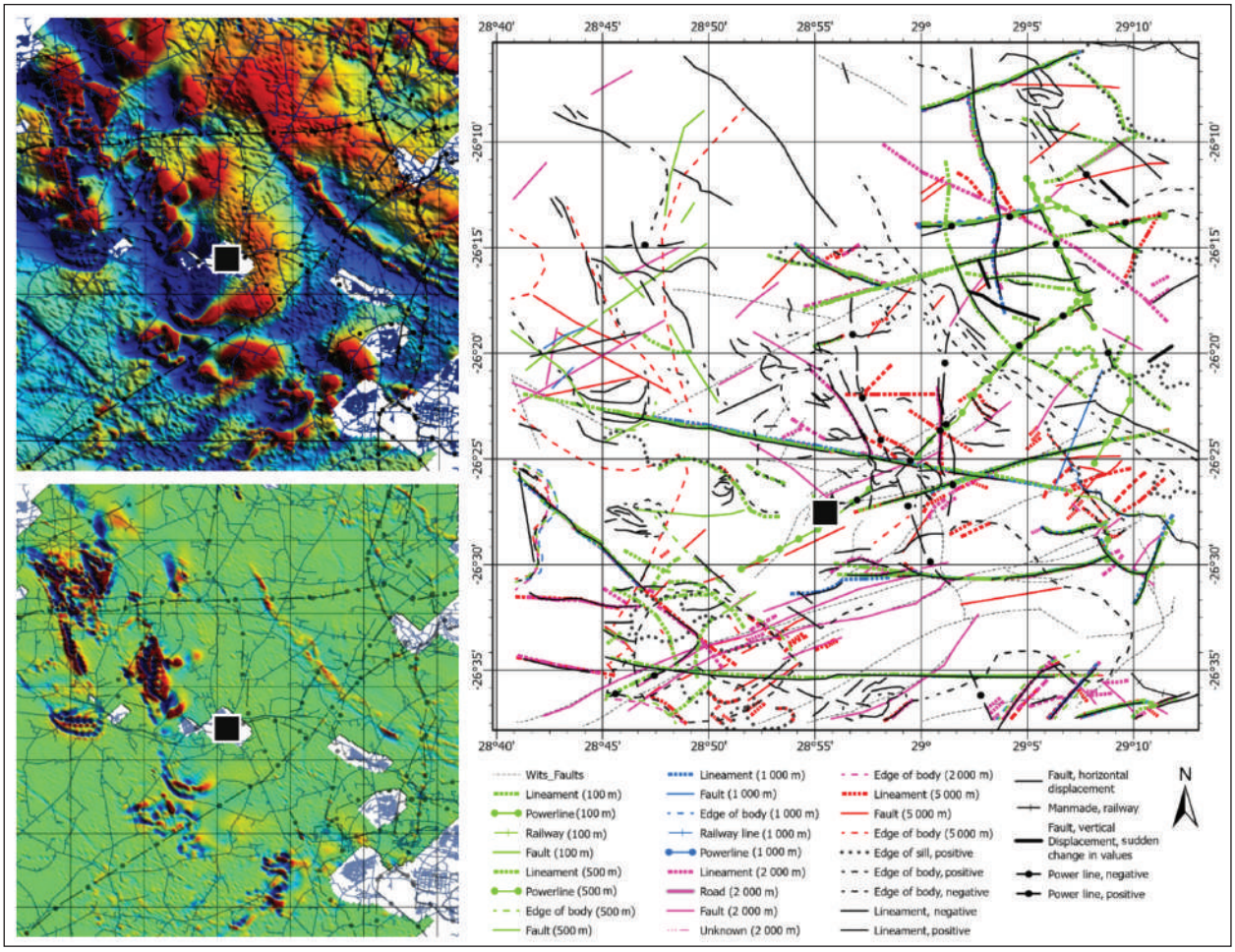

Figure 21. Combination of all inferred lineaments surrounding the proposed injection site (black square). The total magnetic intensity (top left) and the first derivative of the total magnetic intensity (bottom left) are depicted.

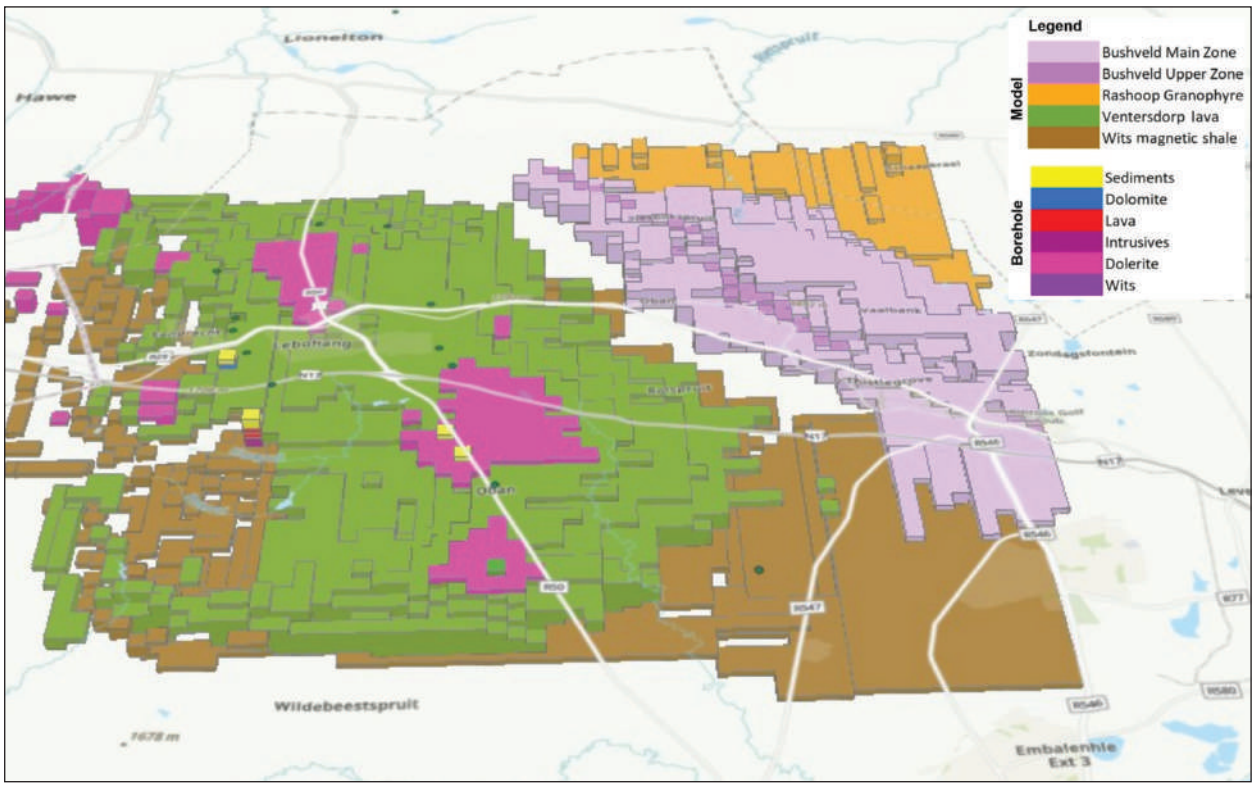

Figure 22. Schematic magnetic model of the area around the proposed injection site.

the surface geology or weathered material from a parent geological sequence. Radiation is measured using a gamma-ray spectrometer, which measures total count radioactivity and potassium-, thorium- and uranium-linked radioactivity.

Figure 23 presents the results of the measurements of radiometric activity in the area surrounding the proposed injection site. In general, the results show relatively higher radiometric readings towards the north and east of Leandra. These signatures may be attributed to possible anthropogenic activities in these areas, for example mining and agriculture causing the reworking of geological sequences that host relatively high abundances of radioactive minerals, as may be expected in the siliciclastic sequences of the Karoo Supergroup.

3.3.4 2D reflection seismic data

Three legacy 2D reflection seismic profile lines are located around the proposed injection site. The seismic lines, collected between 1980 to 1990, particularly targeted the basement Witwatersrand Supergroup. The seismic lines reach a maximum depth of approximately 2 000 km. Figure 24 presents an overview of the available 2D reflection seismic data near the proposed injection site and a schematic interpretation of selected 2D seismic lines. The seismic lines are correlated with selected boreholes and make it possible to characterise the subsurface geology and key structural features associated with the proposed injection site. The seismic lines corroborate the geological model developed from the available borehole data (Figure 7).

3.4 GEOTHERMAL GRADIENT

Understanding the geothermal gradient in and around the proposed injection site is very important. This is because the *in situ* geothermal gradient defines the mechanisms of the proposed working fluids and the anticipated reactivity within the geological reservoir sequences. In general, South Africa is defined by the Kalahari Shield, which consists of several distinctive geological terranes characterising a long-standing tectonic evolution. The shield includes the Kaapvaal Craton, surrounded by several orogenic zones. The Kaapvaal Craton, which encompasses much of the northeast of South Africa, includes a keel extending to approximately 250 km below the surface. This lithospheric mantle keel is defined by ancient highly dense lithologies that deflect most of the convective heat from mantle. Several orogenic belts surround the Kaapvaal Craton. These belts define different phases of tectonic activity, further highlighting various supercontinent cycles. Unlike the Kaapvaal Craton, these orogenic belts are relatively shallow (40 km thick) and are characterised by a higher density of tectonic structures enabling convective heat from the mantle to manifest on the surface. Hot springs and mantle-derived gas signatures are prevalent. The proposed CCUS site near the town of Leandra is located in the Witwatersrand Block

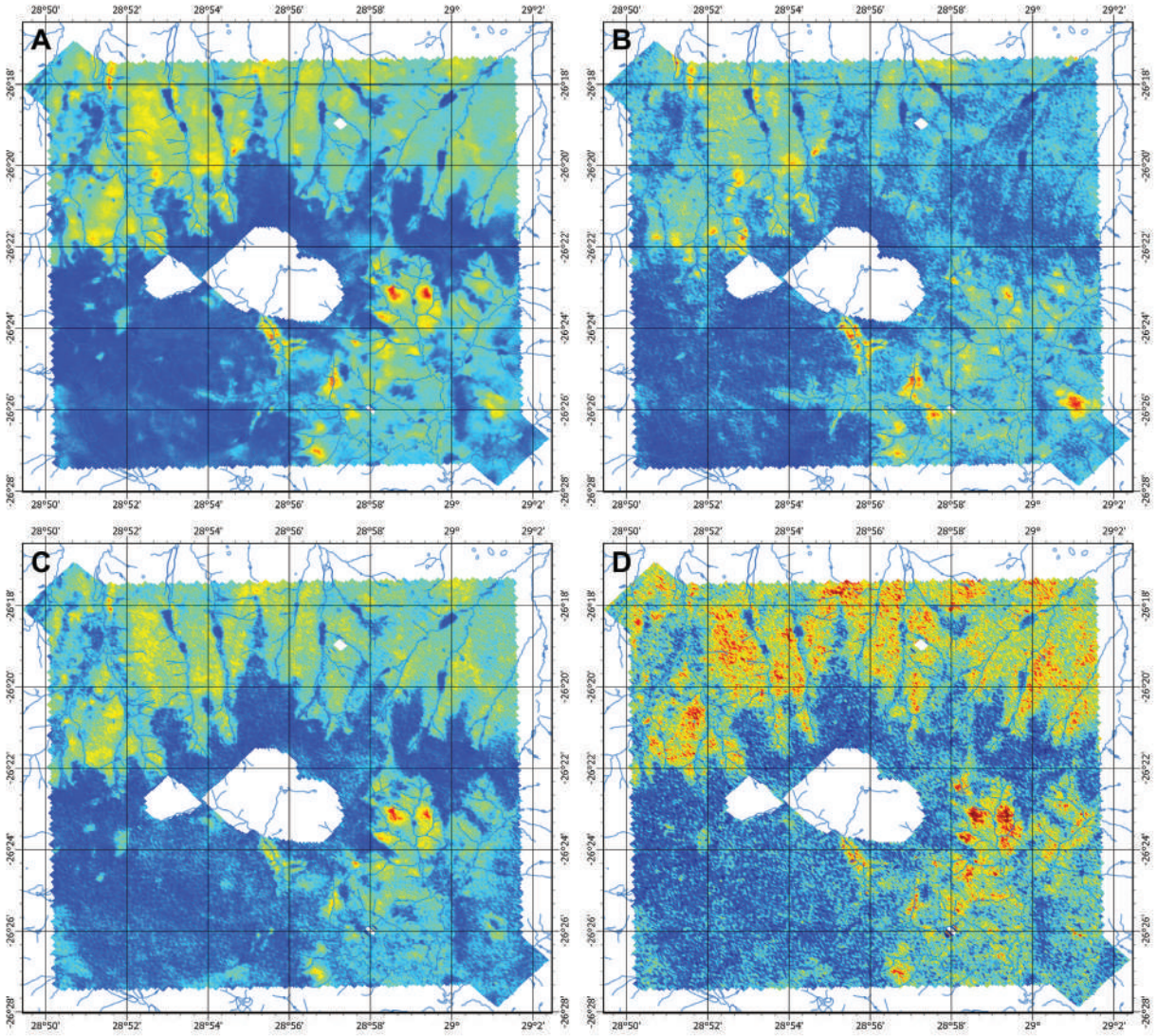

Figure 23. Radiometric ternary images of the area surrounding the proposed injection site. Results show the total count analysed (A), including within the potassium (B), thorium (C) and uranium (D) channels.

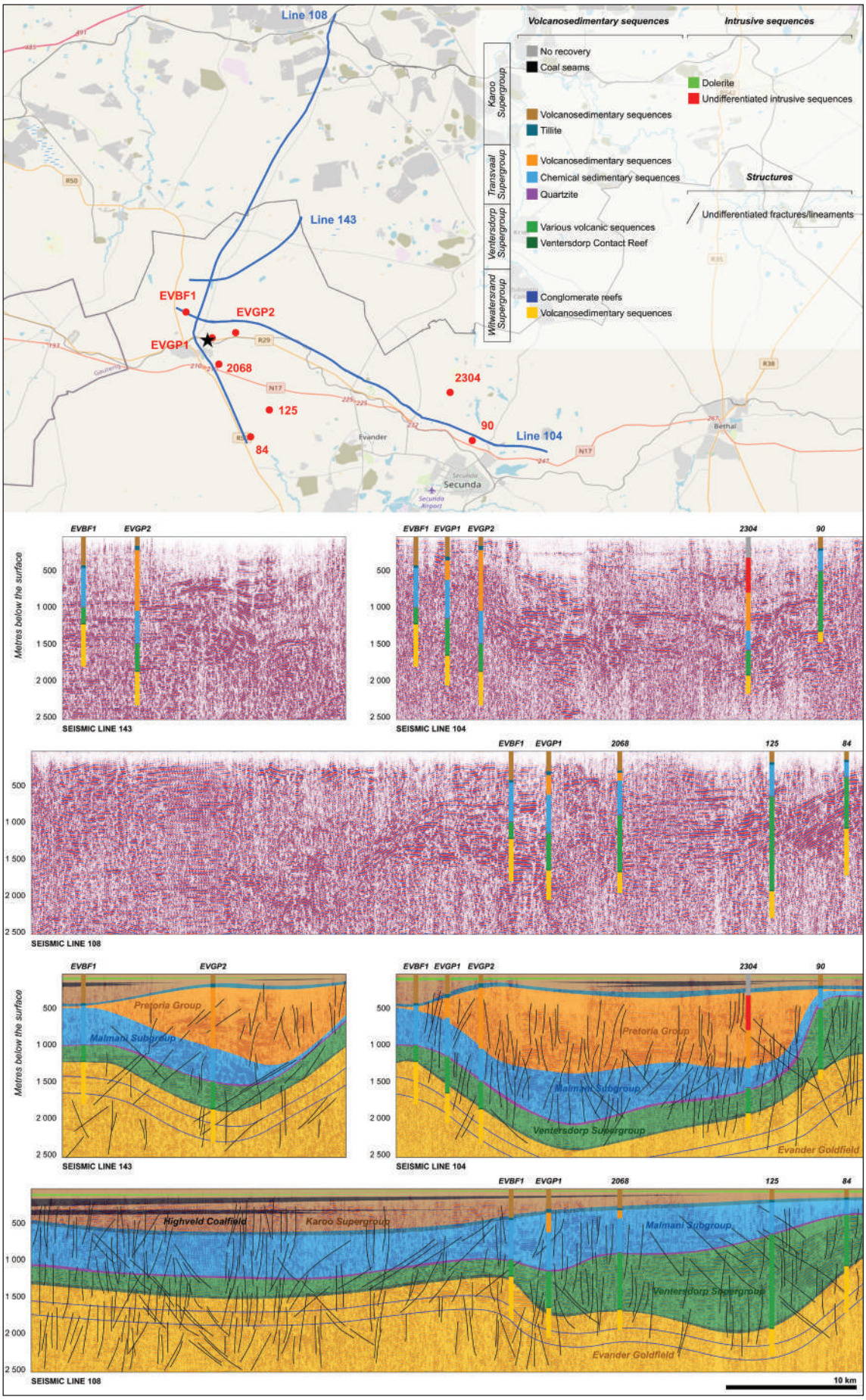

Figure 24. Legacy 2D reflection seismic data surrounding the proposed study area. Schematic geological characterisation supported by available legacy geological borehole information.

of the Kaapvaal Craton near the Makhonjwa Lineament. The lineament separates the Witwatersrand Block from the Eswatini Block. Based on available subsurface temperature measurements (Table 21), collected from deep boreholes and hot springs, the geothermal gradient at the proposed site is approximately 20 °C per kilometre (Figure 25), suggesting possible reservoir temperatures of approximately 30 °C.

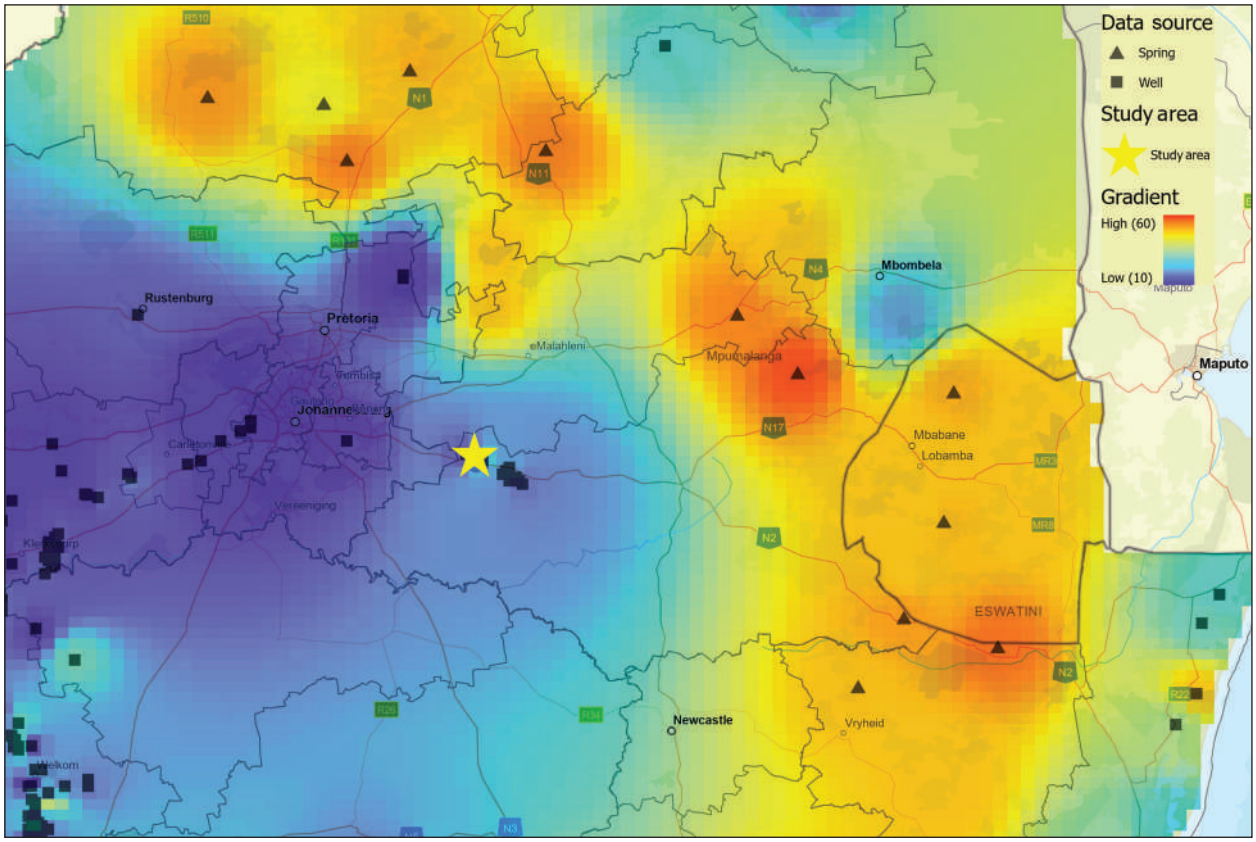

Figure 25. Regional geothermal gradient of the study area and surrounds. Proposed injection site denoted by the yellow star. Geothermal information obtained from from wells (squares) and springs (triangles) is also presented. Data from Dhansay *et al.* (2017).

4. STRUCTURAL GEOLOGY

4.1 STRUCTURAL OVERVIEW

The study area is defined by the lowermost Mesozoic Karoo Supergroup and is relatively flat lying and devoid of significant topographic features that may be linked to recent tectonic activity. However, there is evidence of noteworthy deformation in the underlying geology. The available borehole information suggests that deformation throughout the study area is restricted to brittle deformation with very little to no plastic deformation. The uppermost stratigraphic sequences are relatively flat lying with little to no evidence of folding or significant structural inclination.

Figure 26 presents an overview of the predominant tectonic zones and structural features underlying South

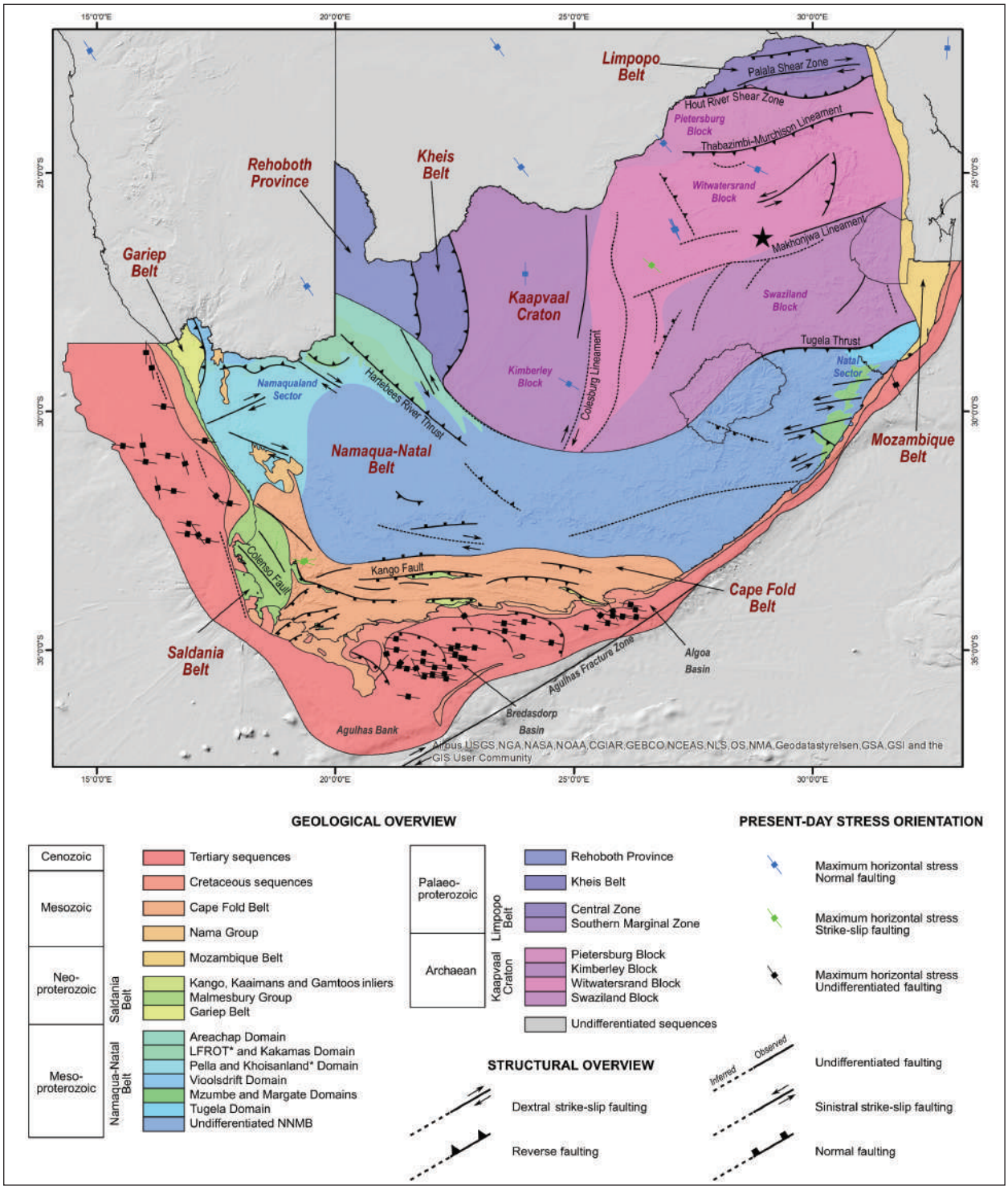

Figure 26. Overview of South Africa's predominant tectonic zones and key structural features. The proposed injection site is represented by a black star. Map after Dhansay (2021).

Africa (Dhansay, 2021). The inherent structural fabric below the study area would have been defined in the Archaean during the amalgamation of the Kaapvaal Craton. The proposed injection site is located near the contact zone between the ca 3.25–3.0 Ga Witwatersrand and ca 3.6–3.1 Ga Eswatini Blocks of the Kaapvaal Craton (Poujol *et al.*, 2003). These blocks would have amalgamated during continental-scale collision not too dissimilar from modern-day tectonic activity. The zone of amalgamation of the Witwatersrand and Eswatini Blocks is defined by the Makhonjwa Lineament. The Makhonjwa Lineament forms an ENE–WSW-oriented tectonic suture zone that displays sinistral transpression movement and extends approximately 500–1 000 km (De Wit *et al.*, 1992; Anhaeusser, 2006; Dhansay, 2021). The geometry of the Makhonjwa Lineament contact zone would have provided the overarching structural fabric apparent in the sequences of the Archaean basement granite-gneiss and the Witwatersrand Supergroup, the lowermost sequences below the proposed injection site.

The Witwatersrand Supergroup displays a predominance of ca ENE–WSW-oriented structures defining discontinuity surfaces. Moreover, these structures appear to have enabled the emplacement of granitoids and younger volcanic sequences. Based on the available geological boreholes and 1:50 000-scale geological mapping, these structures appear as steeply inclined strike-slip faults that often accommodate oblique to normal movement. 2D reflection seismic data further suggests that the structures are limited in their occurrence and that it is possible that they do not extend significantly beyond the Ventersdorp Supergroup. They are also complemented by an array of associated features such as Riedel structures, generally oriented at acute and oblique angles to the predominant fabric. These structures were likely reactivated during the emplacement of the Ventersdorp Supergroup and the deposition of the Transvaal Supergroup. In addition, the Witwatersrand Supergroup may be defined by at least two isoclinal folding orientations, i.e. northwest- and northeast-trending folds (Dankert and Hein, 2010). In general, most of the basement structures do not entirely penetrate the lavas of the Ventersdorp Supergroup and are largely restricted to the lowermost region proximal to the Ventersdorp Contract Reef (Manzi *et al.*, 2013).

4.2 STRESS FIELD

4.2.1 Stress field orientation

Information regarding the *in situ* stress field surrounding the proposed injection site is key to supporting the evaluation of possible permeable migration pathways and ascertaining the likelihood of structural reactivation. Moreover, this information is needed to establish baseline stress conditions, which may provide more information on how additional stress release may be controlled across the proposed injection site. The potential injection of anthropogenic CO_2 will result in changes to the reservoir pore fluid pressure. Any undue migration will follow subtle changes to the *in situ* stress regime. According to the World Stress Map, the proposed injection site is defined by an extension stress regime with a maximum ca northwest–southwest-oriented horizontal stress. Furthermore, the *in situ* stress field is characterised largely by normal faulting and, to a much lesser degree, by strike-slip faulting. The seismic data obtained from the Council for Geoscience's National Seismic Network (Figure 27 and Table 5) corroborates this characterisation. Information from the National Seismic Network suggests that the occurrence of relatively large seismic events is not entirely uncommon in the broader area surrounding the proposed injection site.

The available stress information confirms the occurrence of predominantly normal faulting and, to a lesser extent, of strike-slip earthquakes. Moreover, it also confirms the occurrence of a maximum ca northwest–southeast-oriented horizontal stress. The data also points to the existence of a maximum ca northeast–southwest horizontal stress located south of the proposed injection site

Table 5. Earthquake focal mechanism information used to determine the principal stress orientations around the proposed study site (Midzi *et al.*, 2020; Manzunzu *et al.*, 2021).

No.	Style	Magnitude	Sigma 1		Sigma 2		Sigma 3	
			Azimuth	Plunge	Azimuth	Plunge	Azimuth	Plunge
1	Normal	3.4	329.2	09.7	236.6	15	091	72
2	Normal	5.0	117	04.5	208.9	22.5	016.2	67
3	Normal	4.9	238.8	18.3	332.1	09.9	089.2	69
4	Strike-slip	5.5	136.9	05.1	241	70	045.1	19.3
5	Normal	3.2	154	10.7	056.7	34	259.1	53.9
6	Normal	1.8	221.4	04.8	129.6	20	324.2	69.4
7	Normal	2.1	222.7	16.3	324.5	35	112	50.3

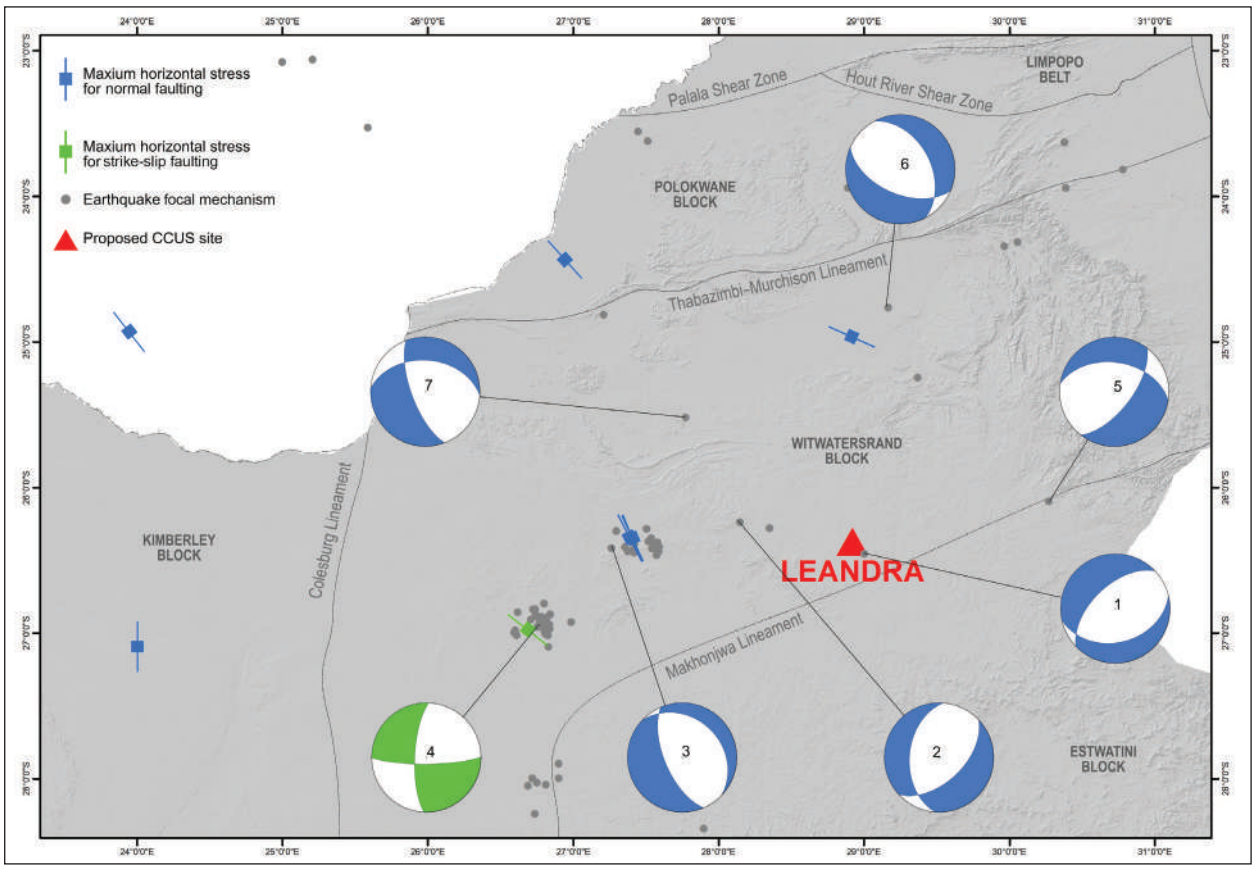

Figure 27. Overview of stress field indicators surrounding the proposed injection site. Stress information derived from the World Stress Map (Heidbach *et al.*, 2019) and earthquake focal mechanisms (Midzi *et al.*, 2020; Manzunzu *et al.*, 2021).

and proximal to the contact zone of the Witwatersrand and Eswatini Cratonic Blocks.

Earthquake moment tensor information for the Leandra site suggests at least three possible localised stress conditions prevailing under two possible faulting regimes — normal and strike-slip faulting (Figure 28).

The available stress information is used to determine the anticipated *in situ* stress fields at the injection site.

These calculations are undertaken by reducing the potential stress axes relative to the predominant observed faulting orientations. The results of these analyses are presented in Table 6.

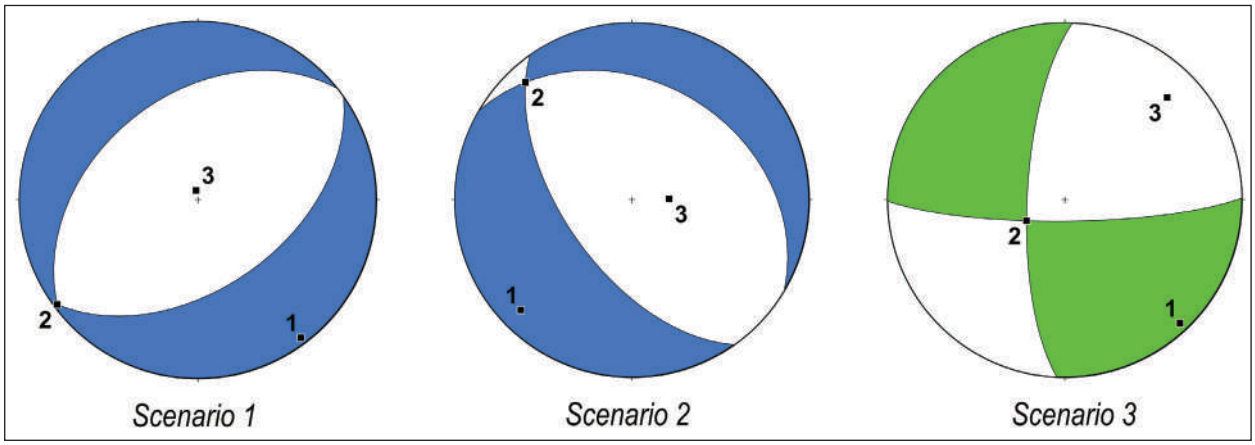

Figure 28. Three possible scenarios for the orientation of *in situ* stresses around the proposed injection site.

Table 6. Detailed *in situ* stress orientation information for the three possible *in situ* stress orientations around the proposed injection site.

Scenario	Style	Sigma 1		Sigma 2		Sigma 3	
		Azimuth	Plunge	Azimuth	Plunge	Azimuth	Plunge
1	Normal	143.2	03.8	233.3	01.9	350	85.7
2	Normal	225.2	12.6	317.8	11.5	088.8	72.8
3	Strike-slip	136.9	05.1	241	70	045.1	19.3

4.2.2 Stress field magnitude

It is very important to determine the amount of *in situ* stresses. Understanding the magnitude of these stresses is needed to design optimal injection mechanisms and to ensure that undue stress release and/or fluid migration is mitigated. *In situ* stress quantification is made possible through experimental work conducted on borehole failures and various rheological studies on a wide range of lithologies (Moos and Zoback, 1990). Importantly, these analyses follow the principle that stress magnitude cannot exceed frictional strength along a pre-existing fracture (Sibson, 1974). *In situ* stress is quantified by means of elastic failure criteria, together with the respective rheological properties particularly to ascertain reservoir depths. In the present case, a depth of 1.5 km is considered, which may be correlated with potential CCUS reservoir depths at the proposed target site. In accordance with the Andersonian stress state of the upper crust, one of the principal stress axes is vertical and perpendicular to the horizontal stresses. The vertical stress corresponds to the lithostatic pressure at reservoir depths and is calculated as follows:

$$Sv = \rho g z$$

Where ρ is the average bulk rock density of the overlying lithologies, g is the gravitational constant and z is the reservoir depth. A value of 2 750 kg/m^3 is considered for the bulk rock density, which takes into account the geology of the upper siliciclastic lithologies, i.e. ca 2 500 kg/m^3, underlain by dolomite, i.e. ca 2 750 kg/m^3 and the lowermost basalt, i.e. 3 000 kg/m^3. The gravitational constant is 9.81 m/s^2 and the reservoir depth is 1.5 km. Pore fluid pressure is taken into account. The pore fluid pressure counteracts normal stress along any plane and may therefore have a bearing on the overall rheological characteristics. The pore fluid pressure at a specific reservoir depth is calculated as follows:

Table 7. *In situ* stress quantities (MPa) for the principal stress orientations at a proposed reservoir depth of 1.5 km.

Style	Sigma 1	Sigma 2	Sigma 3	Pore fluid
Normal	40.47	30.34	20.22	14.72
Strike-slip	57.14	40.47	23.79	14.72

$$f=\rho f g z$$

Where ρf is the density of the pore fluid. At these reservoir depths, it may be assumed that highly saline brines are present and, as a consequence, a pore fluid density of 1 000 kg/m^3 is determined. The maximum and minimum effective stresses are calculated as follows:

$$\frac{1}{\sigma 3 - Pf} = \left(\sqrt{\mu^2 + 1} + \mu\right)^2$$

Where μ represents the coefficient of friction acting on a plane. Here a coefficient of friction of 0.85 is applied (Byerlee, 1978). The *in situ* stress quantification is calculated for an R ratio of 0.5, which is the average mode of deformation between constriction and flattening (Flinn, 1958). Plane strain is a likely mode of deformation present at the proposed CCUS site.

4.2 REACTIVATION POTENTIAL OF PRE-EXISTING STRUCTURES

The relative impermeability of the proposed reservoir can be overcome by artificially increasing its permeability. The calculation of reactivation potential will make it possible to determine which naturally occurring fractures are likely to be reactivated, either through shearing or dilation (Morris *et al.*, 1996). This is an important consideration because the reactivation of pre-existing structures can trigger a number of natural processes such as fluid flow and seismicity. Moreover, the preference of fractures to dilate will increase the likelihood of fracture-trapping mechanisms developing for potential CO_2 storage. These calculations show the relationship between friction and applied normal stress by taking into account frictional reactivation along a pre-existing anisotropic plane. The frictional failure strength of crustal material can be approximated in terms of Byerlee's Law, which expresses normal and shear stress acting on an anisotropic plane as a function of the coefficient of friction (Byerlee, 1978). These are related as follows:

$$\tau=\mu\sigma n$$

Where τ represents shear stress, σn represents normal stress and μ defines the coefficient of friction. The slip tendency is defined by the ratio between the shear and normal stress, expressed as follows:

$$Ts = \frac{\tau}{\sigma n}$$

The dilation tendency is calculated by considering normal and differential stress, expressed as follows:

$$Td = \frac{\sigma 1 - \sigma n}{\sigma 1 - \sigma 3}$$

Figure 29 shows the results of the slip and tendency analyses of CCUS reservoir depths near the proposed CCUS pilot site in Leandra. Under scenarios 1 and 2, moderately inclined ca northeast–southwest and ca northwest–southeast-oriented fractures, respectively, are most likely to undergo reactivation as shear features, while fractures of this same orientation, but that are shallowly inclined, are most likely to undergo reactivation as dilation features. Under scenario 3, steeply inclined ca north–south- and east–west-oriented fractures are most likely to undergo reactivation as shear features, while only steeply inclined ca northwest–southeast-oriented fractures are likely to undergo reactivation as dilation features.

Anticipated basement structures are also considered based on the structures mapped in the Witwatersrand Supergroup (Pretorius *et al.*, 1986). The structures are presented on Mohr's diagrams for normal and strike-slip faulting regimes (Figure 29) to allow for the determination of the structures that are likely to be reactivated under increased pore fluid pressure. The results suggest that the moderately and steeply inclined structures are likely to undergo reaction under increased pore fluid pressures of ca 2–5 MPa above the inherent pore fluid pressure. These structures may form suitable zones under carefully controlled induced pore fluid pressures, where it may be possible to increase reservoir permeability artificially.

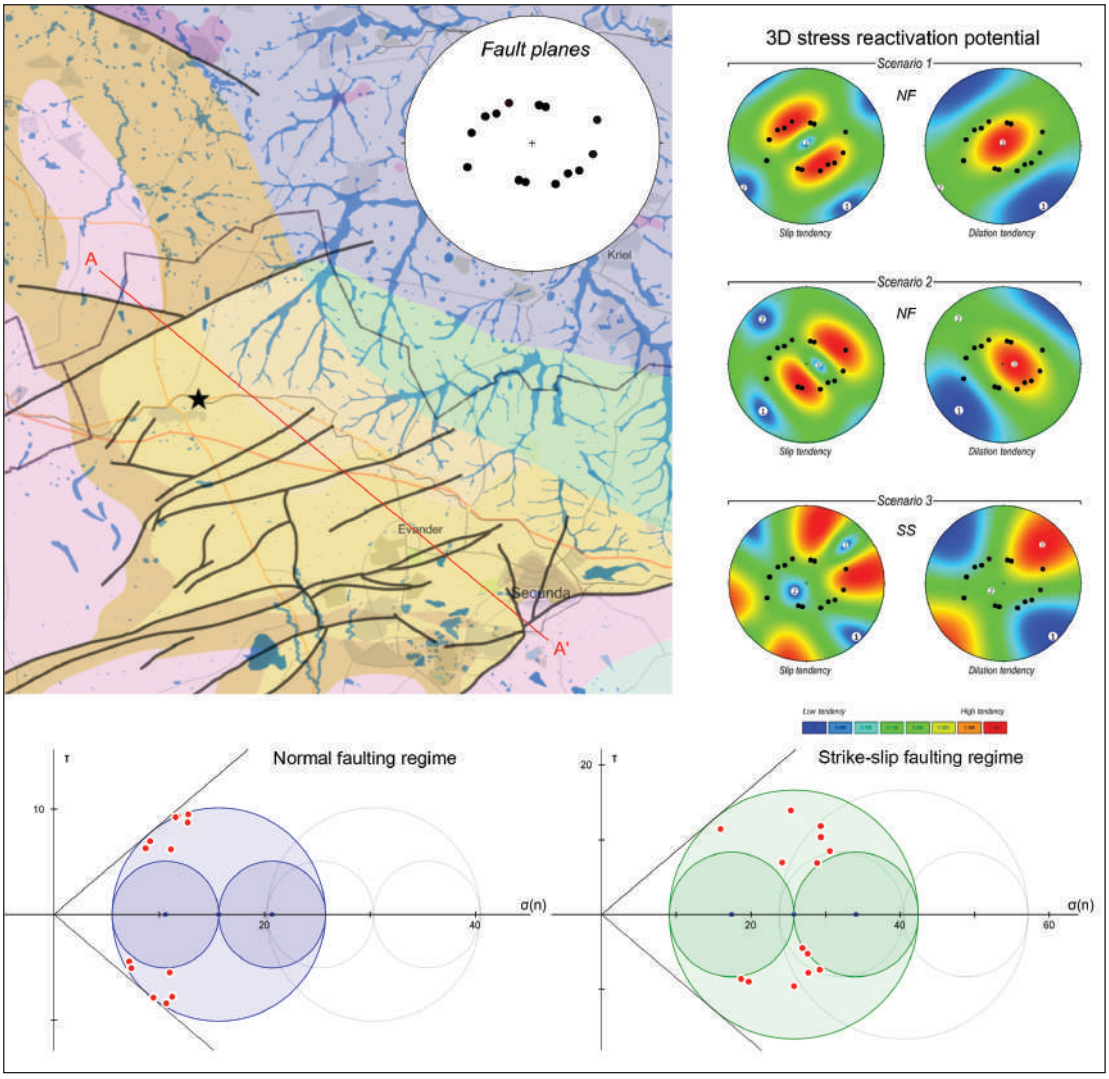

Figure 29. Anticipated basement structures surrounding the proposed injection site (top left). 3D stress plots of the slip and dilation tendency analyses for the three possible stress orientation scenarios at the proposed injection site (top right). Mohr's plots for possible normal and strike-slip faulting, including plots of the anticipated basement structures (bottom).

5. SEISMIC HAZARD ASSESSMENT

The process of injecting anthropogenic CO_2 into a proposed geological reservoir may trigger changes in the pore fluid pressure. Under certain circumstances, these changes will result in induced seismic activity. A probabilistic seismic hazard assessment (PSHA) was therefore conducted around the proposed study site to determine the sensitivity of the area to possible seismic occurrences linked to the proposed injection. In addition, this study was complemented by a deterministic seismic hazard assessment (DSHA) to determine potential seismic impacts to surrounding communities.

The PSHA was undertaken using a multiparameter logic-based approach incorporating several key parameters. Calculations were performed using the OPENQUAKE software (Pagani *et al*., 2014) taking into account surrounding seismic source zone models, ground motion models and the catalogue of seismic events surrounding the proposed injection site. The hazard calculations were undertaken using a return period of 475 years or a 10% probability of exceedance in 50 years. A minimum magnitude of 5 was used in the hazard calculations. Finally, hazard curves for eight periods were calculated, namely PGA; 0.1 s; 0.15 s; 0.2 s; 0.3 s; 0.5 s; 1.0 s; and 2.0 s, as well as hazard maps for three periods (PGA, 0.15 s and 2.0 s).

5.1 EARTHQUAKE CATALOGUE

The probabilistic seismic hazard calculations depend on a reliable catalogue of seismic events. Seismic data used in this study forms part of the Council for Geoscience's South African National Seismograph Network database. The calculations are based on seismic events within a 500 km radius surrounding the proposed injection site. In general, the study area is in an area characterised by a moderately high occurrence of anthropogenic seismicity associated with mining and mineral exploration activities. Recorded seismic events are modified to ensure that they are recorded within the moment magnitude scale, which is the standard scale used to calibrate ground motion predictions (Manzunzu *et al*., 2021). The seismic events are declustered to ensure that only independent events are considered and dependent events, such as aftershocks, are removed and not taken into account for the calculations. Finally, the seismic events are assumed to have a relatively shallow depth range of ca 0 to 15 km. Precise depth range estimates are limited owing to the insufficient number of seismic stations in the region.

5.2 SEISMIC SOURCE ZONES

The identification of seismic sources is a critical part of seismic hazard analysis and involves a range of data types and scientific interpretations. The seismic source model includes all seismic sources deemed capable of contributing to the ground motion hazard in the study area. The model defines the seismogenic potential, location, size and rate of occurrence of future earthquakes. In this study, a model consisting of fifteen area source zones was considered (Midzi *et al*., 2020). Each of the identified seismic sources was then characterised in terms of its earthquake recurrence (relative frequency of occurrence of earthquakes of different magnitudes, as well as the expected maximum magnitude (Mmax) for each seismic source zone) (Table 8).

The characterisation of sources also includes the determination of earthquake depth values. Using the available information on the depths of earthquakes in South Africa, a model was prepared for the identified source zones. Given the limited available information, an alternative set of values for all source zones was used (Table 9). These values cover the range of available depth values and are consistent with typical values observed on the continental crust.

5.3 GROUND MOTION MODELS

Ground motion or attenuation models are used to predict the distribution of expected ground motion during a potential seismic event. These models are generally based on moment magnitude, source to site distance, style of seismic source zone and specific site conditions. The ground motion models aim to predict parameters linked to potential ground motion, i.e. ground shaking intensity that may be linked to seismic wave propagation pathways and local ground and soil conditions. These factors include peak ground acceleration, spectral acceleration, peak ground velocity and peak ground displacement. There are no ground motion models for South Africa, largely because South Africa has relatively moderate seismicity within a relatively low-magnitude range. Furthermore, the geographic distribution of South Africa's regional seismic stations is not sufficiently dense. Although South Africa lacks ground motion models, existing models can be used as a proxy. These models are selected based on similar geological, tectonic and seismicity characteristics. Given the obvious uncertainties in the modelling of ground motion, it is necessary to account for epistemic uncertainty in hazard calculation by selecting more than one attenuation model and assigning weights to individual models. Proxy ground motion models (as observed in Europe and the Middle East (Akkar *et al*., 2014) and for shallow crustal regions (Boore and Atkinson, 2008)), were applied for the purpose of hazard calculations using weights of 0.6 and 0.4, respectively (Table 10). Furthermore, appropriate parameter adjustments were applied to the ground motion models to ensure consistency in respect of the anticipated conditions at the proposed injection site(Table 11) (Bommer *et al*., 2005).

5.4 PSHA CALCULATIONS

The results of the PSHA are presented in two forms, i.e. seismic hazard maps and uniform hazard spectra. The

Table 8. Recurrence parameters applied within the PSHA around the proposed injection site. See Midzi *et al.* (2020) for further information.

Zone	b value	a value	Mmax	Mmax weight
CEDAR	1.06	3.64	5.50	1.00
ERAND	1.27	4.15	5.37	0.65
			5.10	0.35
FWRAND	1.30	4.04	5.10	0.65
			5.50	0.35
KOFFIE	0.74	2.44	6.94	1.00
KOSH	1.23	5.42	6.00	0.70
			6.3	0.30
KVAAL	0.87	4.41	5.77	0.65
			5.5	0.35
LESOTHO	0.86	2.42	5.47	0.65
			6.84	0.35
MDSN	0.81	2.07	6.32	1.0
MOZA	0.94	3.76	7.50	0.35
			7.98	0.65
TUGELA	0.96	2.86	6.23	0.65
			6.50	0.35
WBOTS	1.22	2.22	6.16	0.65
			6.31	0.35
WELKOM	1.30	4.92	6.00	0.65
			6.49	0.35
WRAND	1.35	6.93	5.20	0.70
			5.5	0.30
ZEBED	0.96	2.86	5.48	0.70
			6.10	0.30
ZOET	1.09	2.83	6.80	0.35
			7.07	0.65

Table 9. Earthquake depth estimations used for the seismic source zone considered in and around the study site.

Source	Depth (km)	Weight
Continental tectonic source zone	5	0.2
	10	0.6
	15	0.2
Mining-related sources (e.g. ERAND, CRAND, WRAND, FWRAND, KOSH and WELKOM)	2	0.7
	5	0.3
Mixture of tectonic and mining-related sources (KVAAL)	2	0.3
	5	0.2
	10	0.3
	15	0.2

Table 10. Ground motion models considered for the probabilistic seismic hazard calculations.

Model	Region	Weight	Comments
Akkar *et al.* (2014)	Europe and Middle East	0.6	Active shallow crust. Mostly events of normal faulting used.
Boore and Atkinson (2008)	Global dataset from active shallow crust regions	0.4	Active shallow crust. Data used had a mixture of focal mechanisms.

Table 11. Metrics used in the selected ground motion models.

Equation	Distance metric	Event magnitude	Style of faulting adjustment	Site conditions
Akkar *et al.* (2014)	Closest distance to surface projection of fault rupture (Rjb). No adjustment required.	No adjustment required as Mw is used for events.	Explicit	Explicit (Vs30 value of 760 m/s)
Boore and Atkinson (2008)	Closest distance to surface projection of fault rupture (Rjb). No adjustment required.	No adjustment required as Mw is used for events.	Explicit	Explicit (Vs30 value of 760 m/s)

calculations were conducted for a grid of sites within approximately 20 km around the proposed injection site. Seismic hazard maps were produced for the eight spectral periods. Three periods are presented, i.e. 0 s; 0.15 s; and 2.0 s (Figure 30). The results suggest that the area around the proposed injection site is characterised by a low to moderate seismic hazard with potentially high spectral acceleration. The results suggest a relatively low possible ground motion of approximately 0.089–0.11 g with a predominant period of 0.15 s spectral acceleration.

The PSHA is complemented by a DSHA. Given the possibility that carbon storage at a site may trigger earthquakes, it was also necessary to assess the possible impact of such earthquakes on nearby communities and infrastructure. This assessment was conducted by implementing the DSHA technique. In the present study, an effort was made to assess the possible impact of large earthquakes at the proposed study site on nearby communities. The assessment entailed several key steps, namely the identification of earthquake sources, determining controlling earthquakes for each source, selecting a ground motion relationship and computing the ground motion parameters. The results of the assessment suggest that potentially large earthquakes may result in moderate seismic-related ground motion in nearby towns.

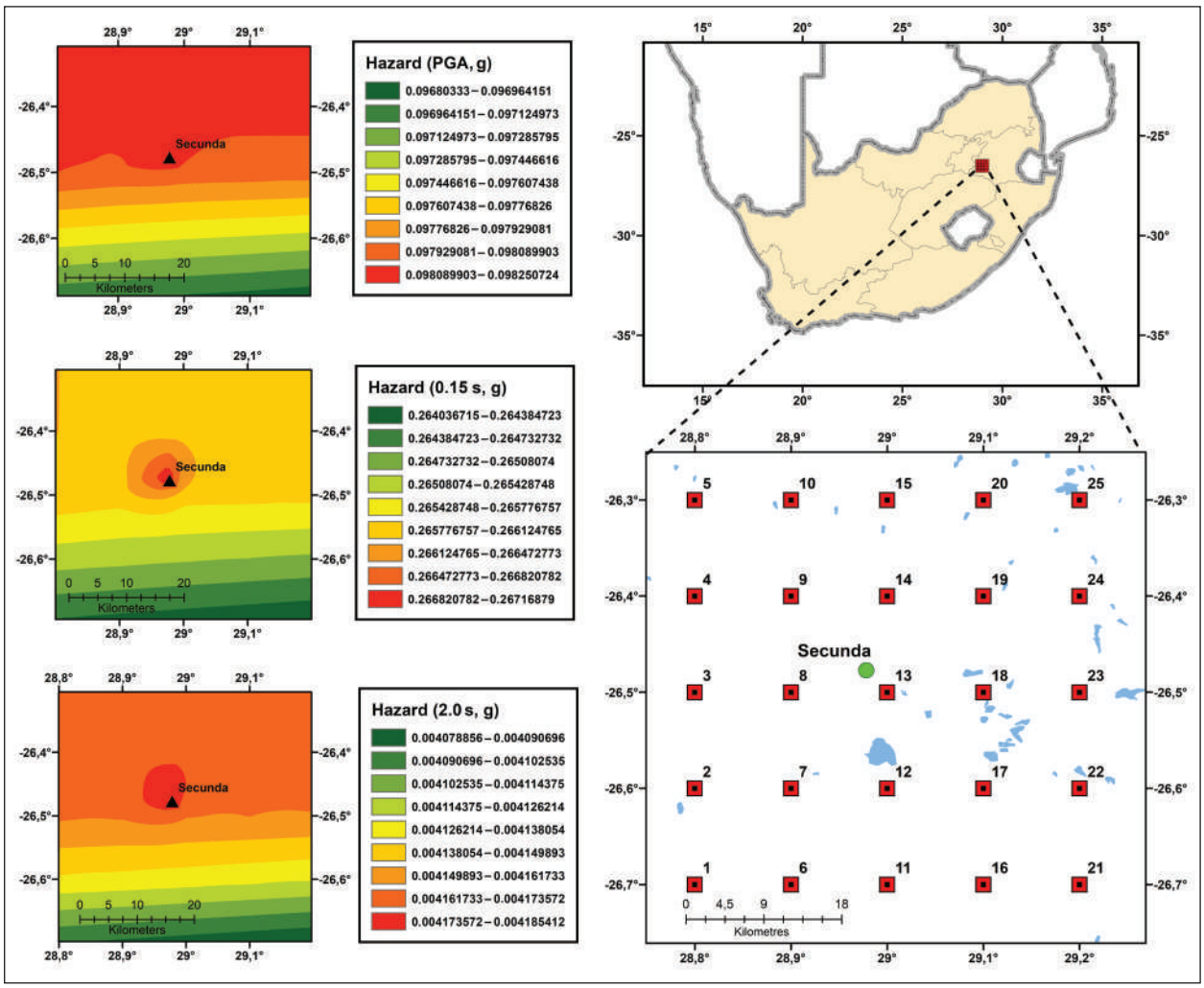

Figure 30. Grid of points where PSHA was conducted around the proposed injection site (right). Seismic hazard maps developed around the proposed injection site near the town of Secunda (left).

6. HYDROGEOLOGY

6.1 HYDROGEOLOGICAL OVERVIEW

The injection of anthropogenic CO_2 into an underground reservoir may result in the undue migration and mixing of groundwater systems, potentially contaminating fresh groundwater resources. Prior assessment of groundwater resources in the vicinity is therefore a pertinent addition to support CCUS technology development. The results of such an investigation will provide crucial information on the characteristics of the underlying groundwater systems and contribute to our understanding of the hydrological baseline conditions.

Therefore, a hydrogeological survey was conducted on various groundwater sources within a 5 km radius of the proposed injection site. The survey included the collection of existing and newly sampled hydrogeological physical and chemical information. The existing information was sourced from the National Groundwater Archive, hosted by South Africa's Department of Water and Sanitation. In total, 80 hydrogeological boreholes surrounding the proposed injection site were verified. Groundwater levels were measured from 62 of these boreholes, while physical and chemical data was collected from 70 boreholes. The remaining 10 boreholes were either dry or inaccessible. Table 22 presents the full dataset that was collected.

The proposed injection site is located near the confluence zone between two Quaternary catchments, i.e. the Olifants River and Vaal River catchments. The correlation between the topography and groundwater is low, at 40%. This shows that the groundwater around the planned injection location may be significantly constrained due to cracks and dolerite dykes and sills.

6.2 AQUIFER TYPES

The project area is surrounded by a combination of intergranular, fractured and karstic aquifers. Intergranular aquifers generally occur within Tertiary and Quaternary deposits and are located along river channels and within the alluvial sediments. Intergranular aquifers generally occur within Tertiary and Quaternary deposits and are located along river channels and within the alluvial sediments. Fractured aquifers are generally encountered within underlying siliciclastic rocks exhibiting a high degree of brittle deformation. These strata include felsic volcanic and other siliciclastic sequences within the Karoo, Transvaal, Ventersdorp and Witwatersrand Supergroups. Intergranular aquifers are generally associated with relatively porous sequences, for example, coarse-grained siliciclastic sequences of the Karoo Supergroup. Karstic aquifers, in turn, are confined to the dolomite sequences of the Malmani Subgroup. These rocks include dolomites, limestones and carbonaceous siliciclastic sequences. Table 12 lists the degrees of groundwater potential anticipated from the various aquifers surrounding the proposed injection site. On average, the different aquifer types are expected to produce between 0.5 and 2.0 litres per second.

Table 12. Anticipated groundwater potential of the various aquifer types surrounding the proposed injection site.

Aquifer	Groundwater potential (litres per second)
Intergranular	0.1 to 1.0
Intergranular and fractured	0.1 to 0.5
Karst	2.0 to 5.0

6.3 GROUNDWATER QUALITY

Determining groundwater quality is essential to the characterisation of the natural baseline conditions surrounding the proposed injection site. Physical, chemical and biological parameters are considered in groundwater quality assessments. Physical properties of groundwater include aspects such as water temperature and clarity. Chemical properties include factors that are affected by the ambient geology, such as pH (acidity or alkalinity), electrical conductivity (EC), mineral content (total dissolved solids —TDS) and total dissolved gas. Biological properties are associated with the presence and concentration of microorganisms living in the groundwater.

In general, the results of groundwater analyses conducted on the boreholes surrounding the proposed injection site are aligned to the recommended standards for drinking water, as prescribed by the South African National Standard (SANS 241:2015). The sampled boreholes display moderate alkalinity (pH 7.6–9.14). The recommended SANS standard for potable water is pH 5–9.7. However, anomalous signatures were recorded in some boreholes. In particular, TDS signatures above 1 200 mg/L were recorded in three boreholes. Several boreholes presented elevated sodium, sulfate, fluoride, chloride, nitrate, arsenic, manganese and uranium.

A Piper diagram (Figure 31) presents the analyses of the groundwater samples around the proposed injection site. The diagram presents a graphical representation of the chemical composition of the sampled groundwater, including the cations (calcium, magnesium, sodium and potassium), anions (bicarbonate, sulfate, chloride and nitrate) and alkalinity. In general, the samples are classified as calcium-magnesium-bicarbonate water. The full hydrochemical datasets are provided in Tables 23–26.

6.4 GROUNDWATER VULNERABILITY

A groundwater aquifer vulnerability assessment was undertaken around the proposed injection site. This assessment aims to establish any likely harm to which the

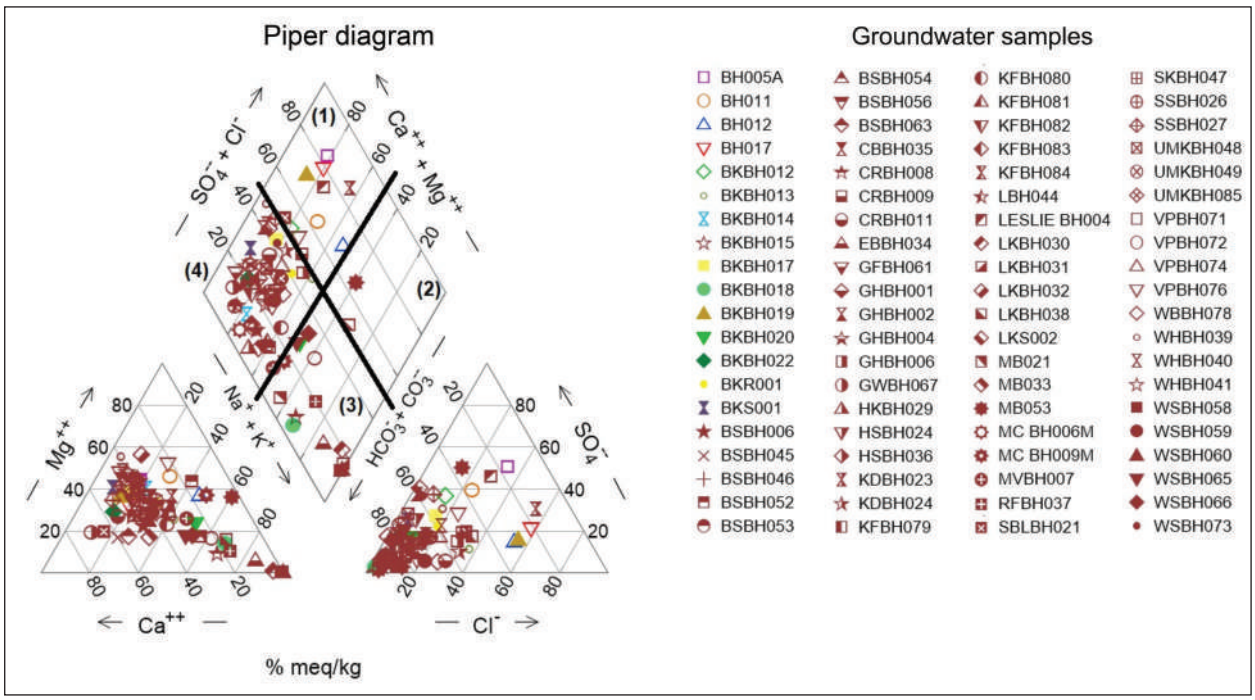

Figure 31. Piper diagram for groundwater analyses conducted on boreholes surrounding the proposed injection site.

underlying groundwater aquifers may be exposed as a consequence of anthropogenic processes (Robins *et al.*, 2007). The assessment takes into account hydraulic connectivity between the underlying groundwater aquifers and the possible penetration of contaminants. Both shallow and deep aquifers can be expected based on the features of the underlying groundwater.

The shallow groundwater aquifers are generally restricted to the overall extent of the weathered zone. The weathered zone surrounding the proposed injection zone is approximately 11 m below the surface. The average soil depth around the site is approximately 3 m below the surface. Although the general elevation of the area does not vary much, the groundwater table in lower-lying areas is generally recorded at approximately 1.2 m below the surface, while the groundwater table in the higher-lying areas lies at a depth of 3.7 m. The average groundwater table is recorded at a depth of approximately 4.5 m in the weathered aquifers around the site. These aquifers are mainly recharged from rainwater infiltrating through the soil horizon.

The total recharge of the groundwater aquifers around the proposed injection site depends on several factors. These include the total precipitation relative to loss associated with runoff, evaporation and transpiration. Other factors include the type of soil horizon, the permeability of the surface layers and topographic features. On average, the recharge rate of groundwater aquifers in the Karoo varies from 2–5% of the mean annual precipitation. Considering the presence of wetlands, soil horizons and the ambient geology, a total average recharge of approximately 3% is assumed. Conditions linked to controlling aspects, such as variable thicknesses and the degree of permeability, result in localised variability.

6.5 REGIONAL GROUNDWATER POTENTIAL MODELLING

The available and collected datasets were used to model groundwater potential around the proposed injection site (Table 13). Modelling is an important application because it enhances the hydrogeological baseline evaluation and assists in forecasting groundwater system flow and concentration. The 500 m line spacing aerial electromagnetic and magnetic surveys, the hydrogeology, the geology and various remotely sensed satellite datasets were all used to create the regional groundwater potential model (Tessema *et al.*, 2014). This data allowed for the development of key input parameters, including geology, lineaments, physical groundwater parameters and regional topographic conditions. These parameters were used to develop a composite thematic map (Ebadi *et al.*, 2004). The groundwater potential modelling process flow is depicted in Figure 32.

The geological input parameters were determined from the existing 1:250 000-scale geological data of the area around the proposed injection site. Lithologies were reclassified based on their perceived importance to groundwater occurrence. They were ranked according to the porosity and permeability of various sequences. Sequences with higher relative porosities and

Table 13. Reclassified lithologies and associated ranks used for the groundwater potential modelling.

Reclassified lithology	Rank
Alluvium	10
Dolomite, subordinate chert, minor carbonaceous shale, limestone and quartzite	9
Network of dolerite sills, sheets and dykes, mainly intrusive into the Karoo Supergroup	6
Fine- to coarse-grained sandstone, shale, coal seams	7
Dolomite, subordinate chert, minor carbonaceous shale, limestone and quartzite	9
Massive porphyritic rhyolite, pyroclastic rocks	6
Diabase	6
Granite	3
Diamictite (polymictic clasts, set in a poorly sorted, fine-grained matrix) with varved shale, mudstone with dropstones and fluvioglacial gravel, common in the north	2
Mudrock, quartzite, minor diamictite	2
Chert	9
Andesitic lava, subordinate pyroclastic rocks, minor quartzite, shale and conglomerate	6
Quartzite with minor shale and siltstone	2
Quartzite (ferruginous in places), wacke, siltstone, shale, magnetic ironstone	2
Undifferentiated granite and gneiss	3
Tholeiitic basalt	6
Water	1
Subequal shale and quartzite, minor conglomerate	2
Lava (mainly andesite and quartz porphyry), shale, quartzite, conglomerate	3

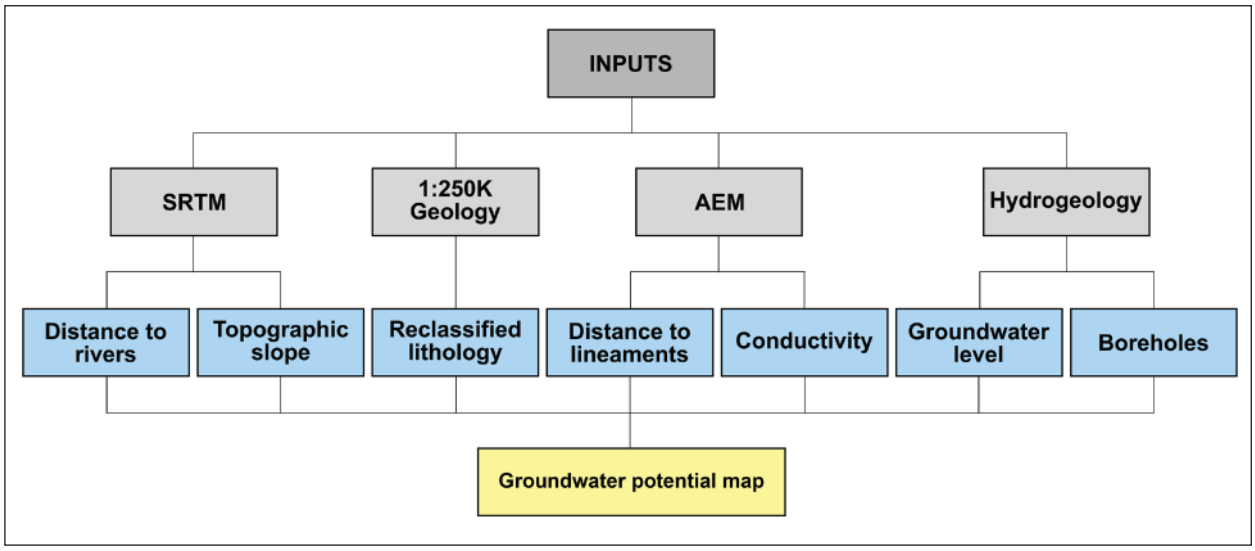

Figure 32. Generalised groundwater potential modelling process map.

permeability were assigned higher ranks (Vaessen and Brentführer, 2015). The ranking was complemented by conductivity information. For example, the majority of semi-unconsolidated sediments would typically allow the most groundwater infiltration.

The topographic slope was another key input parameter. The slope of the target area was derived from available 30 m shuttle radar topographic mission (SRTM) digital elevation model (DEM) data. The surrounding groundwater level, as derived from available boreholes, was also taken into account. The derived slope and information for rivers and the key catchment areas were used to estimate drainage. This information was further complemented by lineament data. The lineament data was extracted from existing geological information and, particularly, from airborne magnetic data. Lineament data provides information about brittle features that will increase the permeability of the area around the proposed injection site (Adams *et al.*, 2004).

The various derived layers were integrated using a knowledge-driven approach (index and overlay), defined

by the various ranks and weights assigned to features in the surrounding area. The following weights were assigned according to the model: geology (6), slope (5), conductivity (4), drainage (4), groundwater level (3) and proximity to lineaments (4). Figure 33 presents the results of the groundwater potential modelling. In general, the highest potential zones are closely related to the natural drainage patterns observed throughout the area. The modelled results suggest that the intergranular aquifers have the highest groundwater potential in the area around the proposed injection site. Moreover, some of the linear features may be linked to underlying fractured lithologies, which are likely to contribute to fractured groundwater potential.

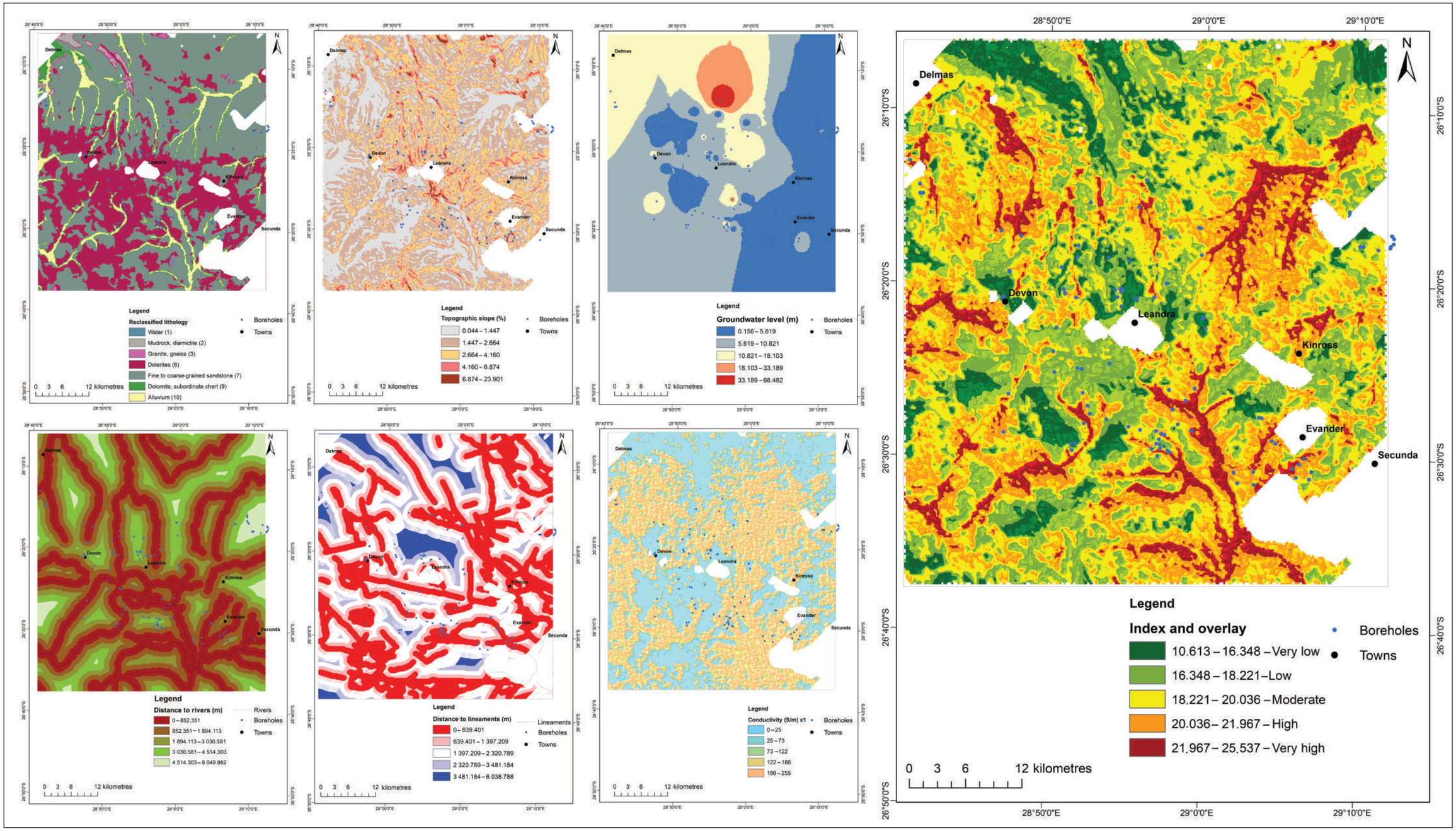

Figure 33. Regional groundwater potential map derived for the area surrounding the proposed injection site (G). Also shown are the various thematic input layers for reclassified lithology (A), topographic slope (B), groundwater level (C), distance to rivers (D), distance to lineaments (E) and conductivity (F).

7. DISCUSSION

7.1 GEOGRAPHICAL CHARACTERISTICS

The proposed injection site is located near the town of Leandra in the Govan Mbeki Municipality, which is part of the larger Gert Sibande District in Mpumalanga Province. The unemployment rate is approximately 25% in the municipality, with at least 50–60% of the population living below the poverty line (Govan Mbeki Municipality, 2022). The region is heavily reliant on coal and its associated downstream industries including numerous coal mines and coal-energy generation and petrochemical industries. The reliance of the community on coal has resulted in negative environmental impacts, for example atmospheric and groundwater pollution. Notwithstanding these drawbacks, these industries are key drivers of municipal and district development programmes. Govan Mbeki Municipality is demarcated as an innovation hub for the development of the petrochemical industry. Accordingly, there is a strong focus on accelerating the development of the large surrounding coal reserves and growing petrochemical industries. The success or failure of South Africa's Just Transition will depend on the country's ability to strike a balance between this planned development of the hydrocarbon sector and achieving the predicted reduction in carbon emissions.

7.2 GEOLOGICAL CHARACTERISTICS

Geologically, the proposed injection site overlies the convergence of three distinct volcanosedimentary basins and their associated sequences. These are the Karoo Supergroup (ca 0–300 m), the Transvaal Supergroup (ca 300–1 100 m), the Ventersdorp Supergroup (ca 1 100–1 600 m) and the Witwatersrand Supergroup (Dhansay *et al.*, 2022). The depth ranges of these sequences are defined by available borehole information, 2D reflection seismic data and aerial electromagnetic information. The Karoo Supergroup is predominantly characterised by carbonaceous shale and coal seams of the Ecca Group and underlying glacial diamictite of the Dwyka Group (Johnson *et al.*, 1996). These, and the underlying sequences, are also intersected by an array of dykes and sills of the Karoo Large Igneous Province. The Transvaal Supergroup underlies the Karoo Supergroup and is predominantly defined by the largely siliciclastic sequences of the Pretoria Group and underlying chemical sedimentary rocks of the Chuniespoort Group. The Ventersdorp Supergroup underlies the Transvaal Supergroup. These are the target sequences and the horizons are generally restricted to the lowermost portion of the Ventersdorp Supergroup including the massive, porphyritic and amygdaloidal lavas of the Klipriviersberg Group (Gumsley *et al.*, 2020; Dhansay *et al.*, 2022). Finally, the Witwatersrand Supergroup, defined by highly fractured quartzite and intercalated conglomerate sequences, underlies the Ventersdorp Supergroup. Archaean basement granite-gneiss of the Devon Dome is also present toward the northernmost extremity of the study area. The presence of approximately 500 m of Ventersdorp Supergroup lavas suggests that the geology of the planned injection location is suitable for the storage of anthropogenic CO_2.

Structurally, the proposed injection site is defined by geological structures linked to the tectonic evolution of the northeastern portion of the Kaapvaal Craton defined by the Archaean amalgamation of the Witwatersrand and Eswatini Cratonic Blocks along the Makhonjwa Lineament (Dhansay, 2021). The lineament demarcates a significant tectonic boundary that would have controlled the development of much of the regional structural fabric and would have undergone several reactivation phases linked to regional tectonic processes. Structural reactivation would have taken place during the emplacement of the Ventersdorp and Transvaal Supergroups. In general, there are very few observed structural features surrounding the proposed injection site. The largest structural complexity is mostly restricted to the Witwatersrand Supergroup. The structures are characterised by isoclinal folding and a high degree of fracture development. In general, these features diminish towards the shallower sequences. Borehole and 2D reflection seismic data suggests that the Ventersdorp Supergroup is generally devoid of folding although it features an array of subvertical and shallow fractures. These fractures are generally filled, but occasionally present evidence of reactivation. The limited structural complexity of the injection site area suggests that it is well suited to the storage of anthropogenic CO_2. The limited occurrence of structural features suggests that the possibility of undue fluid migration is mitigated. Moreover, the highly fractured underlying Witwatersrand Supergroup quartzite presents an additional deep saline storage reservoir, significantly increasing South Africa's overall storage prospects.

7.3 MINERAL REACTIVITY POTENTIAL

Mineralogy and petrography analyses of the proposed Klipriviersberg Group storage reservoir suggest that these sequences possess an abundance of potentially reactive minerals, such as plagioclase and orthopyroxene. These silicate minerals typically appear as large phenocrysts, but they can also be found in the fine-grained matrix. Texturally, the target horizons comprise porphyritic and amygdaloidal lavas. The porphyries are generally defined by plagioclase, while the amygdales are largely filled with quartz. Alteration phases include chlorite, epidote, calcite and dolomite. Alteration is limited in the upper portions of the sequence and increases significantly towards the base of the Klipriviersberg Group. The increase in alteration is likely linked to the occurrence of the basal Ventersdorp Contact Reef. This horizon constitutes a major permeable horizon, which would

have enabled significant fluid flow and accelerated alteration. The availability of reactive minerals and the relatively low alteration suggest that the proposed target horizon is suitable for the storage of anthropogenic CO_2.

7.4 POROSITY AND PERMEABILITY

Porosity and permeability analyses were conducted on approximately 50 samples collected across the proposed injection zone. Porosity analyses included water and mercury intrusion porosimetry and helium expansion pycometry. Permeability analyses were undertaken using the Hoek cell methodology. In addition, XCT was undertaken to establish the porosity and permeability on a microscale. In general, the intrusive porosity analyses suggest that the target horizon is relatively nonporous. Helium expansion pycrometry estimates a porosity range of approximately 1–5%. The Hoek cell analyses further indicate that the target horizons are impermeable under pressures of at least 3 500 kpa. The XCT analyses suggest that, to the extent that the target horizon is porous and permeable, these attributes are restricted to the microscale. In general, results confirm that the target horizon has low porosity and is relatively impermeable. This presents a significant technical challenge and will require the permeability of the horizon to be artificially increased, for example by inducing fracture reactivation.

Fracture reactivation modelling was undertaken to investigate the possibility of enhancing the permeability of the proposed reservoir. The modelling included a 3D stress determination and the development of Mohr's diagrams. These models suggested an *in situ* stress field largely defined by the Makhonjwa Lineament region of the northeastern Kaapvaal Craton. This presumed stress field is defined by normal faulting and/or strike-slip faulting. These findings are corroborated by borehole logging, which confirms the occurrence of normal and strike-slip faulting across the area. The fracture reactivation modelling suggests that pre-existing ca ENE-WSW-oriented fractures are likely to undergo reactivation as normal faults at pore fluid pressures of approximately 1–5 MPa above the *in situ* pore fluid pressure. A PSHA suggests that the region is relatively tectonically stable, although activities linked to artificially increasing permeability may induce seismic events. Therefore, any possible anthropogenic CO_2 storage within this region must be accompanied by a high-resolution seismic monitoring system.

7.5 HYDROGEOLOGICAL CHARACTERISTICS

The hydrogeology characterising the proposed injection site is defined by at least three different groundwater aquifer types. These are relatively shallow intergranular aquifers and fractured and karstic aquifers, at intermediate depths. The intergranular aquifers are generally restricted to the overlying Cenozoic sequences. The fractured and karstic aquifers are generally located in the fractured sequences of the Karoo Supergroup and the underlying dolomites of the Chuniespoort Group, respectively. Deep fractured aquifers are expected, particularly within the lowermost Witwatersrand Supergroup. A hydrogeological census, including an assessment of the physical and chemical parameters of the surrounding groundwater sources, suggests that the region is defined by calcium-magnesium-bicarbonate groundwaters. Moreover, the groundwater quality surrounding the proposed injection site falls within an acceptable range. Several anomalous groundwater signatures have been identified for high TDS and elevated sodium, sulfate, fluoride, chloride, nitrate, arsenic, manganese and uranium. These signatures are likely linked to localised controls. The results of the hydrogeological assessments provide an important baseline dataset to support the potential storage of anthropogenic CO_2.

7.6 POTENTIAL CO_2 STORAGE

Silicate minerals within basaltic sequences promote potential reactivity with anthropogenic CO_2. The mineralogy and petrographic results suggest that the basaltic sequences surrounding the proposed injection site host 25–30% reactive minerals. Potentially, 70 kg CO_2 can be stored in 1 m^3 of basaltic rock (Gislason and Oelkers, 2014; Matter *et al.*, 2016). The result of a regional electromagnetic survey further estimates at least 284 km^3 basaltic material in the surrounding area. This would suggest, theoretically, that the region can store significantly more than several million tonnes of anthropogenic CO_2.

7.7 LIMITATIONS

The geological characterisation took a wide variety of integrated geoscience datasets into account. These included geological, structural, mineralogy and petrography datasets. The data suggests that the proposed storage reservoir meets the general criteria for the reactive storage of anthropogenic CO_2. However, several key limitations will need to be addressed before development of the site is undertaken. These include:

1. The porosity and permeability of the proposed reservoir sequences are generally low. The porosity is ca 1–5% and the sequences are generally impermeable. Ideally, porosities of 5–40% and permeability of 300–2 000 mD are expected (Snæbjörnsdóttir *et al.*, 2018). This implies that the permeability of the proposed reservoir will need to be artificially increased (Liu *et al.*, 2022; Cossins *et al.*, 2023). Fracture reactivation modelling suggests that pre-existing fractures are likely to undergo reactivation at pore fluid pressures of at least 2–5 MPa above the *in situ* pore fluid pressure.

2. Inducing an increase in permeability will require additional baseline data including high-resolution

seismicity information, such as ambient noise seismicity data. This information can be used to identify potential pathways that may enable undue fluid migration (Arts *et al*., 2013; Cheraghi *et al*., 2017; Stork *et al*., 2018).

3. The proposed reservoir sequences are extremely deep, i.e. approximately 1 100–1 600 m below the surface. This is much deeper than existing basaltic storage projects at, for example, 500–800 m (Snæbjörnsdóttir *et al*., 2018) and 800–900 m (McGrail *et al*., 2014). However, greater depths imply more difficult technical challenges, requiring detailed injection, flow and mineralisation modelling. Such modelling is needed to optimise any potential injection.

4. In addition to the basaltic sequences of the Ventersdorp Supergroup, the highly fractured siliciclastic sequences of the Witwatersrand Supergroup provide an additional deep saline storage reservoir that should be considered.

5. The development and implementation of CCUS technologies are expensive (Davies *et al*., 2013; Anderson *et al*., 2021; Lau *et al*., 2021). Detailed technical, economic and financial modelling will be needed to ensure that CCUS deployment in South Africa is successful. Technologies must be tailored to South African conditions and aligned with the country's Just Transition planning, taking into consideration South Africa's coal and associated industries. The adoption of CCUS in South Africa will not be practicable unless adequate provisions are made for precise scenario planning.

6. The development and implementation of carbon capture technologies are key to South Africa's future development (Wilberforce *et al*., 2021). Currently, South Africa does not have such technologies in place. Considering the country's ageing coal-fired fleet, the we may need to consider pre-capture carbon technologies, or consider adopting capture technologies within the petrochemical industry (Choi *et al*., 2017). The success or failure of South Africa's transition to more environmentally friendly energy sources will depend on how well carbon capture technology is implemented.

8. CONCLUSIONS

A prospective CCUS site near the town of Leandra, in the Govan Mbeki Municipality, Mpumalanga Province, was geologically characterised using an integrated geoscience approach. Critical datasets used in this investigation included, among others:

1. 1:50 000-scale geological and structural information, supported by high-resolution aerial electromagnetic and radiometric data and legacy 2D reflection seismic data.

2. 1 500 legacy boreholes logs and 22 legacy physical boreholes generally attaining depths of more than 2 000 m.

3. High-resolution geological and lithological, structural and hyperspectral profiles for the physical boreholes.

4. Sixty-four (64) samples collected across the proposed injection horizon, including the over- and underlying strata.

5. Bulk and trace element geochemistry, mineralogy, petrography, porosity and permeability measurements across the proposed injection horizon.

6. *In situ* stress modelling and anticipated reactivation criteria for the surrounding pre-existing fractures, supported by a PSHA and a regional groundwater assessment.

The integration of these data suggest that the proposed injection meets the key geological requirements to support the reactive storage of anthropogenic CO_2. In other words, the proposed reservoir hosts potentially reactive silicate minerals. However, there are significant challenges, including the significant depth of the proposed reservoir (located at a depth of 1 100–1 600 m) and the relatively nonporous and impermeable nature of the proposed sequences. The formulation of an appropriate government policy framework to ensure the oversight of a CCUS technology relative to South Africa's Just Transition poses an additional challenge. The nation's CCUS programme should take these considerations into account throughout the front-end engineering and design phases.

9. ACKNOWLEDGEMENTS

The Council for Geoscience Analytical Facility is acknowledged for undertaking the sample preparation and analyses.

The Council for Geoscience National Borehole Repository is acknowledged for curating, cataloguing and facilitating the logging activities of the selected boreholes.

The project team wishes to thank Govan Mbeki Municipality leadership, industries, non-profit organisations and communities for supporting the project, providing the research framework and enabling this scientific programme.

10. REFERENCES

Abu-Goodman, M., Güngör, H. and Usman, O., 2023. Are impacts of renewable energy and globalization on carbon neutrality targets asymmetric in South Africa? A reconsideration using nonlinear ARDL approach. Environmental Science and Pollution Research, 30(9), pp. 23736–23746.

Adams, S., Titus, R. and Xu, Y. (2004). Groundwater Recharge Assessment of the Basement Aquifers of Central Namaqualand. WRC Report No. 1093/1/04. In Water Research Commission. Retrieved from http://www.wrc.org.za/wp-content/uploads/mdocs/1093-1-041.pdf.

Akkar, S., Sandıkkaya, M.A. and Ay, B.Ö., 2014. Compatible ground-motion prediction equations for damping scaling factors and vertical-to-horizontal spectral amplitude ratios for the broader Europe region. Bulletin of Earthquake Engineering, 12, pp. 517–547.

Anders, E. and Grevesse, N., 1989. Abundances of the elements: Meteoritic and solar. Geochimica et Cosmochimica acta, 53(1), pp. 197–214.

Anderson, J.J., Rode, D., Zhai, H. and Fischbeck, P., 2021. A techno-economic assessment of carbon-sequestration tax incentives in the US power sector. International Journal of Greenhouse Gas Control, 111, pp. 103–450.

Anhaeusser, C.R., 2006. A re-evaluation of Archaean intracratonic terrane boundaries on the Kaapvaal Craton, South Africa: Collisional suture zones? Special Papers — Geological Society of America, 405, 193p.

Arts, R.J., Zhang, X., Verdel, A.R., Santonico, D., Meekes, J.A.C., Noorlandt, R.P., Paap, B.F. and Vandeweijer, V.P., 2013. Experiences with a permanently installed seismic monitoring array at the CO_2 storage site at Ketzin (Germany) — a status overview. Energy Procedia, 37, pp. 4015–4023.

Bommer, J.J., Scherbaum, F., Bungum, H., Cotton, F., Sabetta, F. and Abrahamson, N.A., 2005. On the use of logic trees for ground-motion prediction equations in seismic-hazard analysis. Bulletin of the Seismological Society of America, 95(2), pp. 377–389.

Boore, D.M. and Atkinson, G.M., 2008. Ground-motion prediction equations for the average horizontal component of PGA, PGV and 5%-damped PSA at spectral periods between 0.01 s and 10.0 s. Earthquake spectra, 24(1), pp. 99–138.

Boot-Handford, M.E., Abanades, J.C., Anthony, E.J., Blunt, M.J., Brandani, S., Mac Dowell, N., Fernández, J.R., Ferrari, M.C., Gross, R., Hallett, J.P. and Haszeldine, R.S., 2014. Carbon capture and storage update. Energy and Environmental Science, 7(1), pp. 130–189.

Bryan, S.E. and Ernst, R.E., 2008. Revised definition of large igneous provinces (LIPs). Earth-Science Reviews, 86(1–4), pp. 175–202.

Byerlee, J., 1978. Friction of rocks. In Rock friction and earthquake prediction (pp. 615–626). Birkhäuser, Basel.

Cheraghi, S., White, D.J., Draganov, D., Bellefleur, G., Craven, J.A. and Roberts, B., 2017. Passive seismic reflection interferometry: A case study from the Aquistore CO_2 storage site, Saskatchewan, Canada. Geophysics, 82(3), pp. B79–B93.

Choi, Y.H., Jang, Y.J., Park, H., Kim, W.Y., Lee, Y.H., Choi, S.H. and Lee, J.S., 2017. Carbon dioxide Fischer-Tropsch synthesis: A new path to carbon-neutral fuels. Applied catalysis B: environmental, 202, pp. 605–610.

Cloete, M., 2010. Atlas on geological storage of carbon dioxide in South Africa. Council for Geoscience, 65 pp.

Cornell, D.H., Meintjes, P.G., Van der Westhuizen, W.A., Kristoffersen, M. and Frei, D., 2021. Dating detrital zircon from the gold-bearing Ventersdorp Contact Reef in the Ventersdorp Supergroup of South Africa. Precambrian Research, 357, pp. 106–131.

Cossins, T., Mishra, A. and Haese, R.R., 2023. The feasibility of enhanced pore space utilization in CO_2 storage reservoirs using an artificially emplaced Si-gel flow barrier. Scientific Reports, 13(1), p. 9334.

Coward, M.P., Spencer, R.M. and Spencer, C.E., 1995. Development of the Witwatersrand Basin, South Africa. Geological Society, London, Special Publications, 95(1), pp. 243–269.

Crow, C. and Condie, K.C., 1988. Geochemistry and origin of late Archean volcanics from the Ventersdorp Supergroup, South Africa. Precambrian Research, 42(1–2), pp. 19–37.

Dankert, B.T. and Hein, K.A., 2010. Evaluating the structural character and tectonic history of the Witwatersrand Basin. Precambrian Research, 177(1–2), pp. 1–22.

Davies, L.L., Uchitel, K. and Ruple, J., 2013. Understanding barriers to commercial-scale carbon capture and sequestration in the United States: An empirical assessment. Energy Policy, 59, pp. 745–761.

De la Roche, H.D., Leterrier, J.T., Grandclaude, P. and Marchal, M., 1980. A classification of volcanic and plutonic rocks using R1R2-diagram and major-element analyses—its relationships with current nomenclature. Chemical geology, 29(1–4), pp. 183–210.

De la Rosa, R., Tolosana-Delgado, R., Kirsch, M. and Gloaguen, R., 2022. Automated Multi-Scale and Multivariate Geological Logging from Drill-Core Hyperspectral Data. Remote Sensing, 14(11), p. 2676.

Department of Mineral Resources and Energy, 2019. Integrated Resource Plan 2019. South African Government Notice, pp. 100. Available from: https://www.energy.gov.za/irp/2019/IRP-2019.pdf.

De Wit, M.J., de Ronde, C.E., Tredoux, M., Roering, C., Hart, R.J., Armstrong, R.A., Green, R.W., Peberdy, E. and Hart, R.A., 1992. Formation of an Archaean continent. Nature, 357(6379), pp. 553–562.

Dhansay, T., 2021. Shattered crust: how brittle deformation enables Critical Zone processes beneath southern Af-

rica. South African Journal of Geology 2021, 124(2), pp. 519–536.

Dhansay, T., Musekiwa, C., Ntholi, T., Chevallier, L., Cole, D. and De Wit, M.J., 2017. South Africa's geothermal energy hotspots inferred from subsurface temperature and geology. South African Journal of Science, 113(11–12), pp. 1–7.

Dhansay, T., Maupa, T., Twala, M., Sibewu, Z., Nengovhela, V., Mudau, P., Schalenkamp, M., Mashale, N., Muedi, T., Ndou, C. and Zilibokwe, N., 2022. CO_2 storage potential of basaltic rocks, Mpumalanga: Implications for the Just Transition. South African Journal of Science, 118(7–8), pp. 1–7.

Ebadi, H., Shad, R., Valadanzoej, M.J. and Vafaeinezhad, A., 2004, July. Evaluation of indexing overlay, fuzzy logic and genetic algorithm methods for industrial estates site selection In GIS environment. In International Congress for Photogrammetry and Remote Sensing, July, Istanbul, Turkey.

Eskom, 2022. Integrated report: 31 March 2022. Eskom Holdings SOC Ltd, pp. 81. Available from: https://www.eskom.co.za/investors/integrated-results/.

Evans, R.L., Jones, A.G., Garcia, X., Muller, M., Hamilton, M., Evans, S., Fourie, C.J.S., Spratt, J., Webb, S., Jelsma, H. and Hutchins, D., 2011. Electrical lithosphere beneath the Kaapvaal craton, southern Africa. Journal of Geophysical Research: Solid Earth, 116(B4).

Flinn, D., 1958. On tests of significance of preferred orientation in three-dimensional fabric diagrams. The Journal of Geology, 66(5), pp. 526–539.

Friedlingstein, P., O'Sullivan, M., Jones, M.W. andrew, R.M., Hauck, J., Olsen, A., Peters, G.P., Peters, W., Pongratz, J., Sitch, S. and Le Quéré, C., 2020. Global carbon budget 2020. Earth System Science Data, 12(4), pp. 3269–3340.

Gislason, S.R. and Oelkers, E.H., 2014. Carbon storage in basalt. Science, 344(6182), pp. 373–374.

Govan Mbeki Municipality, 2022. Annual Report 2021/22. Govan Mbeki Municipality, pp. 372. Available from: https://www.govanmbeki.gov.za/annual-reports/.

Gumsley, A., Stamsnijder, J., Larsson, E., Söderlund, U., Naeraa, T., De Kock, M., Sałacińska, A., Gawęda, A., Humbert, F. and Ernst, R., 2020. Neoarchean large igneous provinces on the Kaapvaal Craton in southern Africa re-define the formation of the Ventersdorp Supergroup and its temporal equivalents. GSA Bulletin, 132(9–10), pp. 1829–1844.

Heidbach, O., Rajabi, M., Reiter, K. and Ziegler, M., 2019. World stress map. In Encyclopedia of petroleum geoscience (pp. 1–8). Springer.

Hollocher, K., Robinson, P., Walsh, E. and Roberts, D., 2012. Geochemistry of amphibolite-facies volcanics and gabbros of the Støren Nappe in extensions west and southwest of Trondheim, Western Gneiss Region, Norway: a key to correlations and paleotectonic settings. American Journal of Science, 312(4), pp. 357–416.

Johnson, M.R., Van Vuuren, C.J., Hegenberger, W.F., Key, R. and Show, U., 1996. Stratigraphy of the Karoo Supergroup in southern Africa: an overview. Journal of African Earth Sciences, 23(1), pp. 3–15.

Kearey, P., Brooks, M. and Hill, I., 2002. An introduction to geophysical exploration (4), John Wiley & Sons.

Kruger, A.C., 2018. Africa and the Paris agreement. Nature Climate Change, 8(5), pp. 365–366.

Lau, H.C., Ramakrishna, S., Zhang, K. and Radhamani, A.V., 2021. The role of carbon capture and storage in the energy transition. Energy and Fuels, 35(9), pp. 7364–7386.

Liu, P., Wang, Z., Lu, K. and Zhang, Z., 2022. Effect of sandstone and mudstone thickness on artificial fracturing for hydrocarbon extraction from low-permeability reservoirs. Natural Gas Industry B, 9(4), pp. 411–425.

Manzunzu, B., Brandt, M.B.C., Midzi, V., Durrheim, R.J., Saunders, I. and Mulabisana, T.F., 2021. Towards a homogeneous moment magnitude determination for earthquakes in South Africa: Reduction of associated uncertainties. Journal of African Earth Sciences, 173, p. 104051.

Manzi, M.S., Hein, K.A., King, N. and Durrheim, R.J., 2013. Neoarchaean tectonic history of the Witwatersrand Basin and Ventersdorp Supergroup: New constraints from high-resolution 3D seismic reflection data. Tectonophysics, 590, pp. 94–105.

Marsh, J.S., Bowen, M.P., Rogers, N.W. and Bowen, T.B., 1992. Petrogenesis of late Archaean flood-type basic lavas from the Klipriviersberg Group, Ventersdorp Supergroup, South Africa. Journal of Petrology, 33(4), pp. 817–847.

Matter, J.M., Stute, M., Snæbjörnsdottir, S.Ó., Oelkers, E.H., Gislason, S.R., Aradottir, E.S., Sigfusson, B., Gunnarsson, I., Sigurdardottir, H., Gunnlaugsson, E. and Axelsson, G., 2016. Rapid carbon mineralization for permanent disposal of anthropogenic carbon dioxide emissions. Science, 352(6291), pp. 1312–1314.

McDonough, W.F. and Sun, S.S., 1995. The composition of the Earth. Chemical geology, 120(3–4), pp. 223–253.

McGrail, B.P., Spane, F.A., Amonette, J.E., Thompson, C.R. and Brown, C.F., 2014. Injection and monitoring at the Wallula basalt pilot project. Energy Procedia, 63, pp. 2939–2948.

Meintjes, P.G. and Van der Westhuizen, W.A., 2018. Stratigraphy and geochemistry of the Goedgenoeg and Makwassie Formations, Ventersdorp Supergroup, in the Bothaville area of South Africa. South African Journal of Geology 2018, 121(4), pp. 339–362.

Metz, B., Davidson, O., De Coninck, H.C., Loos, M. and Meyer, L., 2005. IPCC special report on carbon dioxide capture and storage. Cambridge: Cambridge University Press.

Middlemost, E.A., 1994. Naming materials in the magma/igneous rock system. Earth-science reviews, 37(3–4), pp. 215–224.

Midzi, V., Manzunzu, B., Mulabisana, T., Zulu, B.S., Pule, T. and Myendeki, S., 2020. Probabilistic seismic hazard maps for South Africa. Journal of African Earth Sciences, 162, p. 103689.

Moos, D. and Zoback, M.D., 1990. Utilization of observations of well bore failure to constrain the orientation and magnitude of crustal stresses: application to continental, Deep Sea Drilling Project and Ocean Drilling Program boreholes. Journal of Geophysical Research: Solid Earth, 95(B6), pp. 9305–9325.

Morris, A., Ferrill, D.A. and Henderson, D.B., 1996. Slip-tendency analysis and fault reactivation. Geology, 24(3), pp. 275–278.

Muedi, T., Maclennan, S., Szymanowski, D., Schoene, B., Ramezani, J., Oalmann, J. and Linol, B., 2022. Constraining the timescales of mafic magmatism of the Central Karoo Large Igneous Province using high precision U-Pb zircon geochronology. South African Journal of Geology 2022, 125(1), pp. 99–112.

Nelson, D.R., Trendall, A.F., De Laeter, J.R., Grobler, N.J. and Fletcher, I.R., 1992. A comparative study of the geochemical and isotopic systematics of late Archaean flood basalts from the Pilbara and Kaapvaal Cratons. Precambrian Research, 54(2–4), pp. 231–256.

Pagani, M., Monelli, D., Weatherill, G., Danciu, L., Crowley, H., Silva, V., Henshaw, P., Butler, L., Nastasi, M., Panzeri, L. and Simionato, M., 2014. OpenQuake engine: An open hazard (and risk) software for the global earthquake model. Seismological Research Letters, 85(3), pp. 692–702.

Palacky, G.J., 1993. Use of airborne electromagnetic methods for resource mapping. Advances in space research, 13(11), pp. 5–14.

Pearce, J.A., 1996. A user's guide to basalt discrimination diagrams. Trace element geochemistry of volcanic rocks: applications for massive sulphide exploration. Geological Association of Canada, Short Course Notes, 12(79), p. 113.

Pearce, J.A., 2008. Geochemical fingerprinting of oceanic basalts with applications to ophiolite classification and the search for Archean oceanic crust. Lithos, 100(1–4), pp. 14–48.

Poujol, M. and Anhaeusser, C.R., 2001. The Johannesburg Dome, South Africa: new single zircon U–Pb isotopic evidence for early Archaean granite–greenstone development within the central Kaapvaal Craton. Precambrian Research, 108(1–2), pp. 139–157.

Poujol, M., Robb, L.J., Anhaeusser, C.R. and Gericke, B., 2003. A review of the geochronological constraints on the evolution of the Kaapvaal Craton, South Africa. Precambrian research, 127(1–3), pp. 181–213.

Pretorius, D.A., Brink, W.C.J., Fouche, J., 1986. Geological map of the Witwatersrand Basin. *In*: (C.R. Anhaeusser, and S. Maske, editors). Mineral Deposits of Southern Africa, vol. I. Geological Society of South Africa, Johannesburg.

Robins, N.S., Chilton, P.J. and Cobbing, J.E., 2007. Adapting existing experience with aquifer vulnerability and groundwater protection for Africa. Journal of African Earth Sciences, 47(1), pp. 30–38.

Scott, V., Gilfillan, S., Markusson, N., Chalmers, H. and Haszeldine, R.S., 2013. Last chance for carbon capture and storage. Nature Climate Change, 3(2), pp. 105–111.

Sibson, R.H., 1974. Frictional constraints on thrust, wrench and normal faults. Nature, 249(5457), pp. 542–544.

Snæbjörnsdóttir, S.Ó., Gislason, S.R., Galeczka, I.M. and Oelkers, E.H., 2018. Reaction path modelling of *in situ* mineralisation of CO_2 at the CarbFix site at Hellisheidi, SW-Iceland. Geochimica et Cosmochimica Acta, 220, pp. 348–366.

Stork, A.L., Allmark, C., Curtis, A., Kendall, J.M. and White, D.J., 2018. Assessing the potential to use repeated ambient noise seismic tomography to detect CO_2 leaks: Application to the Aquistore storage site. International Journal of Greenhouse Gas Control, 71, pp. 20–35.

Sun, S.S. and McDonough, W.F., 1989. Chemical and isotopic systematics of oceanic basalts: implications for mantle composition and processes. Geological Society, London, Special Publications, 42(1), pp. 313–345.

Szulczewski, M.L., MacMinn, C.W., Herzog, H.J. and Juanes, R., 2012. Lifetime of carbon capture and storage as a climate-change mitigation technology. Proceedings of the National Academy of Sciences, 109(14), pp. 5185–5189.

Telford, W.M., Geldart, L.P. and Sheriff, R.E., 1990. Applied geophysics. Cambridge University Press.

Tessema, A., Nzotta, U. and Chirenje, E., 2014. Assessment of groundwater potential in fractured hard rocks around Vryburg, North West Province, South Africa. Water Research Commission, Pretoria, WRC Report (2055/1), p. 13.

Vaessen, V. and Brentführer, R., 2014. Integration of groundwater management: Into transboundary basin organizations in Africa.

Wilberforce, T., Olabi, A.G., Sayed, E.T., Elsaid, K. and Abdelkareem, M.A., 2021. Progress in carbon capture technologies. Science of The Total Environment, 761, p. 143203.

Winchester, J.A. and Floyd, P.A., 1977. Geochemical discrimination of different magma series and their differentiation products using immobile elements. Chemical geology, 20, pp. 325–343.

Zeh, A., Wilson, A.H. and Gerdes, A., 2020. Zircon U-Pb-Hf isotope systematics of Transvaal Supergroup Constraints for the geodynamic evolution of the Kaapvaal Craton and its hinterland between 2.65 and 2.06 Ga. Precambrian Research, 345, p. 105760.

11. APPENDICES

11.1 MINERALOGY RESULTS

Table 14. Automated SEM results for selected borehole samples (anticipated non-reactive sequences).

Sample	Cpx	Plag	Kspar	An	Qtz	Bt	Chl	Epi	Tal	Tit	Hem	Ilm	Cal	Dol	Sul	Oth
DBS001A	33.24	27.02	6.74	9.32	1.79	1.61	15.45	2.76	-	1.99	-	-	-	-	0.06	<0.1
DBS002A	24.77	22.02	11.30	19.06	1.42	3.19	16.12	1.48	0.00	0.54	-	<0.1	<0.1	<0.1	0.07	<0.1
DBS003A	36.33	22.66	4.40	9.60	9.21	0.83	11.42	4.04	-	1.28	-	-	<0.1	-	0.08	0.07
DBS004A	29.35	21.13	9.79	16.12	0.71	1.89	15.95	2.79	-	2.19	-	-	<0.1	-	<0.1	<0.1
DBS005A	25.38	32.90	1.75	6.93	6.23	0.96	16.40	8.90	-	0.44	-	<0.1	<0.1	-	0.08	<0.1
DBS006A	19.18	27.30	8.71	0.95	10.88	0.23	16.55	15.20	-	0.59	-	<0.1	0.26	-	<0.1	0.10
DBS007A	21.21	45.36	0.84	2.72	6.79	0.89	17.94	3.50	-	0.68	-	<0.1	<0.1	-	<0.1	<0.1
DBS008A	22.72	33.77	16.08	4.07	2.52	0.82	13.99	4.92	-	0.94	-	<0.1	<0.1	-	0.09	<0.1
DBS009A	17.60	42.45	4.77	1.44	10.95	0.48	16.51	2.20	<0.1	3.06	-	<0.1	0.40	-	0.06	0.07
DBS010A	24.94	18.82	14.90	2.32	3.78	1.91	27.41	1.90	-	3.28	-	<0.1	0.56	-	0.16	<0.1
DBS011A	32.34	28.11	<0.1	<0.1	9.24	0.48	23.80	-	-	-	-	1.67	<0.1	0.54	3.72	0.10
DBS012A	23.53	27.83	<0.1	<0.1	14.60	1.01	15.43	0.01	-	-	-	6.51	<0.1	3.46	7.58	<0.1
DBS013A	8.55	24.00	-	<0.1	14.96	2.94	37.95	0.00	-	-	-	6.53	<0.1	0.83	4.18	<0.1
DBS014A	27.31	31.72	3.04	11.77	4.54	0.60	18.18	1.97	-	0.76	-	<0.1	-	-	0.06	<0.1
DBS015A	32.88	28.46	3.32	10.15	1.11	1.33	9.54	12.44	-	0.67	-	<0.1	<0.1	-	0.05	<0.1
DBS016A	20.65	47.43	1.32	2.26	<0.1	0.41	22.92	2.14	-	2.70	-	-	-	-	<0.1	0.08
DBS017A	22.67	33.66	3.99	5.77	6.49	0.60	18.86	5.58	-	2.25	-	-	<0.1	-	<0.1	0.07
DBS018A	22.19	40.03	12.87	2.01	0.44	1.22	17.07	1.77	-	2.26	-	-	<0.1	-	0.05	0.08
DBS019A	20.66	27.91	0.88	1.39	5.59	0.52	32.61	6.47	-	2.10	0.00	-	1.68	-	0.18	<0.1
DBS020A	33.92	-	-	-	-	-	28.19	-	30.60	-	4.00	1.33	1.10	-	0.79	0.07
LP001D	-	<0.1	10.46	0.00	69.47	0.07	17.95	0.02	-	1.88	-	-	<0.1	-	0.08	0.07
LP002D	-	<0.1	17.19	0.00	80.37	<0.1	2.04	-	-	-	-	-	-	-	0.32	<0.1
LP003D	-	<0.1	11.22	0.00	87.25	<0.1	1.30	0.00	-	-	-	-	<0.1	-	0.14	<0.1
LP004D	<0.1	0.23	13.14	0.00	86.42	<0.1	0.11	<0.1	-	<0.1	-	-	<0.1	-	<0.1	<0.1
PM001A	12.18	22.12	4.73	5.20	2.99	2.63	46.38	0.77	-	2.92	-	-	<0.1	-	<0.1	<0.1
PM002A	39.25	16.30	4.04	7.16	4.67	0.73	17.70	6.03	-	2.03	-	-	1.93	-	0.11	<0.1
PM003A	10.96	14.72	3.17	5.30	23.17	3.77	34.23	0.33	-	2.01	-	<0.1	2.30	-	<0.1	<0.1
PM004A	28.49	32.15	6.43	8.75	0.68	1.24	10.46	8.75	-	2.98	-	<0.1	-	-	<0.1	<0.1
PM005A	12.18	30.60	1.41	2.13	21.55	0.62	13.58	16.19	-	1.43	-	-	<0.1	-	0.25	<0.1
PM006A	22.94	0.36	0.87	<0.1	23.42	0.27	5.50	43.92	-	2.57	-	-	<0.1	-	<0.1	0.14
PM007A	6.99	13.46	3.86	4.81	37.93	1.11	24.37	3.66	-	3.51	-	-	<0.1	<0.1	0.08	0.20
PM008A	17.34	16.00	0.81	3.13	23.35	0.34	15.33	21.60	-	2.06	-	-	<0.1	-	<0.1	<0.1
PM009A	24.68	31.02	0.23	1.67	12.33	0.30	17.02	11.60	-	1.06	-	0.00	-	-	0.06	<0.1
PM010A	20.50	26.90	0.11	0.27	30.91	<0.1	10.32	9.15	-	1.76	-	-	<0.1	-	<0.1	<0.1
PM011A	19.99	35.27	1.35	5.87	17.32	1.03	14.52	1.55	-	3.03	-	-	<0.1	-	<0.1	<0.1
PM012A	13.16	23.05	1.93	10.15	18.44	0.36	17.17	12.77	-	2.64	-	-	<0.1	-	0.28	<0.1
PM013A	20.25	32.11	3.79	6.90	3.72	1.06	13.85	16.24	-	1.25	-	<0.1	0.54	-	0.24	<0.1
PM014A	9.34	-	-	-	-	-	24.51	-	47.85	1.35	-	0.12	13.40	0.00	3.38	0.06
PM015A	28.81	-	-	-	-	-	30.51	-	36.78	-	-	0.26	1.17	0.00	2.36	0.10
PM016A	27.65	29.07	2.94	4.65	1.88	0.55	15.88	13.91	-	3.38	-	-	<0.1	-	<0.1	0.06
PM017A	12.80	34.60	0.70	0.84	27.32	0.04	17.88	3.87	-	1.78	-	-	0.06	-	0.08	<0.1
PM018A	27.31	36.17	1.80	4.42	5.16	0.48	17.80	3.89	-	2.85	-	-	<0.1	-	0.07	0.07
PM019A	24.26	20.91	11.24	15.09	10.98	1.50	9.53	3.28	-	1.14	-	-	2.05	-	<0.1	<0.1
PM020A	13.05	38.16	7.04	1.51	24.66	0.24	4.66	8.20	-	1.48	-	-	0.93	-	0.06	<0.1
PM021A	17.41	-	-	-	-	-	35.31	-	41.50	<0.1	-	0.84	4.29	<0.1	0.58	0.06
PM022A	15.17	47.48	3.05	2.01	2.92	0.29	17.30	8.68	<0.1	0.72	-	-	2.28	-	<0.1	0.07
PM023A	15.40	43.70	1.65	1.21	1.41	0.05	4.75	28.29	<0.1	2.83	-	-	0.53	-	0.09	0.08
PM024A	4.69	-	-	-	-	-	26.78	-	63.22	-	-	0.87	3.79	<0.1	0.62	<0.1
PM025A	11.71	45.93	0.63	3.42	14.52	0.62	18.06	4.45	-	0.45	-	-	<0.1	-	0.16	<0.1

Table 15. Automated SEM results for selected borehole samples (anticipated reservoir sequences).

Sample	Cpx	Plag	Kspar	An	Qtz	Bt	Chl	Epi	Tal	Tit	Cal	Sul	Oth
DBS024A	25.63	33.98	9.37	9.40	2.93	1.01	13.08	3.62	-	0.87	-	0.09	<0.1
DBS025A	23.22	26.90	10.73	18.29	1.47	2.69	15.29	0.30	-	1.05	<0.1	<0.1	<0.1
DBS026A	35.48	27.85	1.87	1.06	2.18	0.66	15.50	13.26	-	1.93	<0.1	<0.1	0.16
DBS028A	12.15	39.01	6.98	4.34	8.09	1.34	16.91	8.32	-	2.49	-	0.34	<0.1
DBS029A	24.81	36.25	7.92	0.98	2.03	2.56	12.90	10.42	-	2.04	<0.1	0.05	<0.1
DBS031A	29.06	37.98	2.68	6.74	1.91	1.81	14.93	4.26	-	0.52	<0.1	0.06	0.05
DBS032A	20.05	38.86	2.72	1.28	5.12	0.82	19.13	9.34	-	2.59	<0.1	<0.1	0.05
DBS033A	20.58	30.49	14.87	2.43	5.05	1.40	18.37	4.50	-	2.23	-	0.05	<0.1
DBS035A	21.13	42.39	3.00	3.37	2.27	0.61	17.29	7.76	-	2.10	<0.1	<0.1	0.05
DBS037A	21.16	24.85	11.20	3.09	4.67	0.37	23.19	10.29	-	0.86	0.20	0.06	0.06
DBS039A	23.98	19.68	24.09	10.77	0.66	5.20	13.20	0.10	-	2.27	<0.1	<0.1	<0.1
DBS040A	23.04	25.76	4.48	12.45	11.37	1.65	17.98	0.37	-	0.42	2.41	0.05	<0.1
DBS041A	39.23	20.71	1.66	0.79	0.71	0.34	11.94	22.84	-	1.45	0.28	<0.1	<0.1
DBS042A	41.17	30.23	1.40	1.27	3.90	0.33	15.37	5.24	-	1.03	<0.1	<0.1	<0.1
DBS043A	23.54	30.65	11.16	2.07	6.76	0.99	15.12	7.37	-	2.20	<0.1	0.07	0.08
DBS044A	21.85	33.79	0.27	0.41	3.87	0.08	26.33	12.23	-	1.12	<0.1	<0.1	<0.1
DBS045A	24.07	47.59	0.82	1.38	<0.1	0.41	21.89	1.39	-	2.34	<0.1	0.05	0.07
DBS049A	18.34	38.43	5.42	3.49	11.86	1.22	16.97	0.96	-	3.12	<0.1	0.07	0.13
DBS050A	26.20	26.55	6.20	1.16	3.32	0.17	17.54	14.42	-	3.24	<0.1	1.09	0.08
PPM024D	6.91	34.27	0.36	0.14	31.35	0.06	11.43	14.26	-	1.13	0.05	<0.1	<0.1
PPM025D	18.26	30.12	2.47	8.62	14.72	1.60	21.34	2.06	-	0.65	-	0.12	<0.1
PM026D	12.88	31.71	3.41	3.45	24.10	0.74	19.16	2.29	-	2.13	<0.1	0.09	<0.1
PM027D	13.03	40.95	0.52	0.46	26.26	0.29	11.89	5.01	-	1.50	<0.1	0.08	<0.1
PM029D	15.70	28.06	18.70	5.50	13.24	2.31	13.31	0.69	-	2.44	-	<0.1	<0.1
PM030D	21.41	32.50	7.07	5.53	9.11	0.95	12.74	8.10	-	2.43	<0.1	0.11	<0.1
PM031D	10.11	26.49	8.06	4.76	19.79	0.60	11.27	16.31	-	2.42	0.12	<0.1	0.05
PM033D	24.73	42.65	2.47	1.89	<0.1	0.87	22.11	1.25	-	3.88	<0.1	<0.1	0.13
PM034D	18.47	35.98	3.33	2.83	1.54	0.60	25.63	8.75	-	2.73	<0.1	<0.1	0.11
PM035D	10.09	59.17	1.51	1.62	<0.1	0.41	15.31	8.05	-	3.73	-	<0.1	0.07
PM036D	1.74	4.26	0.14	0.19	3.09	<0.1	26.25	63.93	-	0.15	0.19	<0.1	<0.1
PM038D	12.20	14.88	15.91	4.34	38.49	1.55	4.93	4.83	-	2.58	0.14	0.10	<0.1
PM042D	26.81	44.11	1.09	1.14	1.44	0.25	12.32	8.80	-	3.83	<0.1	<0.1	0.18
PM043D	12.62	28.14	17.56	0.53	2.38	0.13	19.67	17.33	-	1.58	<0.1	<0.1	<0.1
PM044D	8.38	<0.1	<0.1	<0.1	-	-	36.03	-	45.63	-	7.89	1.32	0.75
PM047D	40.23	1.59	4.78	0.10	20.76	0.45	8.80	20.92	-	2.15	0.18	<0.1	<0.1
PM048D	37.52	30.05	1.48	1.16	10.85	0.07	7.40	9.19	-	1.98	0.26	<0.1	<0.1

11.2 POROSITY RESULTS

Table 16. Porosity results for selected samples. He-Pyc refers to the helium pycrometer method (undertaken at Particle Physics Lab, US) and XCT refers to the X-ray computed tomography method (undertaken at Necsa, South Africa).

No.	Borehole	From	To	Size	Description	Type	He-Pyc	XCT
DBS009	687	745.12	745.47	35	Porphyritic	Non-reactive	14.582	19.155
PM015	687	749.55	749.9	35	Fine	Reactive	0.094	28.176
DBS010	2 068	1 001.42	1 001.67	25	Fine	Non-reactive	-0.203	44.021
DBS011	2 068	1 017.41	1 017.66	25	Fine	Non-reactive	-0.332	34.043
DBS001	2 188	1 101.75	1 102	25	Fine	Non-reactive	1.509	24.657
PM001	2 188	1 105.51	1 105.76	25	Amygdaloidal	Reactive	1.252	42.510
PM002	2 188	1 106.75	1 108	25	Amygdaloidal	Reactive	1.703	29.516
PM003	2 188	1 108.1	1 108.35	25	Amygdaloidal	Reactive	0.638	23.253
DBS002	2 188	1 128	1 128.25	25	Fine	Non-reactive	0.620	23.055
PM004	2 188	1 138.09	1 138.34	25	Amygdaloidal	Reactive	0.940	24.585
PM005	2 188	1 140.69	1 140.94	25	Amygdaloidal	Reactive	1.023	38.846
DBS012	2 068	1 166.85	1 167.1	25	Fine	Non-reactive	0.736	18.785
DBS013	2 068	1 275.2	1 275.45	25	Fine	Non-reactive	0.904	16.187
PM016	2 068	1 291.74	1 291.99	25	Fine	Reactive	0.629	34.007
DBS003	2 188	1 315.4	1 315.65	25	Fine	Non-reactive	1.603	19.930
PM006	2 188	1 320.54	1 320.79	25	Amygdaloidal	Reactive	1.171	22.523
DBS014	2 068	1 347.75	1 348	25	Fine	Non-reactive	1.229	12.208
PM017	2 068	1 356.4	1 356.65	25	Amygdaloidal	Reactive	1.602	9.974
PM018	2 068	1 361.15	1 361.4	25	Amygdaloidal	Reactive	0.787	37.626
DBS004	2 188	1 364.14	1 364.39	25	Fine	Non-reactive	1.262	38.409
PM007	2 188	1 367.2	1 367.45	25	Amygdaloidal	Reactive	1.047	26.975
PM008	2 188	1 367.88	1 368.14	25	Amygdaloidal	Reactive	1.100	22.525
PM009	2 188	1 375.45	1 375.7	25	Amygdaloidal	Reactive	0.855	18.130
DBS015	2 068	1 378.15	1 378.4	25	Fine	Non-reactive	0.880	33.736
PM019	2 068	1 382.74	1 383.09	25	Coarse	Reactive	1.356	19.689
DBS005	2 188	1 431.11	1 431.26	25	Fine	Non-reactive	1.480	19.575
DBS016	2 068	1 436.54	1 436.79	25	Coarse	Non-reactive	1.669	24.259
PM020	2 068	1 443.4	1 443.65	25	Amygdaloidal	Reactive	1.680	19.528
DBS017	2 068	1 450.76	1 451.01	25	Coarse	Non-reactive	1.659	21.718
PM010	2 188	1 459.08	1 459.33	25	Amygdaloidal	Reactive	1.046	20.336
PM025	2 068	1 464.7	1 464.95	25	Coarse	Reactive	1.429	38.665
DBS006	2 188	1 491.8	1 492.05	25	Fine	Non-reactive	1.397	29.015
PM011	2 188	1 508	1 508.25	25	Amygdaloidal	Reactive	0.865	23.812
DBS007	2 188	1 513.7	1 514.05	25	Amygdaloidal	Non-reactive and reactive	1.228	30.596
DBS018	2 068	1 562	1 562.25	25	Fine	Non-reactive	0.921	20.171
PM022	2 068	1 573.6	1 573.85	25	Amygdaloidal	Reactive	3.522	17.092
PM023	2 068	1 576.15	1 576.4	25	Amygdaloidal	Reactive	2.030	20.659
DBS008	2 188	1 640	1 640.25	25	Fine	Non-reactive	-0.380	22.242
PM012	2 188	1 644.96	1 145.21	25	Amygdaloidal	Reactive	1.572	34.269
DBS019	2 068	1 686.37	1 686.62	25	Fine	Non-reactive	-0.003	44.290
DBS020	2 068	1 690.8	1 691.05	25	Fine	Non-reactive and reactive	1.371	15.457
PM024	2 068	1 692.5	1 692.75	25	Coarse	Reactive	7.114	25.499
PM021	2 068	1 698.5	1 698.75	25	Coarse	Reactive	2.674	11.210
PM013	2 188	1 755.24	1 755.49	25	Porphyrtic	Reactive	1.649	28.683
PM014	2 188	1 778.61	1 778.86	25	Coarse	Reactive	1.222	31.544
LP001	2 068	1 793.85	1 794.2	35	Quartzite	Reactive	0.485	30.343
LP002	2 068	1 939.49	1 939.84	35	Quartzite	Reactive	0.539	40.411
LP003	2 068	1 991.02	1 991.37	35	Quartzite	Reactive	1.174	43.132
LP004	2 068	2 043.34	2 043.69	35	Quartzite	Reactive	0.094	37.332

11.3 PERMEABILITY RESULTS

Table 17. Permeability results for selected samples. Analyses undertaken at RockLab, South Africa.

No.	ID	Area	Length	W_head	F_rate	H_grad	Co_per	Darcy	Note
PMT-PM24	PM24	252.2	43.39	3 500	0	8 227.7	0.00 × 10-7	0	Not permeable
PMT-PM25	PM25	181.1	47.85	3 500	0	7 460.8	0.00 × 10-7	0	Not permeable
PMT-PM26	PM26	220	45.22	3 500	0	7 894.7	0.00 × 10-7	0	Not permeable
PMT-PM27	PM27	199.4	40.17	3 500	0	8 887.2	0.00 × 10-7	0	Not permeable
PMT-PM29	PM29	207.9	45.08	3 500	0	7 919.3	0.00 × 10-7	0	Not permeable
PMT-PM30	PM30	244.1	51.6	3 500	0	6 918.6	0.00 × 10-7	0	Not permeable
PMT-PM31	PM31	215.8	47.69	3 500	0	7 485.8	0.00 × 10-7	0	Not permeable
PMT-PM33	PM33	176.2	54.56	3 500	0	6 543.3	0.00 × 10-7	0	Not permeable
PMT-PM34	PM34	202	53.03	3 500	0	6 732	0.00 × 10-7	0	Not permeable
PMT-PM35	PM35	195.3	66.93	3 500	0	5 333.9	0.00 × 10-7	0	Not permeable
PMT-PM36	PM36	218.6	63.75	3 500	0	5 600	0.00 × 10-7	0	Not permeable
PMT-PM38	PM38	180.3	42.28	3 500	0	8 443.7	0.00 × 10-7	0	Not permeable
PMT-PM42	PM42	211.2	54.2	3 500	0	6 586.7	0.00 × 10-7	0	Not permeable
PMT-PM43	PM43	212.6	45.93	3 500	0	7 772.7	0.00 × 10-7	0	Not permeable
PMT-PM44	PM44	198.4	52.59	3 500	0	6 788.4	0.00 × 10-7	0	Not permeable
PMT-PM47	PM47	203.1	61.41	3 500	0	5 813.4	0.00 × 10-7	0	Not permeable
PMT-PM48	PM48	218	54.61	3 500	0	6 537.3	0.00 × 10-7	0	Not permeable
PMT-DBS-24	DBS-24	210.8	29.03	3 500	0	12 297.6	0.00 × 10-7	0	Not permeable
PMT-DBS-25	DBS-25	186.2	42.09	3 500	0	8 481.8	0.00 × 10-7	0	Not permeable
PMT-DBS-26	DBS-26	204.7	48.4	3 500	0	7 376	0.00 × 10-7	0	Not permeable
PMT-DBS-28	DBS-28	228.2	49.39	3 500	0	7 228.2	0.00 × 10-7	0	Not permeable
PMT-DBS-29	DBS-29	237.4	54.73	3 500	0	6 522.9	0.00 × 10-7	0	Not permeable
PMT-DBS-31	DBS-31	210.9	63.28	3 500	0	5 641.6	0.00 × 10-7	0	Not permeable
PMT-DBS-32	DBS-32	247.6	61.41	3 500	0	5 813.4	0.00 × 10-7	0	Not permeable
PMT-DBS-33	DBS-33	198.4	58.29	3 500	0	6 124.5	0.00 × 10-7	0	Not permeable
PMT-DBS-35	DBS-35	205.6	41.39	3 500	0	8 625.3	0.00 × 10-7	0	Not permeable
PMT-DBS-37	DBS-37	178.4	52.28	3 500	0	6 828.6	0.00 × 10-7	0	Not permeable
PMT-DBS-39	DBS-39	205.9	44.41	3 500	0	8 038.7	0.00 × 10-7	0	Not permeable
PMT-DBS-40	DBS-40	195	55.96	3 500	0	6 379.6	0.00 × 10-7	0	Not permeable
PMT-DBS-41	DBS-41	203.3	42.07	3 500	0	8 485.9	0.00 × 10-7	0	Not permeable
PMT-DBS-42	DBS-42	222.5	42.25	3 500	0	8 449.7	0.00 × 10-7	0	Not permeable
PMT-DBS-43	DBS-43	230.9	52.93	3 500	0	6 744.8	0.00 × 10-7	0	Not permeable
PMT-DBS-44	DBS-44	231.3	61.78	3 500	0	5 778.6	0.00 × 10-7	0	Not permeable
PMT-DBS-45	DBS-45	228.2	37.11	3 500	0	9 620	0.00 × 10-7	0	Not permeable
PMT-DBS-49	DBS-49	215.1	31.34	3 500	0	11 391.2	0.00 × 10-7	0	Not permeable
PMT-DBS-50	DBS-50	198.6	56.71	3 500	0	6 295.2	0.00 × 10-7	0	Not permeable

11.4 WHOLE ROCK GEOCHEMICAL ANALYSES

Table 18. Whole rock analyses of selected samples collected from the Ventersdorp Supergroup. Loc refers to samples collected from the Klipriviersberg Group (Kl), Platberg Group (Pl) and the Pniel Group (Pn). Ref refers to analyses/samples ascertained from Dhansay *et al*., 2022 (A), Marsh *et al*. (1992) (B), Nelson *et al*. (1992) (C), Meintjes and Van der Westhuizen (2018) (D), Crow and Condie (1988) (E).

Sample	Loc	Ref	SiO_2	TiO_2	Al_2O_3	Fe_2O_3 (t)	MnO	MgO	CaO	Na_2O	K_2O	P_2O_5	Cr_2O_3	LOI
DBS001D	Kl	A	55.74	0.69	12.76	10.74	0.14	6.14	6.76	3.55	1.44	0.09	0.05	1.86
DBS002D	Kl	A	53.83	0.90	14.59	11.54	0.19	4.58	6.36	3.69	2.94	0.12	0.01	1.27
DBS003D	Kl	A	52.21	0.71	11.83	12.16	0.18	8.04	8.86	2.91	1.53	0.08	0.08	1.44
DBS004D	Kl	A	53.95	0.93	14.27	11.77	0.17	4.51	6.16	3.30	3.23	0.12	0.01	1.43
DBS005D	Kl	A	53.57	0.91	14.51	12.27	0.16	4.83	7.80	3.37	1.01	0.12	0.01	1.54
DBS006D	Kl	A	54.87	1.04	14.18	12.60	0.15	4.37	6.34	3.05	1.43	0.15	0.02	1.85
DBS007D	Kl	A	59.71	0.96	13.79	9.99	0.11	3.44	5.02	4.78	0.77	0.14	0.01	1.31
DBS008D	Kl	A	53.49	1.16	14.41	11.39	0.15	5.02	6.16	3.66	2.43	0.18	0.03	1.57
DBS009D	Kl	A	53.12	1.22	14.67	11.51	0.18	4.97	6.04	4.45	1.11	0.19	0.02	1.98
DBS010D	Kl	A	46.67	1.37	14.58	13.77	0.18	6.46	8.48	3.20	1.88	0.22	0.03	2.60
DBS011D	Kl	A	52.54	0.79	13.69	11.14	0.13	7.02	7.29	4.39	0.93	0.09	0.04	2.01
DBS012D	Kl	A	54.30	0.87	14.43	12.14	0.16	4.84	5.96	3.60	1.71	0.12	0.01	1.80
DBS013D	Kl	A	50.90	1.08	15.85	13.27	0.14	6.35	3.02	3.25	2.93	0.14	0.01	3.04
DBS014D	Kl	A	54.35	0.90	13.85	11.72	0.16	5.24	5.94	3.94	1.60	0.12	0.01	1.72
DBS015D	Kl	A	54.22	0.90	14.23	11.88	0.17	4.43	7.70	4.08	0.97	0.12	0.01	1.22
DBS016D	Kl	A	51.34	1.07	15.64	13.12	0.15	4.47	5.78	5.59	0.50	0.15	0.02	1.96
DBS017D	Kl	A	53.75	1.03	14.65	12.23	0.14	4.68	5.94	4.10	1.35	0.15	0.02	1.71
DBS018D	Kl	A	53.63	1.17	14.73	11.07	0.23	5.29	5.66	4.28	2.00	0.18	0.03	1.60
DBS019D	Kl	A	50.01	1.36	14.68	12.30	0.27	7.12	7.21	3.18	0.45	0.22	0.03	3.26
DBS020D	Kl	A	47.16	0.73	3.54	17.41	0.19	23.01	2.69	0.06	0.01	0.07	0.19	4.91
PM001D	Kl	A	53.80	0.84	14.31	10.82	0.10	6.67	4.34	3.97	1.08	0.20	0.04	3.61
PM002D	Kl	A	52.90	0.69	11.83	11.03	0.15	8.18	8.58	3.62	0.73	0.10	0.04	1.76
PM003D	Kl	A	67.81	0.45	8.73	8.43	0.07	6.24	2.76	1.55	0.88	0.07	0.03	2.89
PM004D	Kl	A	54.36	0.83	14.28	11.67	0.16	4.39	7.29	3.32	1.66	0.11	0.01	1.89
PM005D	Kl	A	51.22	0.82	14.00	11.72	0.19	4.49	11.77	3.57	0.42	0.11	0.01	1.33
PM006D	Kl	A	59.29	0.63	12.04	8.51	0.16	2.14	16.31	0.03	0.00	0.08	0.01	0.65
PM007D	Kl	A	60.90	0.97	11.70	10.32	0.10	2.78	9.77	1.25	0.73	0.06	0.01	1.36
PM008D	Kl	A	56.66	0.62	14.21	10.31	0.13	3.66	8.66	3.24	0.80	0.04	0.01	1.62
PM009D	Kl	A	56.00	0.92	13.44	11.85	0.14	4.56	6.92	3.70	0.40	0.12	0.01	1.87
PM010D	Kl	A	51.87	0.65	13.01	10.78	0.14	7.65	10.11	2.65	0.35	0.10	0.03	2.71
PM011D	Kl	A	54.40	0.99	14.81	11.48	0.15	3.85	7.63	4.45	0.75	0.14	0.01	1.41
PM012D	Kl	A	56.48	0.90	13.11	11.17	0.16	4.35	6.57	4.68	0.55	0.14	0.02	1.40
PM013D	Kl	A	53.49	1.19	15.22	11.20	0.14	4.40	6.77	3.97	1.50	0.19	0.02	1.65
PM014D	Kl	A	41.83	0.62	3.09	11.98	0.22	19.17	11.44	0.04	0.00	0.05	0.15	11.05
PM015D	Kl	A	44.19	0.62	3.19	19.03	0.19	23.38	3.67	0.14	0.02	0.02	0.15	4.93
PM016D	Kl	A	48.74	1.27	13.86	13.73	0.21	5.79	9.25	4.07	0.57	0.21	0.02	1.85
PM017D	Kl	A	56.77	0.69	12.73	11.27	0.13	4.90	7.34	3.99	0.20	0.10	0.01	1.72
PM018D	Kl	A	53.21	0.87	13.85	11.36	0.19	4.62	8.75	4.54	0.94	0.13	0.01	1.35
PM019D	Kl	A	48.01	1.19	13.92	14.21	0.18	5.41	9.36	2.99	1.73	0.09	0.02	2.42
PM020D	Kl	A	54.72	0.84	13.63	11.00	0.16	3.53	9.74	4.18	0.96	0.13	0.01	1.00
PM021D	Kl	A	44.08	0.74	4.00	15.89	0.27	20.16	7.21	0.09	0.02	0.06	0.15	7.10
PM022D	Kl	A	52.00	0.93	15.30	11.01	0.21	3.65	8.89	4.64	0.85	0.13	0.02	1.82
PM023D	Kl	A	53.91	1.17	14.72	10.35	0.21	4.19	8.15	5.29	0.32	0.18	0.03	1.32
PM024D	Kl	A	46.03	0.59	3.00	17.53	0.16	23.66	2.91	0.06	0.02	0.03	0.16	5.87
PM025D	Kl	A	64.56	0.86	11.92	9.60	0.10	2.98	4.66	3.42	0.37	0.10	0.01	1.48
KA102	Kl	B	55.49	1.09	15.62	11.60	0.11	5.69	5.39	4.09	0.75	0.16	ND	3.47
KA104	Kl	B	55.29	1.08	14.92	10.72	0.15	4.85	7.27	4.00	1.54	0.18	ND	3.51
KA106	Kl	B	55.46	1.02	15.00	10.66	0.14	4.71	8.18	3.38	1.29	0.17	ND	3.36
KA291	Kl	B	56.60	1.05	15.39	11.74	0.12	5.07	5.23	3.92	0.74	0.14	ND	3.48
KA347	Kl	B	58.13	1.01	14.13	10.10	0.14	4.89	6.43	4.46	0.58	0.14	ND	2.25
KA348	Kl	B	53.26	1.08	15.13	12.27	0.13	5.16	8.13	2.80	0.87	0.17	ND	2.23
KA376	Kl	B	52.77	1.17	16.66	12.23	0.16	4.66	6.81	3.39	1.97	0.17	ND	5.54
KA452	Kl	B	53.91	1.05	13.76	12.30	0.15	6.57	9.52	2.23	1.38	0.14	ND	4.15
NL793	Kl	B	55.45	1.27	14.08	13.17	0.14	4.22	7.03	3.76	0.69	0.19	ND	1.96
100 532	Kl	C	53.70	1.05	14.50	9.17	0.14	4.73	7.63	2.77	1.74	0.15	ND	ND
KL131	Kl	B	54.10	0.77	13.79	11.51	0.18	6.62	7.12	3.72	2.09	0.10	ND	1.79
KL134	Kl	B	56.31	0.65	12.53	10.72	0.18	6.54	9.15	3.12	0.72	0.08	ND	2.02
KL135	Kl	B	53.10	0.49	10.35	11.88	0.18	13.62	8.29	1.85	0.18	0.05	ND	3.35

Sample	Loc	Ref	SiO_2	TiO_2	Al_2O_3	Fe_2O_3 (t)	MnO	MgO	CaO	Na_2O	K_2O	P_2O_5	Cr_2O_3	LOI
KL138	Kl	B	51.82	0.69	15.13	11.94	0.20	6.84	8.46	3.37	1.46	0.09	ND	2.94
KL140	Kl	B	53.32	0.53	11.30	10.99	0.21	9.91	9.44	2.39	1.85	0.06	ND	1.55
KL141	Kl	B	52.54	0.57	11.87	11.69	0.18	10.60	9.21	1.58	1.68	0.08	ND	2.74
KL142	Kl	B	50.97	0.63	13.46	12.06	0.18	8.33	10.55	3.08	0.68	0.06	ND	2.69
KL146	Kl	B	51.77	0.52	12.72	11.08	0.19	12.87	7.19	1.98	1.60	0.08	ND	4.00
KL152	Kl	B	56.82	0.64	14.24	13.23	0.15	5.23	6.91	3.38	2.27	0.13	ND	2.02
KL153	Kl	B	52.25	0.74	15.38	12.10	0.23	7.11	6.29	3.31	2.49	0.10	ND	2.57
KL154	Kl	B	53.59	0.48	12.73	10.79	0.18	10.75	7.75	2.16	1.52	0.07	ND	3.12
KL157	Kl	B	54.23	0.42	10.58	10.86	0.17	14.27	7.68	1.64	0.12	0.04	ND	4.40
KL159	Kl	B	53.82	0.41	10.57	11.24	0.19	14.07	7.94	1.40	0.28	0.07	ND	4.42
KL204	Kl	B	55.60	0.50	12.42	10.17	0.17	9.22	7.99	2.39	1.47	0.07	ND	2.54
KL467	Kl	B	56.34	0.74	14.47	10.90	0.14	5.53	7.90	3.09	0.82	0.08	ND	2.08
KL468	Kl	B	52.81	0.40	8.59	12.17	0.17	17.46	8.06	0.19	0.11	0.04	ND	4.95
100 527	Kl	C	50.20	0.40	10.00	8.49	0.20	13.20	8.50	0.93	1.03	0.05	ND	ND
100 528	Kl	C	53.80	0.74	14.20	9.44	0.16	5.91	6.98	3.24	1.32	0.09	ND	ND
100 529	Kl	C	52.10	0.64	12.80	9.27	0.18	7.56	9.57	2.70	0.58	0.07	ND	ND
KO109	Kl	B	53.80	1.08	14.90	13.94	0.17	5.53	5.81	3.43	1.22	0.13	ND	2.19
KO110	Kl	B	54.30	1.05	14.77	13.22	0.15	5.19	6.49	3.91	0.79	0.12	ND	2.00
KO111	Kl	B	52.31	1.10	15.54	14.46	0.17	5.49	5.66	3.90	0.95	0.13	ND	2.11
KO112	Kl	B	53.26	1.00	14.96	12.77	0.15	4.49	9.82	2.69	0.76	0.12	ND	1.89
KO118	Kl	B	53.26	0.93	15.05	11.78	0.13	4.80	10.66	2.91	0.34	0.13	ND	2.34
KO126	Kl	B	51.87	0.93	15.27	12.87	0.16	5.47	8.24	3.22	1.85	0.12	ND	1.98
KO129	Kl	B	51.11	1.01	15.59	13.72	0.16	4.85	9.28	3.22	0.91	0.13	ND	2.05
KO130	Kl	B	55.65	0.90	14.59	11.55	0.16	4.47	7.58	2.32	2.63	0.14	ND	2.25
KO295	Kl	B	55.55	1.07	14.66	13.47	0.15	5.23	5.52	3.34	0.90	0.12	ND	2.89
NL791	Kl	B	54.19	0.98	15.07	12.62	0.14	5.01	7.34	3.87	0.67	0.13	ND	2.17
100 530	Kl	C	53.40	0.93	14.20	9.99	0.17	5.07	7.84	3.16	1.08	0.12	ND	ND
100 531	Kl	C	54.10	1.00	14.30	9.89	0.15	4.60	6.92	3.15	1.97	0.12	ND	ND
100 521	Pl	C	58.40	1.45	11.30	9.50	0.07	6.12	3.26	0.09	0.42	0.74	ND	ND
100 522	Pl	C	56.60	1.32	13.50	7.31	0.13	4.03	6.13	3.97	0.21	0.58	ND	ND
100 523	Pl	C	63.90	1.15	13.00	5.62	0.11	2.34	2.49	2.26	2.98	0.48	ND	ND
100 524	Pl	C	69.30	0.93	11.00	5.34	0.10	1.91	2.44	1.47	3.28	0.38	ND	ND
FVM216	Pl	D	64.44	1.04	12.59	5.87	0.10	0.87	3.70	2.08	4.56	0.39	ND	3.59
FVM217	Pl	D	64.82	1.06	12.53	5.96	0.10	1.33	3.44	3.16	3.63	0.39	ND	2.96
FVM293	Pl	D	63.29	1.18	13.95	7.29	0.09	2.27	2.57	2.17	2.77	0.48	ND	2.43
FVM294	Pl	D	62.95	1.11	13.24	6.42	0.10	1.76	3.31	2.03	3.12	0.44	ND	3.17
FVM295	Pl	D	65.74	1.06	12.64	6.19	0.09	0.55	3.23	2.88	3.78	0.42	ND	2.32
FVM361	Pl	D	69.68	0.70	12.71	4.31	0.05	0.88	1.90	2.41	5.33	0.21	ND	1.89
FVM362	Pl	D	71.04	0.66	12.73	3.72	0.05	0.92	1.40	2.38	5.51	0.19	ND	1.51
FVM227	Pl	D	72.90	0.36	11.98	1.82	0.06	0.66	1.75	1.19	6.98	0.06	ND	1.87
FVM228	Pl	D	75.81	0.36	11.81	1.60	0.04	1.54	1.21	1.39	6.55	0.06	ND	1.45
FVM229	Pl	D	74.87	0.36	11.93	1.90	0.04	0.60	1.09	3.44	4.39	0.06	ND	1.38
FVM379	Pl	D	73.22	0.59	13.42	3.16	0.04	1.36	0.36	0.53	5.76	0.16	ND	1.91
FVM380	Pl	D	72.44	0.64	13.59	3.06	0.05	1.29	1.09	0.40	5.66	0.18	ND	2.54
FVM345	Pl	D	50.98	1.40	13.71	9.48	0.12	4.60	6.65	1.87	1.42	0.58	ND	6.56
FVM322	Pl	D	65.09	1.33	13.29	6.71	0.11	1.20	3.48	4.10	2.28	0.48	ND	1.53
FVM323	Pl	D	62.98	1.26	12.81	7.50	0.11	1.30	4.17	3.24	3.38	0.45	ND	2.19
FVM324	Pl	D	62.92	1.27	12.86	7.01	0.10	1.22	4.31	3.53	3.21	0.46	ND	2.34
FVM401	Pl	D	63.24	1.28	12.38	6.39	0.09	1.13	3.82	2.40	3.60	0.46	ND	3.40
FVM402	Pl	D	62.56	1.32	13.25	7.12	0.09	1.75	3.54	1.18	4.12	0.48	ND	3.67
FVM403	Pl	D	62.19	1.27	12.58	6.78	0.12	1.61	4.06	1.86	3.97	0.45	ND	3.97
100 525	Pl	C	53.60	1.39	14.50	7.55	0.12	3.58	5.99	3.82	2.36	0.62	ND	ND
100 526	Pl	C	54.60	1.57	13.70	8.26	0.16	5.15	6.12	3.35	0.83	0.72	ND	ND
J1A	Pn	E	50.50	1.52	14.80	13.20	0.17	6.02	4.20	3.74	0.30	0.70	ND	4.91
J2A	Pn	E	58.90	1.13	13.90	9.10	0.09	1.87	4.55	4.88	1.62	0.20	ND	4.09
J3A	Pn	E	58.70	1.11	13.90	9.20	0.09	1.86	4.50	4.92	1.63	0.21	ND	3.98
J4A	Pn	E	56.80	0.65	14.60	9.00	0.11	4.74	5.68	3.35	1.49	0.11	ND	3.66
J5A	Pn	E	60.70	1.12	13.80	10.70	0.11	3.48	2.39	2.86	2.45	0.20	ND	3.14
J6A	Pn	E	51.40	1.64	15.40	10.10	0.11	5.94	4.56	4.79	0.60	0.84	ND	4.92
J7A	Pn	E	57.30	1.14	14.00	10.00	0.11	3.39	5.60	4.78	1.11	0.19	ND	2.39
J9A	Pn	E	54.70	1.13	13.20	10.30	0.13	4.70	6.22	4.05	1.10	0.21	ND	4.47
J10A	Pn	E	55.50	1.17	14.10	9.80	0.12	3.83	5.49	3.73	1.50	0.32	ND	4.79
100 519	Pn	C	52.80	1.19	13.10	10.06	0.15	4.40	5.88	4.11	1.30	0.24	ND	ND
100 520	Pn	C	55.40	1.11	13.10	9.07	0.14	3.28	5.60	3.76	1.93	0.18	ND	ND

11.5 TRACE ELEMENT GEOCHEMICAL ANALYSES

Table 19. Trace element analyses of selected samples collected from the Ventersdorp Supergroup (elements Ni – La). Ref refers to analyses/samples ascertained from Dhansay *et al.* (2022) (A), Marsh *et al.* (1992) (B), Nelson *et al.* (1992) (C), Meintjes and Van der Westhuizen (2018) (D), Crow and Condie (1988) (E). Location information consistent with that presented in Table 18.

Sample	Ref	Ni	Cr	V	Sc	Co	Cu	Zn	Ga	Rb	Sr	Y	Zr	Nb	Cs	Ba	La
DBS002D	A	113.80	27.90	191.70	21.20	61.90	122.50	94.70	22.00	84.40	221.80	20.00	104.60	5.00	5.00	681.20	8.70
DBS003D	A	299.90	475.90	198.80	12.50	64.70	80.30	100.10	15.40	62.30	209.90	17.20	70.40	5.00	5.00	618.00	11.40
DBS004D	A	144.40	23.60	185.70	20.50	63.50	104.40	95.20	17.90	117.70	218.40	20.00	103.00	5.00	5.00	983.30	7.80
DBS005D	A	156.60	31.20	189.30	21.40	65.10	136.50	114.30	23.20	42.10	457.80	20.10	100.00	5.00	5.00	590.70	15.70
DBS006D	A	167.30	42.00	167.70	18.50	69.40	77.20	154.20	19.90	48.30	559.20	21.60	120.40	5.10	5.00	428.80	16.10
DBS007D	A	128.20	68.60	133.30	16.10	54.50	43.20	88.30	21.00	24.20	118.80	17.30	112.10	5.40	5.00	114.00	13.10
DBS010D	A	109.20	147.30	207.50	20.40	67.00	85.60	140.30	24.70	59.70	344.60	30.50	115.00	5.70	5.00	441.20	10.70
DBS011D	A	205.80	274.50	191.70	24.60	67.10	80.80	118.30	18.00	28.30	219.70	17.00	89.60	5.00	5.00	266.70	14.80
DBS012D	A	125.10	38.40	179.40	22.50	65.90	95.70	107.10	23.30	53.60	411.20	19.00	101.10	5.00	5.00	486.70	12.80
DBS013D	A	169.50	24.40	198.00	26.40	77.30	62.00	121.30	20.80	80.50	50.20	20.10	119.30	5.80	5.20	359.90	11.10
DBS014D	A	138.20	18.00	185.30	20.30	62.80	130.10	116.00	19.70	56.00	388.50	20.20	99.20	5.00	5.00	622.60	13.80
DBS016D	A	183.10	48.80	175.00	20.80	66.20	83.20	133.60	23.10	13.80	139.00	21.90	121.70	5.90	5.00	112.80	17.10
DBS017D	A	157.80	70.60	162.40	14.10	63.10	79.20	109.90	20.60	50.00	412.30	21.50	120.30	5.60	5.00	755.80	17.00
DBS020D	A	2 027.40	1 536.80	97.50	10.20	152.60	177.10	153.90	7.30	5.00	48.90	8.10	55.30	9.80	5.00	5.00	5.00
PM001D	A	212.70	298.30	118.80	24.10	69.60	93.90	95.80	21.10	26.90	84.40	17.60	92.70	5.00	6.60	132.80	10.20
PM002D	A	196.00	208.10	163.30	23.60	66.80	52.20	82.50	20.40	17.70	171.90	16.00	80.40	5.00	5.00	95.10	17.60
PM003D	A	128.60	198.10	129.20	15.30	43.50	41.10	69.10	14.10	23.30	73.40	11.60	50.40	5.00	5.00	144.00	6.20
PM005D	A	130.70	50.30	175.50	19.60	58.40	135.60	95.50	26.80	10.90	390.60	20.30	96.20	5.00	5.00	46.90	11.30
PM006D	A	53.40	31.00	166.60	20.40	51.30	7.80	28.50	34.90	5.00	437.60	15.60	72.10	5.00	5.00	5.10	13.90
PM007D	A	119.00	29.10	130.90	19.10	45.20	62.40	64.50	24.20	21.90	270.60	18.80	101.50	5.00	5.00	77.60	11.00
PM009D	A	148.70	20.10	169.90	21.50	65.40	89.90	108.60	21.30	13.00	86.20	19.50	100.60	5.10	5.00	74.50	6.60
PM010D	A	186.10	207.60	172.90	17.50	65.70	64.60	87.50	25.40	8.80	146.70	20.10	76.50	5.00	5.00	53.80	8.80
PM011D	A	142.40	70.60	170.80	21.40	58.70	152.20	87.70	26.10	22.80	191.70	21.00	116.80	5.60	5.00	116.20	18.00
PM012D	A	154.00	122.20	139.90	13.60	52.40	145.30	135.20	20.40	14.60	93.30	15.90	109.20	5.00	5.00	81.80	11.90
PM013D	A	144.60	119.30	145.40	14.60	54.50	130.10	99.10	23.90	37.90	637.20	22.00	144.00	6.60	5.00	1 802.10	23.70
PM015D	A	2 049.30	1 159.50	83.90	9.50	143.90	149.20	129.20	6.00	5.00	46.70	7.10	50.90	8.90	5.00	5.00	11.50
PM016D	A	96.20	149.30	196.00	7.90	55.90	55.30	109.70	20.00	12.70	210.60	28.40	108.90	5.50	5.00	128.30	15.80
PM017D	A	125.40	26.40	143.40	17.40	58.10	66.10	109.90	21.40	5.90	60.10	13.00	75.90	5.00	5.00	38.10	11.90
PM019D	A	139.80	85.60	244.00	21.50	65.40	97.70	121.70	28.50	49.90	121.70	24.80	133.70	7.40	5.00	248.10	32.70
PM020D	A	128.90	60.50	167.40	18.00	51.30	137.20	92.80	22.10	27.90	110.20	17.60	98.10	5.00	5.00	129.30	13.30
PM021D	A	1 125.90	1 302.30	105.80	13.10	97.10	237.30	183.40	8.10	5.00	243.70	10.70	63.70	9.80	5.00	14.30	23.20
PM023D	A	158.90	165.60	148.20	20.00	51.90	129.50	267.80	24.70	6.30	389.10	22.10	139.60	5.80	5.00	68.70	14.90
PM024D	A	2 073.60	1 282.00	83.20	10.20	154.80	158.70	171.80	5.40	5.00	94.20	6.50	45.30	7.20	5.00	6.30	7.00
PM025D	A	119.20	62.90	128.80	14.20	51.10	75.50	89.30	21.90	10.20	139.80	21.50	102.50	5.00	5.00	45.00	16.00
KA102	B	172.00	98.00	201.00	19.80	65.00	88.00	86.00	ND	29.00	232.00	23.00	126.00	6.20	ND	226.00	ND
KA104	B	164.00	64.00	169.00	19.20	57.00	107.00	84.00	ND	52.00	396.00	22.50	124.00	6.20	ND	495.00	ND
KA106	B	159.00	66.00	168.00	19.00	57.00	108.00	82.00	ND	47.00	517.00	21.70	117.00	4.90	ND	344.00	15.30
KA291	B	167.00	81.00	180.00	18.10	59.00	72.00	92.00	ND	26.00	560.00	21.40	122.00	5.50	ND	304.00	ND
KA347	B	101.00	124.00	179.00	17.50	54.00	77.00	67.00	ND	12.00	257.00	20.70	108.00	5.20	ND	204.00	ND
KA348	B	167.00	64.00	171.00	16.50	63.00	122.00	103.00	ND	27.00	588.00	23.70	118.00	6.40	ND	391.00	ND
KA376	B	173.00	86.00	188.00	19.70	59.00	59.00	95.00	ND	64.00	249.00	22.40	137.00	6.00	ND	355.00	ND
KA452	B	226.00	415.00	194.00	21.80	64.00	109.00	73.00	ND	10.00	566.00	22.00	106.00	4.00	ND	241.00	ND
NL793	B	191.00	71.00	206.00	ND	68.00	70.00	100.00	ND	30.00	172.00	26.60	133.00	8.30	ND	281.00	ND
100 532	C	169.00	61.00	170.00	20.00	61.00	113.00	90.00	ND	68.00	466.00	20.00	141.00	7.00	ND	ND	17.50
KL131	B	172.00	272.00	193.00	25.00	64.00	79.00	90.00	ND	75.00	64.00	19.10	86.00	3.20	ND	328.00	10.10
KL134	B	190.00	400.00	195.00	23.40	59.00	71.00	77.00	ND	20.00	155.00	17.80	68.00	2.00	ND	179.00	ND
KL135	B	438.00	2 086.00	171.00	29.40	78.00	52.00	78.00	ND	9.00	54.00	12.50	43.00	ND	ND	70.00	4.80
KL138	B	166.00	251.00	197.00	26.70	67.00	80.00	81.00	ND	43.00	173.00	18.40	71.00	2.20	ND	644.00	9.00
KL140	B	281.00	783.00	201.00	46.60	66.00	55.00	81.00	ND	55.00	107.00	14.60	45.00	ND	ND	468.00	6.00
KL141	B	308.00	900.00	219.00	36.50	75.00	64.00	76.00	ND	80.00	270.00	14.90	52.00	ND	ND	599.00	4.30
KL142	B	221.00	475.00	224.00	32.90	71.00	79.00	93.00	ND	20.00	208.00	17.40	56.00	1.80	ND	206.00	6.50
KL146	B	422.00	1 369.00	190.00	27.70	72.00	48.00	118.00	ND	60.00	109.00	12.70	60.00	2.30	ND	433.00	6.70
KL152	B	145.00	156.00	132.00	25.10	56.00	80.00	74.00	ND	74.00	314.00	18.60	75.00	2.40	ND	735.00	ND
KL153	B	163.00	171.00	207.00	30.10	67.00	82.00	97.00	ND	59.00	140.00	20.20	81.00	3.00	ND	680.00	ND
KL154	B	294.00	1 200.00	156.00	25.00	69.00	56.00	92.00	ND	61.00	361.00	14.60	56.00	ND	ND	435.00	8.20

Sample	Ref	Ni	Cr	V	Sc	Co	Cu	Zn	Ga	Rb	Sr	Y	Zr	Nb	Cs	Ba	La
KL157	B	402.00	2 289.00	171.00	29.20	76.00	45.00	114.00	ND	4.00	137.00	12.40	41.00	ND	ND	49.00	5.60
KL159	B	405.00	1 771.00	171.00	31.50	78.00	40.00	112.00	ND	9.00	180.00	12.20	41.00	ND	ND	120.00	4.20
KL204	B	258.00	1 032.00	180.00	25.80	62.00	52.00	84.00	ND	51.00	67.00	16.50	66.00	2.20	ND	419.00	ND
KL467	B	123.00	186.00	206.00	29.50	57.00	88.00	73.00	ND	25.00	498.00	20.60	78.00	3.40	ND	262.00	ND
KL468	B	516.00	2 618.00	178.00	27.70	88.00	43.00	76.00	ND	8.00	20.00	10.40	34.00	ND	ND	16.00	3.90
100 527	C	418.00	1 831.00	156.00	26.00	72.00	56.00	105.00	ND	47.00	97.00	12.00	47.00	7.00	ND	ND	5.90
100 528	C	174.00	194.00	191.00	29.00	64.00	96.00	112.00	ND	46.00	305.00	17.00	96.00	7.00	ND	ND	12.10
100 529	C	249.00	441.00	205.00	33.00	71.00	89.00	88.00	ND	25.00	342.00	15.00	76.00	7.00	ND	ND	8.60
KO109	B	163.00	72.00	249.00	27.00	75.00	104.00	105.00	ND	44.00	332.00	23.60	103.00	4.20	ND	505.00	ND
KO110	B	160.00	79.00	239.00	25.80	74.00	113.00	95.00	ND	28.00	269.00	23.40	104.00	5.60	ND	549.00	12.40
KO111	B	163.00	72.00	258.00	28.80	79.00	112.00	107.00	ND	34.00	282.00	24.80	109.00	5.40	ND	278.00	13.20
KO112	B	152.00	65.00	234.00	25.30	75.00	119.00	93.00	ND	27.00	671.00	23.40	98.00	6.60	ND	251.00	14.10
KO118	B	143.00	49.00	228.00	20.40	63.00	65.00	76.00	ND	11.00	781.00	22.10	91.00	3.10	ND	128.00	ND
KO126	B	133.00	26.00	209.00	23.20	63.00	96.00	94.00	ND	66.00	247.00	21.60	96.00	4.50	ND	453.00	12.00
KO129	B	131.00	28.00	235.00	26.60	72.00	103.00	104.00	ND	34.00	207.00	25.50	107.00	5.70	ND	178.00	ND
KO130	B	111.00	16.00	215.00	26.20	59.00	91.00	87.00	ND	109.00	411.00	21.20	97.00	4.60	ND	816.00	11.60
KO295	B	161.00	60.00	208.00	22.60	76.00	68.00	105.00	ND	32.00	197.00	21.30	110.00	5.40	ND	233.00	ND
NL791	B	169.00	69.00	222.00	ND	69.00	65.00	97.00	ND	29.00	258.00	21.40	100.00	4.80	ND	276.00	ND
100 530	C	155.00	59.00	198.00	24.00	62.00	105.00	91.00	ND	45.00	471.00	21.00	120.00	7.00	ND	ND	15.00
100 531	C	173.00	49.00	210.00	24.00	71.00	122.00	98.00	ND	85.00	404.00	19.00	120.00	7.00	ND	ND	14.00
100 521	C	100.00	202.00	226.00	17.00	45.00	29.00	132.00	ND	16.00	80.00	39.00	274.00	14.00	ND	ND	50.40
100 522	C	109.00	247.00	184.00	17.00	43.00	34.00	125.00	ND	3.00	927.00	44.00	407.00	19.00	ND	ND	63.20
100 523	C	23.00	13.00	94.00	12.00	28.00	11.00	119.00	ND	138.00	275.00	60.00	537.00	25.00	ND	ND	97.50
100 524	C	22.00	11.00	86.00	12.00	49.00	5.00	124.00	ND	144.00	182.00	51.00	436.00	19.00	ND	ND	84.90
FVM216	D	10.00	14.00	100.00	ND	11.00	3.00	96.00	ND	138.00	302.00	54.00	448.00	17.00	ND	1 545.00	104.86
FVM217	D	11.00	18.00	106.00	ND	14.00	6.00	134.00	ND	98.00	322.00	54.00	446.00	17.00	ND	1 283.00	103.60
FVM293	D	19.00	25.00	113.00	ND	14.00	5.00	129.00	ND	113.00	370.00	64.00	487.00	23.00	ND	1 144.00	100.53
FVM294	D	18.00	27.00	107.00	ND	10.00	12.00	106.00	ND	130.00	222.00	61.00	507.00	22.00	ND	987.00	97.85
FVM295	D	17.00	21.00	101.00	ND	14.00	6.00	105.00	ND	92.00	368.00	58.00	474.00	20.00	ND	1 400.00	112.86
FVM361	D	17.00	30.00	70.00	ND	8.00	7.00	44.00	ND	164.00	172.00	49.00	433.00	18.00	ND	1 589.00	113.65
FVM362	D	16.00	27.00	63.00	ND	9.00	4.00	57.00	ND	150.00	168.00	46.00	417.00	18.00	ND	1 755.00	101.99
FVM227	D	5.00	14.00	19.00	ND	8.00	2.00	80.00	ND	211.00	81.00	49.00	297.00	18.00	ND	1 243.00	111.88
FVM228	D	6.00	13.00	18.00	ND	7.00	4.00	43.00	ND	206.00	85.00	43.00	282.00	17.00	ND	1 338.00	95.55
FVM229	D	7.00	13.00	23.00	ND	4.00	2.00	78.00	ND	139.00	77.00	42.00	299.00	17.00	ND	872.00	101.60
FVM379	D	13.00	18.00	49.00	ND	6.00	5.00	65.00	ND	165.00	46.00	46.00	387.00	18.00	ND	1 555.00	83.07
FVM380	D	11.00	17.00	48.00	ND	5.00	2.00	46.00	ND	172.00	49.00	48.00	426.00	18.00	ND	1 426.00	97.82
FVM345	D	119.00	316.00	201.00	ND	25.00	12.00	145.00	ND	34.00	269.00	46.00	324.00	15.00	ND	715.00	37.74
FVM322	D	24.00	21.00	121.00	ND	14.00	30.00	160.00	ND	48.00	319.00	66.00	654.00	21.00	ND	1 066.00	116.16
FVM323	D	14.00	17.00	116.00	ND	11.00	4.00	155.00	ND	77.00	306.00	64.00	631.00	21.00	ND	1 321.00	116.15
FVM324	D	14.00	19.00	112.00	ND	12.00	5.00	141.00	ND	77.00	302.00	62.00	624.00	20.00	ND	1 462.00	110.39
FVM401	D	14.00	17.00	120.00	ND	9.00	3.00	66.00	ND	81.00	111.00	58.00	625.00	20.00	ND	1 119.00	103.34
FVM402	D	14.00	19.00	173.00	ND	8.00	2.00	75.00	ND	143.00	86.00	69.00	649.00	21.00	ND	1 100.00	84.25
FVM403	D	15.00	18.00	129.00	ND	4.00	9.00	88.00	ND	122.00	148.00	65.00	617.00	21.00	ND	1 238.00	107.14
100 525	C	87.00	151.00	184.00	18.00	40.00	39.00	123.00	ND	55.00	376.00	42.00	354.00	15.00	ND	ND	63.00
100 526	C	102.00	140.00	197.00	22.00	39.00	39.00	129.00	ND	20.00	560.00	46.00	351.00	15.00	ND	ND	69.50
J1A	E	125.00	15.00	196.00	17.30	56.00	ND	ND	ND	14.40	458.00	25.20	197.30	11.90	0.20	204.00	27.90
J2A	E	97.00	12.00	165.00	17.10	53.00	ND	ND	ND	37.40	664.00	22.70	186.80	10.20	0.60	604.00	29.60
J3A	E	90.00	12.00	155.00	16.20	54.00	ND	ND	ND	43.50	859.00	22.50	181.60	10.00	1.10	739.00	29.80
J4A	E	107.00	11.00	232.00	16.10	50.00	ND	ND	ND	63.10	204.00	25.20	194.00	13.00	1.10	296.00	22.90
J5A	E	81.00	9.00	173.00	13.40	43.00	ND	ND	ND	43.10	105.00	20.80	165.80	10.20	0.40	884.00	23.40
J6A	E	94.00	9.00	165.00	13.70	47.00	ND	ND	ND	25.10	410.00	21.20	175.00	9.10	0.90	532.00	24.40
J7A	E	98.00	10.00	150.00	14.00	46.00	ND	ND	ND	26.20	958.00	21.80	189.60	10.10	17.50	463.00	26.20
J9A	E	117.00	47.00	180.00	15.90	48.00	ND	ND	ND	22.50	534.00	21.00	180.00	10.80	0.60	5.00	25.20
J10A	E	99.00	15.00	176.00	15.28	49.00	ND	ND	ND	44.12	491.00	22.99	182.63	10.62	2.77	459.00	26.29
100 519	C	192.00	34.00	168.00	16.00	65.00	147.00	128.00	ND	35.00	1 256.00	21.00	217.00	8.00	ND	ND	24.30
100 520	C	109.00	8.00	148.00	13.00	59.00	147.00	152.00	ND	45.00	841.00	23.00	206.00	10.00	ND	ND	27.50

Table 20. Trace element analyses of selected samples collected from the Ventersdorp Supergroup (elements Ce–U). Ref refers to analyses/samples ascertained from Dhansay *et al*. (2022) (A), Marsh *et al*. (1992) (B), Nelson *et al*. (1992) (C), Meintjes and Van der Westhuizen (2018) (D), Crow and Condie (1988) (E). Location information consistent with that presented in Table 18.

Sample	Ref	Ce	Pr	ND	Sm	Eu	Gd	Tb	Dy	Ho	Er	Yb	Lu	Hf	Ta	Pb	Th	U
DBS002D	A	5.00	ND	13.10	5.00	ND	ND	ND	ND	ND	ND	5.00	ND	5.00	5.00	5.00	5.00	5.00
DBS003D	A	5.00	ND	6.20	5.00	ND	ND	ND	ND	ND	ND	5.00	ND	5.20	5.00	5.00	5.00	5.00
DBS004D	A	29.00	ND	17.80	5.00	ND	ND	ND	ND	ND	ND	5.00	ND	5.00	5.00	5.00	5.00	5.00
DBS005D	A	5.00	ND	15.70	5.00	ND	ND	ND	ND	ND	ND	5.00	ND	5.00	5.00	5.00	5.00	5.00
DBS006D	A	19.90	ND	16.30	5.00	ND	ND	ND	ND	ND	ND	5.00	ND	5.00	5.00	5.00	5.00	5.00
DBS007D	A	8.70	ND	15.40	5.00	ND	ND	ND	ND	ND	ND	5.00	ND	6.60	5.00	5.00	5.00	5.00
DBS010D	A	6.70	ND	12.40	5.00	ND	ND	ND	ND	ND	ND	5.00	ND	5.00	5.00	5.00	5.00	5.00
DBS011D	A	5.00	ND	13.00	5.00	ND	ND	ND	ND	ND	ND	5.00	ND	5.00	5.00	5.00	5.00	5.00
DBS012D	A	5.00	ND	8.00	5.00	ND	ND	ND	ND	ND	ND	5.00	ND	5.00	5.00	5.00	5.00	5.00
DBS013D	A	5.00	ND	9.60	5.00	ND	ND	ND	ND	ND	ND	5.00	ND	5.20	5.00	5.00	5.00	5.00
DBS014D	A	10.90	ND	16.30	5.00	ND	ND	ND	ND	ND	ND	5.00	ND	5.00	5.00	5.00	5.00	5.00
DBS016D	A	7.90	ND	15.40	5.00	ND	ND	ND	ND	ND	ND	5.00	ND	5.00	5.00	5.00	5.00	5.00
DBS017D	A	15.60	ND	20.40	5.00	ND	ND	ND	ND	ND	ND	5.00	ND	5.00	5.00	5.00	5.00	5.00
DBS020D	A	5.00	ND	7.60	5.00	ND	ND	ND	ND	ND	ND	5.00	ND	5.00	5.00	5.00	5.00	5.00
PM001D	A	6.00	ND	12.00	5.00	ND	ND	ND	ND	ND	ND	5.00	ND	5.00	5.00	5.00	5.00	5.00
PM002D	A	8.80	ND	7.60	5.00	ND	ND	ND	ND	ND	ND	5.00	ND	5.00	5.00	5.00	5.00	5.00
PM003D	A	5.00	ND	8.50	6.80	ND	ND	ND	ND	ND	ND	5.00	ND	5.00	5.00	5.00	5.00	5.00
PM005D	A	5.00	ND	11.60	5.00	ND	ND	ND	ND	ND	ND	5.00	ND	5.00	5.00	5.00	5.00	5.00
PM006D	A	5.00	ND	8.80	5.00	ND	ND	ND	ND	ND	ND	5.00	ND	5.00	5.00	10.60	5.00	5.00
PM007D	A	19.20	ND	19.40	5.00	ND	ND	ND	ND	ND	ND	5.00	ND	5.00	5.00	9.50	5.00	5.00
PM009D	A	19.60	ND	19.20	5.00	ND	ND	ND	ND	ND	ND	5.00	ND	5.00	5.00	5.00	5.00	5.00
PM010D	A	11.00	ND	11.80	5.00	ND	ND	ND	ND	ND	ND	5.00	ND	5.00	5.00	5.00	5.00	5.00
PM011D	A	13.40	ND	14.80	5.00	ND	ND	ND	ND	ND	ND	5.00	ND	6.00	5.00	5.00	5.00	5.00
PM012D	A	5.20	ND	11.60	5.00	ND	ND	ND	ND	ND	ND	5.00	ND	5.10	5.00	5.00	5.00	5.00
PM013D	A	15.20	ND	19.10	5.00	ND	ND	ND	ND	ND	ND	5.00	ND	5.00	5.00	5.00	5.00	5.00
PM015D	A	5.00	ND	6.10	5.10	ND	ND	ND	ND	ND	ND	5.00	ND	5.00	5.00	5.00	5.00	5.00
PM016D	A	5.00	ND	10.30	5.00	ND	ND	ND	ND	ND	ND	5.00	ND	5.30	5.00	5.00	5.00	5.00
PM017D	A	5.00	ND	11.00	5.00	ND	ND	ND	ND	ND	ND	5.00	ND	5.00	5.00	5.00	5.00	5.00
PM019D	A	37.20	ND	24.60	5.60	ND	ND	ND	ND	ND	ND	5.00	ND	5.00	5.00	5.00	5.00	5.00
PM020D	A	5.00	ND	11.60	9.00	ND	ND	ND	ND	ND	ND	5.00	ND	5.00	5.00	5.40	5.00	5.00
PM021D	A	20.80	ND	17.90	5.00	ND	ND	ND	ND	ND	ND	5.00	ND	5.00	5.00	5.00	5.00	5.00
PM023D	A	27.50	ND	18.80	5.00	ND	ND	ND	ND	ND	ND	5.00	ND	5.00	5.00	388.60	5.00	5.00
PM024D	A	5.00	ND	6.30	5.00	ND	ND	ND	ND	ND	ND	5.00	ND	5.00	5.00	5.00	5.00	5.00
PM025D	A	25.40	ND	17.30	14.50	ND	ND	ND	ND	ND	ND	5.00	ND	5.00	5.00	5.00	5.00	5.00
KA102	B	ND	ND	ND	ND	ND	ND	ND	ND	ND	ND	ND	ND	ND	ND	ND	ND	ND
KA104	B	ND	ND	ND	ND	ND	ND	ND	ND	ND	ND	ND	ND	ND	ND	ND	ND	ND
KA106	B	33.00	ND	17.20	3.78	1.27	ND	0.61	ND	ND	ND	1.56	0.24	3.10	0.39	ND	2.03	ND
KA291	B	ND	ND	ND	ND	ND	ND	ND	ND	ND	ND	ND	ND	ND	ND	ND	ND	ND
KA347	B	ND	ND	ND	ND	ND	ND	ND	ND	ND	ND	ND	ND	ND	ND	ND	ND	ND
KA348	B	ND	ND	ND	ND	ND	ND	ND	ND	ND	ND	ND	ND	ND	ND	ND	ND	ND
KA376	B	ND	ND	ND	ND	ND	ND	ND	ND	ND	ND	ND	ND	ND	ND	ND	ND	ND
KA452	B	ND	ND	ND	ND	ND	ND	ND	ND	ND	ND	ND	ND	ND	ND	ND	ND	ND
NL793	B	ND	ND	ND	ND	ND	ND	ND	ND	ND	ND	ND	ND	ND	ND	ND	ND	ND
100 532	C	33.90	ND	17.90	4.29	1.46	4.12	ND	3.70	0.74	2.02	1.73	0.25	ND	ND	ND	3.00	2.00
KL131	B	20.50	ND	10.30	2.67	0.73	ND	0.47	ND	ND	ND	1.52	0.27	2.34	0.28	ND	1.55	
KL134	B	ND	ND	ND	ND	ND	ND	ND	ND	ND	ND	ND	ND	ND	ND	ND	ND	ND
KL135	B	11.40	ND	6.70	1.57	0.47	ND	0.31	ND	ND	ND	1.08	0.19	1.27	0.14	ND	1.28	ND
KL138	B	18.50	ND	8.90	2.23	0.82	ND	0.42	ND	ND	ND	1.45	0.25	1.92	0.22	ND	1.41	ND
KL140	B	13.40	ND	7.30	1.48	0.48	ND	0.34	ND	ND	ND	1.32	0.21	1.42	0.19	ND	1.09	ND
KL141	B	11.80	ND	5.60	1.61	0.53	ND	0.33	ND	ND	ND	1.18	0.21	1.31	0.14	ND	0.71	ND
KL142	B	13.50	ND	6.30	1.91	0.62	ND	0.35	ND	ND	ND	1.32	0.24	1.51	0.13	ND	0.93	ND
KL146	B	16.10	ND	7.60	1.97	0.58	ND	0.37	ND	ND	ND	1.34	0.23	1.74	0.21	ND	1.63	ND
KL152	B	ND	ND	ND	ND	ND	ND	ND	ND	ND	ND	ND	ND	ND	ND	ND	ND	ND
KL153	B	ND	ND	ND	ND	ND	ND	ND	ND	ND	ND	ND	ND	ND	ND	ND	ND	ND
KL154	B	17.70	ND	9.10	1.91	0.71	ND	0.32	ND	ND	ND	1.26	0.20	1.17	0.12	ND	0.89	ND
KL157	B	12.80	ND	7.00	1.37	0.46	ND	0.31	ND	ND	ND	1.22	0.20	1.21	0.11	ND	1.10	ND
KL159	B	9.60	ND	4.90	1.28	0.38	ND	0.23	ND	ND	ND	1.00	0.19	1.14	0.10	ND	0.65	ND
KL204	B	ND	ND	ND	ND	ND	ND	ND	ND	ND	ND	ND	ND	ND	ND	ND	ND	ND
KL467	B	ND	ND	ND	ND	ND	ND	ND	ND	ND	ND	ND	ND	ND	ND	ND	ND	ND
KL468	B	10.20	ND	5.60	1.29	0.43	ND	0.24	ND	ND	ND	0.90	0.15	1.02	0.11	ND	0.70	ND
100 527	C	11.40	ND	6.70	1.66	0.63	2.02	ND	1.94	0.50	1.35	1.20	0.20	ND	ND	ND	2.00	2.00

Sample	Ref	Ce	Pr	ND	Sm	Eu	Gd	Tb	Dy	Ho	Er	Yb	Lu	Hf	Ta	Pb	Th	U
100 528	C	22.30	ND	11.50	2.77	0.86	2.89	ND	3.05	0.65	1.86	1.67	0.26	ND	ND	ND	2.00	2.00
100 529	C	16.40	ND	9.30	2.35	0.86	2.57	ND	2.77	0.64	1.75	1.56	0.24	ND	ND	ND	2.00	2.00
KO109	B	ND	ND	ND	ND	ND	ND	ND	ND	ND	ND	ND	ND	ND	ND	ND	ND	ND
KO110	B	28.50	ND	14.10	3.47	1.12	ND	0.59	ND	ND	ND	1.79	0.27	2.86	0.37	ND	2.16	ND
KO111	B	28.70	ND	14.10	3.62	1.06	ND	0.59	ND	ND	ND	1.76	0.32	2.85	0.41	ND	2.27	ND
KO112	B	27.30	ND	12.40	3.41	1.33	ND	0.60	ND	ND	ND	1.77	0.29	2.79	0.37	ND	2.07	ND
KO118	B	ND	ND	ND	ND	ND	ND	ND	ND	ND	ND	ND	ND	ND	ND	ND	ND	ND
KO126	B	25.60	ND	11.70	3.11	1.27	ND	0.54	ND	ND	ND	1.69	0.30	2.57	0.29	ND	1.86	ND
KO129	B	ND	ND	ND	ND	ND	ND	ND	ND	ND	ND	ND	ND	ND	ND	ND	ND	ND
KO130	B	26.70	ND	13.50	3.14	1.07	ND	0.57	ND	ND	ND	1.74	0.27	2.70	0.34	ND	1.70	ND
KO295	B	ND	ND	ND	ND	ND	ND	ND	ND	ND	ND	ND	ND	ND	ND	ND	ND	ND
NL791	B	ND	ND	ND	ND	ND	ND	ND	ND	ND	ND	ND	ND	ND	ND	ND	ND	ND
100 530	C	28.60	ND	15.70	3.82	1.33	3.80	ND	3.60	0.76	2.11	1.82	0.27	ND	ND	ND	2.00	2.00
100 531	C	27.50	ND	15.10	3.76	1.18	3.89	ND	3.65	0.76	2.12	1.78	0.26	ND	ND	ND	2.00	2.00
100 521	C	103.00	ND	54.10	9.50	2.49	8.06	ND	6.37	1.37	3.74	3.01	0.46	ND	ND	ND	2.00	2.00
100 522	C	125.00	ND	62.30	11.00	2.73	9.30	ND	7.43	1.53	4.08	3.24	0.47	ND	ND	ND	2.00	2.00
100 523	C	203.00	ND	94.90	15.90	3.45	12.80	ND	10.90	2.23	6.39	5.61	0.81	ND	ND	ND	8.00	2.00
100 524	C	171.00	ND	79.40	13.40	2.81	10.80	ND	9.24	1.89	5.47	4.63	0.68	ND	ND	ND	7.00	2.00
FVM216	D	192.77	24.54	89.50	15.64	3.13	11.61	ND	9.32	1.70	5.00	3.95	ND	ND	ND	ND	ND	ND
FVM217	D	187.18	24.04	88.08	14.79	3.11	10.84	ND	8.56	1.54	4.08	2.90	ND	ND	ND	ND	ND	ND
FVM293	D	185.06	23.63	84.62	12.65	2.67	9.63	ND	9.49	1.77	4.83	3.38	ND	ND	ND	ND	ND	ND
FVM294	D	180.99	23.05	84.59	15.78	3.26	12.39	ND	10.81	2.05	5.90	4.98	ND	ND	ND	ND	ND	ND
FVM295	D	205.37	26.08	95.44	17.33	3.46	13.16	ND	11.47	2.18	6.18	5.04	ND	ND	ND	ND	ND	ND
FVM361	D	205.23	25.59	87.87	15.22	2.67	11.46	ND	9.97	1.88	5.84	5.07	ND	ND	ND	ND	ND	ND
FVM362	D	184.51	22.59	75.82	12.53	2.25	9.51	ND	8.12	1.54	4.77	4.09	ND	ND	ND	ND	ND	ND
FVM227	D	195.44	22.59	79.28	13.54	2.23	10.07	ND	8.50	1.61	5.37	4.69	ND	ND	ND	ND	ND	ND
FVM228	D	169.02	20.01	69.48	11.90	1.88	8.93	ND	7.76	1.50	4.61	3.95	ND	ND	ND	ND	ND	ND
FVM229	D	176.07	21.08	71.50	12.24	1.98	9.42	ND	7.83	1.54	5.07	4.25	ND	ND	ND	ND	ND	ND
FVM379	D	149.91	18.44	62.94	10.95	2.11	9.11	ND	9.09	1.62	4.98	4.47	ND	ND	ND	ND	ND	ND
FVM380	D	180.15	22.13	74.59	12.37	2.39	9.28	ND	9.34	1.65	4.73	4.60	ND	ND	ND	ND	ND	ND
FVM345	D	81.56	12.25	48.39	8.78	2.26	7.13	ND	6.32	1.15	3.22	2.30	ND	ND	ND	ND	ND	ND
FVM322	D	217.82	28.50	107.11	19.43	3.89	14.68	ND	11.62	2.19	6.24	5.06	ND	ND	ND	ND	ND	ND
FVM323	D	216.04	28.17	105.82	19.03	3.83	14.12	ND	11.43	2.15	6.18	4.82	ND	ND	ND	ND	ND	ND
FVM324	D	205.09	26.69	100.37	18.11	3.67	13.33	ND	10.80	2.02	5.94	4.60	ND	ND	ND	ND	ND	ND
FVM401	D	196.10	26.53	99.21	18.64	3.71	13.29	ND	10.98	2.09	5.85	4.89	ND	ND	ND	ND	ND	ND
FVM402	D	166.50	22.43	93.54	15.14	2.89	12.68	ND	11.46	2.21	6.37	4.94	ND	ND	ND	ND	ND	ND
FVM403	D	195.65	26.16	93.95	14.33	2.88	10.80	ND	8.44	1.45	3.67	2.56	ND	ND	ND	ND	ND	ND
100 525	C	128.00	ND	64.40	12.60	3.24	10.10	ND	8.09	1.72	4.37	3.63	0.52	ND	ND	ND	2.00	2.00
100 526	C	142.00	ND	72.60	13.80	3.50	11.50	ND	9.17	1.87	4.86	3.80	0.58	ND	ND	ND	2.00	2.00
J1A	E	65.30	ND	ND	6.90	1.98	ND	1.00	ND	ND	ND	2.33	0.34	5.20	0.72	10.10	3.30	1.10
J2A	E	65.50	ND	ND	6.51	2.08	ND	0.92	ND	ND	ND	2.53	0.36	5.60	0.75	13.40	4.50	1.10
J3A	E	63.20	ND	ND	6.13	1.94	ND	0.79	ND	ND	ND	2.30	0.32	5.10	0.67	8.30	3.40	1.00
J4A	E	56.30	ND	ND	6.33	2.12	ND	0.89	ND	ND	ND	2.12	0.35	5.30	0.78	10.70	3.50	1.00
J5A	E	53.80	ND	ND	5.37	1.23	ND	0.81	ND	ND	ND	1.97	0.29	4.50	0.64	10.20	3.00	0.80
J6A	E	52.80	ND	ND	5.85	1.61	ND	0.77	ND	ND	ND	1.85	0.30	4.50	0.64	10.50	3.10	0.80
J7A	E	55.20	ND	ND	5.89	1.73	ND	0.78	ND	ND	ND	1.88	0.29	4.60	0.64	11.00	3.10	0.90
J9A	E	55.60	ND	ND	5.61	1.62	ND	0.75	ND	ND	ND	1.85	0.29	4.60	0.69	13.00	3.00	0.80
J10A	E	58.49	ND	ND	6.07	1.78	ND	0.84	ND	ND	ND	2.08	0.32	4.91	0.69	11.23	3.34	0.90
100 519	C	51.40	ND	29.10	5.81	1.86	5.32	ND	4.03	0.87	2.23	1.56	0.23	ND	ND	ND	2.00	2.00
100 520	C	54.40	ND	28.30	5.49	1.83	5.20	ND	4.27	0.97	2.45	1.91	0.28	ND	ND	ND	3.00	2.00

11.6 GEOTHERMAL GRADIENT DATA

Table 21. Geothermal gradient data within a radius of 25 km surrounding the proposed injection site. Data from Dhansay *et al.* (2017).

Longitude	Latitude	Type	Gradient (°C/km)
29.183061	-26.517194	Borehole well	16.92
29.149726	-26.500528	Borehole well	15.67
29.166394	-26.500528	Borehole well	16.00
29.149727	-26.483863	Borehole well	19.62
29.116392	-26.500528	Borehole well	17.67
29.116393	-26.467197	Borehole well	17.33
29.099726	-26.450531	Borehole well	19.67
29.116393	-26.433865	Borehole well	20.38
29.083058	-26.467196	Borehole well	20.33
29.116393	-26.450531	Borehole well	21.00
29.083058	-26.467196	Borehole well	18.33
28.983056	-26.400532	Borehole well	23.08
28.89972	-26.3672	Borehole well	14.86

11.7 HYDROGEOLOGICAL CENSUS DATA

Table 22. Groundwater physical data collected at the various sampling sites. Data includes water level (Wlevel), borehole depth (Bdepth), pumping rate (Prate), pumping average (Pave), pumping duration (PDur) and pumping depth (PDep).

ID	Long	Lat	Ele	Date	Wlevel	Type	Bdepth	pH	EC	Temp	PRate	Pave	PDur	PDep
KB01D	29.1872	-26.2632	1 606	2015/02/01	1.49	Borehole	ND	7.80	281	ND	ND	ND	ND	ND
KB01S	29.1872	-26.2632	1 606	2015/02/01	5.97	Borehole	ND	8.20	285	ND	ND	ND	ND	ND
KB06D	29.1912	-26.2792	1 595	2015/02/01	6.30	Borehole	ND	8.80	632	ND	ND	ND	ND	ND
KB06S	29.1912	-26.2792	1 595	2015/02/01	4.49	Borehole	ND	7.90	399	ND	ND	ND	ND	ND
KB08D	29.2033	-26.2714	1 592	2015/02/01	ND	Borehole	ND	7.30	1 370	ND	ND	ND	ND	ND
KB08S	29.2033	-26.2714	1 592	2015/02/01	ND	Borehole	ND	7.10	1 340	ND	ND	ND	ND	ND
KB10D	29.1982	-26.2623	1 600	2015/02/01	ND	Borehole	ND	8.10	388	ND	ND	ND	ND	ND
KB10S	29.1982	-26.2623	1 600	2015/02/01	ND	Borehole	ND	7.90	282	ND	ND	ND	ND	ND
KB12D	29.2167	-26.2769	1 581	2015/02/01	12.40	Borehole	ND	7.10	2 080	ND	ND	ND	ND	ND
KB12S	29.2167	-26.2769	1 581	2015/02/01	12.38	Borehole	ND	7.50	1 590	ND	ND	ND	ND	ND
KB18D	29.2218	-26.2735	1 580	2015/02/01	3.96	Borehole	ND	8.20	1 390	ND	ND	ND	ND	ND
KB18S	29.2218	-26.2735	1 580	2015/02/01	3.93	Borehole	ND	7.80	1 500	ND	ND	ND	ND	ND
KB19	29.2068	-26.2763	1 587	2015/02/01	32.57	Borehole	ND	6.90	2 870	ND	ND	ND	ND	ND
KB20	29.2100	-26.2757	1 586	2015/02/01	33.02	Borehole	ND	7.70	2 750	ND	ND	ND	ND	ND
KB23	29.1694	-26.2504	1 609	2015/02/01	5.27	Borehole	ND	6.50	221	ND	ND	ND	ND	ND
KB24	29.1637	-26.2512	1 609	2015/02/01	2.81	Borehole	ND	6.20	694	ND	ND	ND	ND	ND
KB27	29.1724	-26.2540	1 611	2015/02/01	4.96	Borehole	ND	7.30	501	ND	ND	ND	ND	ND
KB28	29.1941	-26.2796	1 593	2015/02/01	9.63	Borehole	ND	6.40	333	ND	ND	ND	ND	ND
KB29	29.2223	-26.2732	1 580	2015/02/01	3.54	Borehole	ND	7.80	1 200	ND	ND	ND	ND	ND
KB30	29.2004	-26.2829	1 587	2015/02/01	ND	Borehole	ND	8.40	1 810	ND	ND	ND	ND	ND
KB32	29.1778	-26.2680	1 608	2015/02/01	1.50	Borehole	ND	8.10	266	ND	ND	ND	ND	ND
KB34	29.1862	-26.2564	1 606	2015/02/01	1.50	Borehole	ND	7.50	447	ND	ND	ND	ND	ND
KB35	29.1842	-26.2760	1 601	2015/02/01	1.42	Borehole	ND	7.90	631	ND	ND	ND	ND	ND
KB39	29.2137	-26.2811	1 580	2015/02/01	3.29	Borehole	ND	8.60	2 100	ND	ND	ND	ND	ND
KB40	29.2166	-26.2719	1 584	2015/02/01	14.95	Borehole	ND	7.80	1 780	ND	ND	ND	ND	ND
KB41	29.2048	-26.2757	1 589	2015/02/01	19.17	Borehole	ND	8.00	1 980	ND	ND	ND	ND	ND
KB42	29.2026	-26.2741	1 591	2015/02/01	35.36	Borehole	ND	7.50	2 690	ND	ND	ND	ND	ND
KB60	29.1860	-26.2637	1 606	2015/02/01	2.74	Borehole	ND	8.20	2 580	ND	ND	ND	ND	ND
KB61	29.2056	-26.2695	1 592	2015/02/01	ND	Borehole	ND	8.10	382	ND	ND	ND	ND	ND
KB62	29.2056	-26.2695	1 592	2015/02/01	ND	Borehole	ND	8.20	411	ND	ND	ND	ND	ND
KB65	29.1802	-26.2735	1 604	2015/02/01	2.01	Borehole	ND	7.60	389	ND	ND	ND	ND	ND
KB66	29.1875	-26.2551	1 604	2015/02/01	1.26	Borehole	ND	7.20	107	ND	ND	ND	ND	ND
KB67	29.2194	-26.2759	1 580	2015/02/01	6.29	Borehole	ND	8.30	1 110	ND	ND	ND	ND	ND
KB68	29.2194	-26.2759	1 580	2015/02/01	2.69	Borehole	ND	7.40	2 150	ND	ND	ND	ND	ND
KB70	29.2164	-26.2778	1 581	2015/02/01	4.02	Borehole	ND	8.00	2 620	ND	ND	ND	ND	ND
KB71	29.1762	-26.2439	1 603	2015/02/01	6.67	Borehole	ND	9.30	155	ND	ND	ND	ND	ND
KB72	29.1750	-26.2463	1 605	2015/02/01	4.02	Borehole	ND	6.40	1 440	ND	ND	ND	ND	ND
KB73	29.1750	-26.2462	1 605	2015/02/01	3.92	Borehole	ND	7.10	1 240	ND	ND	ND	ND	ND
KB74	29.2031	-26.2838	1 585	2015/02/01	0.23	Borehole	ND	8.40	1 570	ND	ND	ND	ND	ND
KB75	29.2104	-26.2823	1 582	2015/02/01	5.46	Borehole	ND	7.70	1 020	ND	ND	ND	ND	ND
KB76	29.2104	-26.2823	1 582	2015/02/01	4.96	Borehole	ND	7.50	2 640	ND	ND	ND	ND	ND
KB77	29.1862	-26.2627	1 607	2015/02/01	3.13	Borehole	ND	8.20	389	ND	ND	ND	ND	ND
KB78	29.1863	-26.2627	1 606	2015/02/01	1.82	Borehole	ND	8.70	645	ND	ND	ND	ND	ND
KB79	29.2164	-26.2778	1 581	2015/02/01	6.98	Borehole	ND	7.90	1 110	ND	ND	ND	ND	ND
KB80	29.2190	-26.2665	1 586	2015/02/01	8.86	Borehole	ND	8.20	1 390	ND	ND	ND	ND	ND
KB81	29.1858	-26.2560	1 606	2015/02/01	18.10	Borehole	ND	8.30	273	ND	ND	ND	ND	ND
KB82	29.1813	-26.2531	1 606	2015/02/01	2.78	Borehole	ND	7.10	200	ND	ND	ND	ND	ND
LBH002	29.0335	-26.5133	1 582	2022/02/01	1.45	Borehole	ND	7.23	1 088	21.7	ND	ND	ND	ND
LBH003	29.0379	-26.5235	1 580	2022/02/01	2.43	Borehole	ND	6.82	2 312	21.9	ND	ND	ND	ND
LBH004	29.0554	-26.5248	1 583	2022/02/01	4.41	Borehole	ND	7.34	495.5	21.3	ND	ND	ND	ND
LBH005	29.0548	-26.5122	1 586	2022/02/01	1.48	Borehole	ND	6.89	2 691	24	ND	ND	ND	ND
WBH001A	29.0964	-26.5087	1 601	2022/02/01	0.93	Borehole	ND	7.08	2 328	20.8	ND	ND	ND	ND
WBH001B	29.0964	-26.5087	1 601	2022/02/01	ND	Borehole	ND	7.85	576.5	18.4	ND	ND	ND	ND
WBH002A	29.1039	-26.5046	1 607	2022/02/01	0.00	Borehole	ND	7.06	2 373	20.3	ND	ND	ND	ND
WBH002B	29.1039	-26.5046	1 607	2022/02/01	1.60	Borehole	ND	7.06	2 523	21.2	ND	ND	ND	ND
WBH003A	29.1003	-26.5172	1 599	2022/02/01	0.66	Borehole	ND	7.60	2 994	21	ND	ND	ND	ND
WBH003B	29.1003	-26.5172	1 599	2022/02/01	0.38	Borehole	ND	7.50	736.7	21.2	ND	ND	ND	ND
WBH004A	29.1144	-26.5188	1 604	2022/02/01	0.12	Borehole	ND	6.77	10 810	21.3	ND	ND	ND	ND
WBH004B	29.1144	-26.5188	1 604	2022/02/01	11.53	Borehole	ND	7.38	2 020	24.1	ND	ND	ND	ND

ID	Long	Lat	Ele	Date	Wlevel	Type	Bdepth	pH	EC	Temp	PRate	Pave	PDur	PDep
WBH005A	29.1168	-26.5116	1 609	2022/02/01	9.55	Borehole	ND	7.29	3 088	23.4	ND	ND	ND	ND
WBH005B	29.1168	-26.5116	1 609	2022/02/01	19.82	Borehole	ND	7.71	1 370	20.2	ND	ND	ND	ND
WBH006	29.1091	-26.4990	1 612	2022/02/01	ND	Borehole	ND	7.82	4 665	23	ND	ND	ND	ND
8SBH011	29.0600	-26.4601	1 606	2022/02/02	1.88	Borehole	ND	702.00	3 718	21	ND	ND	ND	ND
8SBH012	29.0629	-26.4605	1 606	2022/02/02	1.67	Borehole	ND	7.26	2 222	20.2	ND	ND	ND	ND
KBH002A	29.0780	-26.4848	1 600	2022/02/02	ND	Borehole	ND	7.76	1 716	23.2	ND	ND	ND	ND
KBH002B	29.0780	-26.4848	1 600	2022/02/02	ND	Borehole	ND	7.78	774.7	22.1	ND	ND	ND	ND
KDBH017	29.0740	-26.4826	1 598	2022/02/02	5.27	Borehole	ND	7.02	1 104	20.5	ND	ND	ND	ND
MB001	29.1571	-26.2782	1 610	2022/02/03	1.55	Borehole	ND	7.36	388	20.7	ND	ND	ND	ND
MB002	29.1532	-26.2726	1 611	2022/02/03	1.06	Borehole	ND	6.72	1 110	22.2	ND	ND	ND	ND
MB003	29.1535	-26.2652	1 611	2022/02/03	1.87	Borehole	ND	7.21	194.3	22.6	ND	ND	ND	ND
MB004	29.1533	-26.2620	1 611	2022/02/03	0.60	Borehole	ND	7.21	716.5	22.6	ND	ND	ND	ND
MB017	29.1551	-26.2763	1 610	2022/02/03	1.89	Borehole	ND	6.97	766.5	22.9	ND	ND	ND	ND
MB021	29.1535	-26.2612	1 611	2022/02/03	0.02	Borehole	ND	7.03	158.1	18.1	ND	ND	ND	ND
MB030	29.2011	-26.2863	1 585	2022/02/03	0.00	Borehole	ND	8.27	798	26.3	ND	ND	ND	ND
MB031	29.1688	-26.2943	1 601	2022/02/03	ND	Borehole	ND	7.31	518.1	20.9	ND	ND	ND	ND
MB033	29.1847	-26.2973	1 589	2022/02/03	0.00	Borehole	ND	7.17	287.1	21.1	ND	ND	ND	ND
MB034	29.1257	-26.2794	1 616	2022/02/03	0.00	Borehole	ND	6.96	744.5	22.9	ND	ND	ND	ND
MB035	29.1272	-26.2797	1 616	2022/02/03	0.48	Borehole	ND	7.47	162.3	20.9	ND	ND	ND	ND
MB037	29.1650	-26.2942	1 603	2022/02/03	10.49	Borehole	ND	7.87	588.3	18.9	ND	ND	ND	ND
MB038	29.1651	-26.2942	1 603	2022/02/03	ND	Borehole	ND	7.35	348.3	21.5	ND	ND	ND	ND
MB042A	29.1992	-26.2838	1 588	2022/02/03	0.49	Borehole	ND	8.53	1 222	21.2	ND	ND	ND	ND
MB042B	29.1992	-26.2838	1 588	2022/02/03	1.30	Borehole	ND	8.06	926.6	19.6	ND	ND	ND	ND
MB043	29.1980	-26.2937	1 583	2022/02/03	ND	Borehole	ND	6.87	1 467	19.7	ND	ND	ND	ND
MB047	29.1651	-26.2946	1 603	2022/02/03	1.79	Borehole	ND	7.07	195.8	24.6	ND	ND	ND	ND
MB048	29.1988	-26.2835	1 588	2022/02/03	3.83	Borehole	ND	9.27	151.1	22	ND	ND	ND	ND
MB049	29.1974	-26.2953	1 582	2022/02/03	1.47	Borehole	ND	9.82	362.2	23.3	ND	ND	ND	ND
MB050	29.1974	-26.2952	1 582	2022/02/03	6.46	Borehole	ND	9.91	270.3	20.1	ND	ND	ND	ND
MB053	29.1885	-26.2806	1 596	2022/02/03	0.00	Borehole	ND	8.50	1 141	23.3	ND	ND	ND	ND
MB057	29.2009	-26.2913	1 582	2022/02/03	4.20	Borehole	ND	9.31	233.1	22.2	ND	ND	ND	ND
MCBH004D	28.6945	-26.2396	1 603	2022/02/08	26.36	Borehole	90	8.85	139.1	18.8	ND	ND	ND	ND
MCBH004M	28.6945	-26.2396	1 603	2022/02/08	6.83	Borehole	40	9.31	84.59	18.5	ND	ND	ND	ND
MCBH004S	28.6945	-26.2396	1 603	2022/02/08	4.21	Borehole	10	9.02	206.6	19.3	ND	ND	ND	ND
MCBH006D	28.6839	-26.2169	1 594	2022/02/08	23.98	Borehole	90	7.85	213.9	18.4	ND	ND	ND	ND
MCBH006M	28.6839	-26.2169	1 594	2022/02/08	4.00	Borehole	40	7.86	209.4	20.7	ND	ND	ND	ND
MCBH009D	28.6980	-26.2484	1 606	2022/02/08	42.62	Borehole	96	9.41	137.1	19.7	ND	ND	ND	ND
MCBH009M	28.2484	-26.2484	1 602	2022/02/08	4.06	Borehole	26	9.14	106.5	18.6	ND	ND	ND	ND
MCBH009S	28.6981	-26.2484	1 606	2022/02/08	3.79	Borehole	10	9.21	157.1	19.1	ND	ND	ND	ND
CRBH008	28.9626	-26.2875	1 611	2022/02/15	14.34	Borehole	150	7.80	409.1	21.2	ND	ND	ND	ND
CRBH009	28.9929	-26.2784	1 614	2022/02/15	3.32	Borehole	ND	7.19	498.4	25.3	ND	ND	ND	ND
CRBH011	28.9948	-26.2788	1 614	2022/02/15	0.00	Borehole	ND	7.23	455	17.4	ND	ND	ND	ND
GHBH001	29.1757	-26.5155	1 599	2022/02/15	1.83	Borehole	36	7.59	142.6	22.4	2	48	ND	ND
GHBH002	28.9283	-26.3469	1 640	2022/02/15	6.50	Borehole	12	7.49	507.1	18.5	0.6	14.4	ND	ND
GHBH003	28.9260	-26.3482	1 641	2022/02/15	2.24	Borehole	50	7.22	602.5	21.2	ND	ND	ND	ND
GHBH004	28.9462	-26.3459	1 644	2022/02/15	12.00	Borehole	ND	7.24	440.1	20.3	10	240	ND	ND
GHBH006	28.9592	-26.3323	1 633	2022/02/15	15.37	Borehole	26	7.79	853.7	24.1	6.7	160	ND	ND
MVBH007	28.9963	-26.3046	1 615	2022/02/15	12.98	Borehole	36	8.12	420.6	26.4	ND	ND	ND	ND
BKBH012	28.9112	-26.3550	1 643	2022/02/16	6.33	Borehole	25	7.22	1 098	18.1	2	48	6	23.5
BKBH013	28.9112	-26.3383	1 629	2022/02/16	2.06	Borehole	45	7.47	833.2	22.4	ND	ND	ND	ND
BKBH014	28.9112	-26.3383	1 629	2022/02/16	20.16	Borehole	45	7.39	487.7	21	ND	ND	ND	ND
BKBH015	28.9104	-26.3381	1 628	2022/02/16	10.82	Borehole	45	7.31	511.5	21.7	ND	ND	ND	ND
BKBH016	28.9134	-26.3390	1 630	2022/02/16	1.50	Borehole	ND	7.33	625	23.6	ND	ND	ND	ND
BKBH017	28.9106	-26.3407	1 631	2022/02/16	3.00	Borehole	30	7.33	852.8	27	ND	ND	ND	ND
BKBH018	28.9043	-26.3392	1 628	2022/02/16	15.50	Borehole	62	8.14	473.4	24.1	ND	ND	ND	ND
BKBH019	28.9068	-26.3461	1 635	2022/02/16	1.30	Borehole	ND	6.67	960.6	20.9	ND	ND	ND	ND
BKBH020	28.9187	-26.3110	1 606	2022/02/16	6.96	Borehole	ND	7.76	576.9	23.6	ND	ND	ND	ND
BKS001	28.9138	-26.3388	1 630	2022/02/16	0.00	Spring	ND	7.70	493	27.3	ND	ND	ND	ND
HSBH024	28.8509	-26.3435	1 626	2022/02/17	10.59	Borehole	ND	8.41	347.4	22	2	ND	ND	ND
KDBH022	28.9290	-26.2594	1 584	2022/02/17	1.20	Borehole	30	7.41	376.1	21.1	1	ND	ND	28
KDBH023	28.9363	-26.2333	1 582	2022/02/17	66.57	Borehole	90	7.47	352.5	22.3	ND	ND	ND	84
KDBH024	28.9363	-26.2333	1 582	2022/02/17	ND	Borehole	60	6.83	1 578	24.7	ND	ND	ND	ND
SBLBH021	28.8971	-26.3083	1 600	2022/02/17	12.08	Borehole	60	7.57	597.1	25.3	1	ND	ND	55
SSBH026	28.8470	-26.3179	1 607	2022/02/17	ND	Borehole	ND	7.74	437.3	22.5	5	ND	ND	ND
SSBH027	28.8636	-26.3082	1 593	2022/02/17	ND	Borehole	ND	7.82	338.5	25.1	ND	ND	ND	ND
EBBH034	28.8035	-26.2881	1 609	2022/02/18	ND	Borehole	40	8.22	433.2	21.4	ND	ND	ND	ND

ID	Long	Lat	Ele	Date	Wlevel	Type	Bdepth	pH	EC	Temp	PRate	Pave	PDur	PDep
ECBBH035	28.7821	-26.2837	1 610	2022/02/18	1.75	Borehole	200	7.58	698	25.5	6	ND	ND	ND
HKBH029	28.8773	-26.2554	1 561	2022/02/18	3.60	Borehole	80	7.14	187.4	22.4	ND	ND	ND	ND
LKBH030	28.7833	-26.3490	1 646	2022/02/18	11.80	Borehole	ND	8.82	397.8	21.4	ND	ND	ND	ND
LKBH031	28.7853	-26.3462	1 645	2022/02/18	25.07	Borehole	86	9.22	517	22.4	ND	ND	ND	80
LKBH032	28.7851	-26.3482	1 645	2022/02/18	0.90	Borehole	16	7.71	452.4	19.6	ND	ND	ND	ND
LKBH033	28.7848	-26.3501	1 646	2022/02/18	5.40	Borehole	24	7.39	502.8	20.7	ND	ND	ND	ND
LKS002	28.7860	-26.3511	1 646	2022/02/18	0.00	Spring	ND	7.55	663.9	19	ND	ND	ND	ND
HSBH036	28.8492	-26.3390	1 623	2022/02/22	0.82	Borehole	90	7.50	484.8	24.5	1	ND	ND	ND
LKBH038	28.7918	-26.3229	1 632	2022/02/22	ND	Borehole	ND	8.55	846.1	24.6	ND	ND	ND	ND
RFBH037	28.8625	-26.3470	1 626	2022/02/22	0.00	Well	ND	8.09	549.6	21.6	ND	ND	ND	ND
RFBH042	28.8626	-26.3471	1 626	2022/02/22	0.00	Borehole	ND	7.61	554.6	20	ND	ND	ND	ND
RFBH043	28.7911	-26.3220	1 632	2022/02/22	0.85	Borehole	ND	8.92	474	23.5	ND	ND	ND	ND
WHBH039	28.8079	-26.3699	1 648	2022/02/22	3.57	Borehole	ND	7.35	1 045	21.9	ND	ND	ND	ND
WHBH040	28.8391	-26.3991	1 664	2022/02/22	ND	Borehole	ND	7.55	733.2	27	ND	ND	ND	ND
WHBH041	28.4229	-26.3759	1 597	2022/02/22	0.00	Borehole	ND	7.54	421.7	23.2	ND	ND	ND	14
BSBH045	28.9813	-26.4447	1 625	2022/02/23	9.60	Borehole	ND	7.30	461.9	19.1	1.67	40	ND	ND
BSBH046	28.9908	-26.4329	1 625	2022/02/23	0.10	Borehole	ND	7.45	232.4	19.5	ND	ND	ND	ND
LBH044	28.9412	-26.4016	1 652	2022/02/23	0.00	Well	ND	7.72	474.6	20.5	ND	ND	ND	ND
BKBH047	28.9632	-26.4347	1 639	2022/02/24	21.42	Borehole	27	7.70	142.3	23.2	ND	ND	ND	ND
BSBH052	28.9547	-26.4909	1 611	2022/02/24	ND	Borehole	ND	8.85	351.7	24.7	ND	ND	ND	ND
BSBH053	28.9542	-26.4874	1 613	2022/02/24	ND	Borehole	ND	7.71	380	25.9	ND	ND	ND	ND
BSBH054	28.9649	-26.4945	1 602	2022/02/24	3.40	Borehole	86	7.72	511.6	24.2	ND	ND	ND	ND
BSBH055	28.9625	-26.4929	1 605	2022/02/24	ND	Borehole	ND	7.53	579.2	18.4	ND	ND	ND	ND
RBH050	28.9996	-26.3649	1 659	2022/02/24	10.99	Borehole	100	7.34	643.1	23.1	ND	ND	ND	ND
RBH051	28.9977	-26.3660	1 659	2022/02/24	12.90	Borehole	100	7.73	1 180	20.1	ND	ND	ND	ND
UMKBH048	29.0014	-26.3754	1 651	2022/02/24	10.60	Borehole	50	7.88	571.8	28.1	25	ND	ND	ND
UMKBH049	28.0014	-26.3754	1 668	2022/02/24	7.05	Borehole	50	7.36	497.5	18	ND	ND	ND	ND
GFBH061	28.8697	-26.4158	1 682	2022/02/25	ND	Borehole	ND	7.67	455.9	22.9	ND	ND	ND	ND
WSBH058	28.9518	-26.4984	1 609	2022/02/25	ND	Borehole	ND	9.44	521.5	20.2	ND	ND	ND	ND
WSBH059	28.9455	-26.4917	1 616	2022/02/25	5.00	Borehole	ND	7.38	482.8	19	ND	ND	ND	ND
WSBH060	28.9507	-26.4864	1 615	2022/02/25	24.00	Borehole	ND	7.98	428	22	ND	ND	ND	ND
BSBH063	28.9874	-26.4735	1 609	2022/03/01	3.10	Borehole	13	7.50	380.1	19.1	2.5	ND	ND	ND
BSBH064	28.9880	-26.4739	1 609	2022/03/01	3.00	Borehole	21	7.76	371	20.8	6.5	ND	ND	ND
GFBH067	28.8968	-26.4636	1 650	2022/03/01	ND	Borehole	ND	7.44	212.9	23.8	ND	ND	ND	ND
GFBH068	28.8407	-26.4192	1 673	2022/03/01	1.40	Borehole	ND	7.64	349.1	25	ND	ND	ND	ND
VPBH069	28.8713	-26.4387	1 670	2022/03/01	2.40	Borehole	ND	7.49	456.5	19.3	ND	ND	ND	ND
VPBH070	28.8793	-26.4587	1 657	2022/03/01	6.34	Borehole	ND	7.89	465.8	18.9	ND	ND	ND	ND
VPBH071	28.8729	-26.4679	1 655	2022/03/01	ND	Borehole	ND	7.37	355.2	17.4	ND	ND	ND	ND
VPBH072	28.8767	-26.4510	1 661	2022/03/01	ND	Borehole	ND	8.03	386.1	21	ND	ND	ND	ND
WSBH065	28.9333	-26.4735	1 632	2022/03/01	ND	Borehole	ND	7.62	445.3	21.7	ND	ND	ND	ND
WSBH066	28.9207	-26.4705	1 640	2022/03/01	ND	Borehole	ND	8.23	611.2	22.4	ND	ND	ND	ND
WSBH073	28.8995	-26.4100	1 658	2022/03/01	ND	Borehole	ND	7.70	688.6	21.1	ND	ND	ND	ND
VPBH074	28.8605	-26.4939	1 651	2022/03/02	ND	Borehole	ND	7.42	660.4	ND	ND	ND	ND	ND
VPBH075	28.8596	-26.4883	1 653	2022/03/02	ND	Borehole	ND	7.41	717.1	ND	ND	ND	ND	ND
VPBH076	28.8643	-26.4875	1 652	2022/03/02	ND	Borehole	ND	8.27	830.9	22.3	ND	ND	ND	ND
WBBH078	28.7872	-26.4773	1 662	2022/03/02	10.76	Borehole	ND	7.68	600.1	20.9	ND	ND	ND	ND
WN02	28.8612	-26.1375	1 546	2022/06/01	ND	Borehole	ND	7.97	527.2	26.1	ND	ND	ND	ND

11.8 GROUNDWATER PHYSICAL AND HYDROCHEMICAL DATA

Table 23. Various physical and hydrochemical results of groundwater samples collected from boreholes surrounding the proposed injection site. Dataset 1.

Borehole	pH	Con	TDS	Alk	Har	NH3	F	Cl	NO_2	Br	NO_3	PO_4	SO_4
BH005A	7.6	546.3	2 731	523.5	2 456.2	<0.07	<0.10	766.01	<0.02	5.08	3.83	0.19	1 573.87
BH011	7.73	637.7	3 191	930.5	2 338.7	<0.07	<0.10	447.15	0.37	4.72	<0.02	<0.08	961.5
BH012	8.23	370.5	1 852	579.75	896.6	<0.07	<0.10	715.1	0.03	2.3	0.83	<0.08	260.75
BH017	7.95	151.7	759	137	514.5	<0.07	<0.10	268.8	<0.02	1.32	3.2	0.63	134.83
BKBH012	7.74	191.1	955	547.75	830.6	<0.07	<0.10	116.66	<0.02	0.29	0.22	<0.08	393.73
BKBH013	7.87	141.2	710	378	387.9	<0.07	0.47	193.14	<0.02	0.23	0.38	<0.08	76.11
BKBH014	8.05	84.7	424	498.75	286	<0.07	<0.10	20.18	<0.02	0.14	0.07	<0.08	42.98
BKBH015	8.05	92.3	461	390.75	328.9	<0.07	0.11	43.16	<0.02	0.13	0.07	<0.08	50.76
BKBH017	7.68	143.2	716	413.25	632.5	<0.07	0.11	79.04	<0.02	0.27	21.61	<0.08	188.15
BKBH018	8.35	82.3	411	466.25	119.3	<0.07	0.41	9.69	<0.02	0.09	0.24	<0.08	11.74
BKBH019	7.6	183.5	918	246.75	664	<0.07	<0.10	330.3	1.36	1.58	10.68	<0.08	125.45
BKBH020	8.15	100.7	503	420	214.1	<0.07	<0.10	42.7	<0.02	0.2	2.6	<0.08	95.78
BKBH022	7.99	65.4	327	270.25	248.5	<0.07	<0.10	12.73	<0.02	0.16	4.37	<0.08	55.23
BKR001	8.05	91.8	459	282.5	287.1	<0.07	<0.10	63.65	<0.02	0.18	4.74	7.45	99.49
BKS001	8.12	82.7	414	372.25	440.7	<0.07	<0.10	18.79	<0.02	<0.07	0.08	<0.08	127.3
BSBH006	8.11	60.6	303	293.5	212.1	<0.07	<0.10	10.38	<0.02	0.16	8.57	<0.08	27.18
BSBH045	7.92	79	395	344	448	<0.07	<0.10	44.25	<0.02	0.14	0.36	<0.08	46.7
BSBH046	8.04	78.1	391	312.25	232.7	<0.07	<0.10	18.26	<0.02	0.23	11.59	<0.08	66.74
BSBH052	8.2	57.9	290	303.75	178.3	<0.07	<0.10	18.05	0.38	0.17	0.21	<0.08	23.49
BSBH053	8.05	62.7	313	390	255.2	<0.07	<0.10	16.36	<0.02	0.17	1.03	0.2	16.91
BSBH054	8.1	89.7	448	425	328.6	<0.07	<0.10	50.65	<0.02	0.17	0.38	<0.08	65.36
BSBH056	7.78	68.7	343	270.25	208.1	<0.07	0.11	46.26	<0.02	0.23	9.03	0.46	22.61
BSBH063	7.8	62.3	312	319.25	226.4	<0.07	<0.10	10.8	<0.02	0.15	9.55	<0.08	27.64
CBBH035	7.95	122.3	612	473.25	438.1	<0.07	<0.10	80.27	0.02	0.43	13.68	<0.08	123.77
CRBH008	8.07	71.4	357	416.75	107.4	<0.07	2.68	17.27	<0.02	0.14	0.3	<0.08	13.9
CRBH009	7.91	79.9	399	161.75	247.1	<0.07	<0.10	69.26	<0.02	0.2	28.35	0.69	58.53
CRBH011	7.72	74.4	372	272.25	293.8	<0.07	<0.10	91.68	<0.02	0.21	3.68	<0.08	22.8
EBBH034	8.26	74.9	374	396.75	50.7	<0.07	0.22	29	<0.02	0.24	0.6	<0.08	19.86
GFBH061	7.98	79.6	398	352.5	362.2	<0.07	<0.10	13.49	<0.02	<0.07	13.52	<0.08	56.82
GHBH001	8.12	24.6	123	89.5	73.4	<0.07	<0.10	15.45	<0.02	<0.07	0.88	<0.08	19.44
GHBH002	7.93	76.5	383	334	419.6	<0.07	<0.10	11.25	<0.02	<0.07	3.95	<0.08	199.83
GHBH004	7.94	73.5	367	337.75	302.3	<0.07	<0.10	27.37	<0.02	0.1	3.89	<0.08	79.85
GHBH006	8.15	142.4	713	384.5	398.5	<0.07	0.11	153.52	<0.02	0.54	27.69	<0.08	101.17
GWBH067	7.79	71.9	360	357.5	300.9	<0.07	<0.10	19.23	0.09	0.16	7.01	<0.08	25.63
HKBH029	8	31.8	159	191.5	109.1	<0.07	<0.10	4.05	<0.02	0.08	0.57	<0.08	5.58
HSBH024	8.18	60.1	301	184.5	230.9	<0.07	0.22	15.85	<0.02	0.15	6.86	<0.08	67.77
HSBH036	8.06	42.1	841	421.5	372.1	<0.07	<0.10	15.31	<0.02	0.16	1.46	<0.08	87.59
KDBH023	7.78	281.7	1 410	118.25	774.5	0.08	<0.10	316.59	<0.02	1.74	117.2	<0.08	232.72
KDBH024	8.03	61.6	308	168	201.7	<0.07	<0.10	71.68	<0.02	0.55	2.79	<0.08	29.23
KFBH079	8.35	66.4	332	342.75	188.1	<0.07	0.11	17.73	<0.02	0.13	4.22	<0.08	25.27
KFBH080	7.9	54.7	274	250	163.8	<0.07	<0.10	21.9	<0.02	0.17	1.15	<0.08	43.09
KFBH081	8.03	79.4	397	419.5	251.1	<0.07	<0.10	33.03	<0.02	0.2	7.92	<0.08	22.47
KFBH082	8.21	42.6	213	186.5	177.6	<0.07	<0.10	10.01	<0.02	<0.07	3.77	<0.08	30.22
KFBH083	8.09	65.3	327	249.5	281.2	<0.07	<0.10	30.53	<0.02	0.15	7.39	<0.08	44.07
KFBH084	7.93	62	310	260	265.1	<0.07	<0.10	29.11	<0.02	0.12	4.64	<0.08	42.33
LBH044	8.04	82.8	414	488.25	355.1	<0.07	<0.10	17.82	<0.02	0.2	0.97	<0.08	30.87
LESLIE BH004	8.02	81.1	405	106.25	282.1	<0.07	0.12	85.6	<0.02	0.36	0.32	<0.08	184.91
LKBH030	8.62	69.6	348	311	15.1	<0.07	0.55	18.13	<0.02	0.1	0.36	<0.08	48.64
LKBH031	9.04	90.2	451	470.5	4.9	<0.07	2.54	48.64	<0.02	0.28	0.44	<0.08	25.23
LKBH032	7.83	78.8	394	477.5	360.6	<0.07	<0.10	3.48	<0.02	<0.07	1.19	<0.08	94.34
LKBH038	8.06	141.4	707	363.5	230.2	0.1	0.1	193.56	0.31	0.26	0.24	<0.08	124.17
LKS002	7.95	117.1	586	414.25	622.9	<0.07	<0.10	12.09	<0.02	0.09	1.95	<0.08	277.55
MB021	8.5	25.4	127	166.25	58.3	<0.07	0.12	5.32	<0.02	<0.07	0.22	0.09	3.69
MB033	7.92	48.1	240	285.25	146.9	<0.07	0.42	7.2	<0.02	<0.07	0.46	0.17	18.07
MB053	8.4	202.7	1 013	383.5	402.6	<0.07	<0.10	117.28	<0.02	1.11	1.44	<0.08	529.97
MC BH006M	8.08	39.3	197	238	158.3	<0.07	<0.10	8.65	<0.02	0.25	0.24	<0.08	3.05
MC BH009M	8.35	18	90	92.25	40.6	<0.07	<0.10	11.15	<0.02	0.16	0.47	<0.08	2.49
MVBH007	7.97	66.6	333	374.75	179.1	<0.07	0.54	12.17	<0.02	0.29	0.22	<0.08	26.57
RANDWATER	8.08	24.5	122	78.25	77.1	<0.07	0.41	16.04	<0.02	<0.07	0.89	<0.08	19.14
RFBH037	8.3	96.1	480	460.5	129	<0.07	2.56	51.32	<0.02	0.47	1.79	<0.08	41.37

Borehole	pH	Con	TDS	Alk	Har	NH3	F	Cl	NO_2	Br	NO_3	PO_4	SO_4
SBLBH021	7.98	105.5	528	198.5	406.6	<0.07	<0.10	93.13	<0.02	0.32	37	<0.08	76.98
SKBH047	7.91	24.9	124	100.25	78.6	<0.07	0.45	15.94	<0.02	<0.07	0.95	<0.08	18.84
SSBH026	8.12	75.6	378	458.5	282.9	<0.07	0.68	15.94	<0.02	0.2	0.1	<0.08	40.87
SSBH027	8.1	58.8	294	146.75	239.1	<0.07	<0.10	18.78	<0.02	0.17	4.09	<0.08	99.56
UMKBH048	8.14	99.9	500	456.25	444.8	<0.07	0.37	16.94	<0.02	<0.07	0.14	<0.08	177.3
UMKBH049	7.98	87.1	435	448.5	412.5	<0.07	0.27	11.15	<0.02	<0.07	0.37	<0.08	131.83
UMKBH085	7.82	125.8	629	521	504.2	<0.07	<0.10	86.42	<0.02	0.31	13.88	<0.08	103.12
VPBH071	7.93	62.3	311	231.25	222.9	<0.07	<0.10	8.91	<0.02	0.15	3.74	<0.08	73.35
VPBH072	8.08	67	335	249.75	123.8	<0.07	2.67	35.93	<0.02	0.3	1.77	<0.08	55.1
VPBH074	7.81	116.4	582	387	419.1	<0.07	0.13	98.94	<0.02	0.56	14.01	<0.08	103.25
VPBH076	7.95	147.7	739	388	547.2	<0.07	0.13	139.87	<0.02	0.19	0.31	<0.08	222.37
WBBH078	7.94	102.7	513	390.5	339.6	<0.07	1.2	111.04	<0.02	0.7	6.56	<0.08	28.01
WHBH039	7.85	186.3	931	530.75	999.5	<0.07	<0.10	119.08	<0.02	0.37	44.51	<0.08	288.97
WHBH040	7.99	127.7	640	463.5	599.8	<0.07	0.15	115.44	<0.02	0.11	5	<0.08	173.44
WHBH041	8	73.9	370	366.25	356.8	<0.07	<0.10	10.73	<0.02	<0.07	3.32	<0.08	95.13
WSBH058	9.14	90.7	453	468	3.5	<0.07	1.47	45.21	<0.02	0.39	0.46	<0.08	12.63
WSBH059	7.95	84.8	424	300.75	289.6	<0.07	0.19	64.9	<0.02	0.31	3.12	<0.08	21.13
WSBH060	8.5	75	375	379.25	<0.5	<0.07	0.33	28.3	<0.02	0.29	1.36	<0.08	26.65
WSBH065	7.93	78.6	393	343.75	198.2	<0.07	0.67	19.95	<0.02	0.11	0.4	<0.08	90.97
WSBH066	8.31	107.7	539	426.5	240.6	<0.07	2.73	73.67	<0.02	0.3	0.29	<0.08	107.3
WSBH073	8.04	120.4	603	420.25	534.6	<0.07	<0.10	28.52	<0.02	0.16	8.91	<0.08	252.95

Table 24. Various physical and hydrochemical results of groundwater samples collected from boreholes surrounding the proposed injection site. Dataset 2.

Borehole	Ag	Al	As	Au	B	Ba	Be	Bi	Ca	Cd	Co	Cr	Cu	Fe	Hg
BH005A	<0.002	<0.010	<0.002	<0.005	<0.150	0.043	<0.005	<0.005	445.277	<0.002	0.005	<0.002	<0.005	0.036	<0.005
BH011	<0.002	0.013	<0.002	<0.005	1.003	0.134	<0.005	<0.005	318.212	<0.002	0.003	<0.002	0.009	<0.025	<0.005
BH012	<0.002	<0.010	0.003	<0.005	0.563	0.082	<0.005	<0.005	109.859	<0.002	<0.002	<0.002	<0.005	0.025	<0.005
BH017	<0.002	<0.010	<0.002	<0.005	<0.150	0.064	<0.005	<0.005	121.919	<0.002	0.048	<0.002	<0.005	<0.025	<0.005
BKBH012	<0.002	<0.010	<0.002	<0.005	<0.150	0.113	<0.005	<0.005	166.374	<0.002	<0.002	<0.002	0.007	<0.025	<0.005
BKBH013	<0.002	<0.010	<0.002	<0.005	<0.150	0.236	<0.005	<0.005	87.966	<0.002	<0.002	<0.002	<0.005	<0.025	<0.005
BKBH014	<0.002	<0.010	<0.002	<0.005	<0.150	0.087	<0.005	<0.005	54.487	<0.002	<0.002	<0.002	<0.005	<0.025	<0.005
BKBH015	<0.002	<0.010	<0.002	<0.005	<0.150	0.108	<0.005	<0.005	65.381	<0.002	<0.002	<0.002	<0.005	<0.025	<0.005
BKBH017	<0.002	<0.010	<0.002	<0.005	<0.150	0.051	<0.005	<0.005	135.594	<0.002	<0.002	<0.002	0.01	0.063	<0.005
BKBH018	<0.002	<0.010	<0.002	<0.005	<0.150	0.133	<0.005	<0.005	26.758	<0.002	<0.002	<0.002	<0.005	<0.025	<0.005
BKBH019	<0.002	<0.010	<0.002	<0.005	<0.150	0.153	<0.005	<0.005	152.333	<0.002	<0.002	<0.002	<0.005	<0.025	<0.005
BKBH020	<0.002	<0.010	<0.002	<0.005	<0.150	0.075	<0.005	<0.005	43.394	<0.002	<0.002	<0.002	0.009	<0.025	<0.005
BKBH022	<0.002	0.01	<0.002	<0.005	<0.150	0.195	<0.005	<0.005	65.61	<0.002	<0.002	<0.002	<0.005	<0.025	<0.005
BKR001	<0.002	0.01	<0.002	<0.005	<0.150	0.048	<0.005	<0.005	58.881	<0.002	<0.002	<0.002	0.005	<0.025	<0.005
BKS001	<0.002	<0.010	<0.002	<0.005	<0.150	0.041	<0.005	<0.005	97.838	<0.002	<0.002	<0.002	<0.005	<0.025	<0.005
BSBH006	<0.002	<0.010	<0.002	<0.005	<0.150	0.151	<0.005	<0.005	57.624	<0.002	<0.002	<0.002	0.022	<0.025	<0.005
BSBH045	<0.002	<0.010	<0.002	<0.005	<0.150	0.393	<0.005	<0.005	139.803	<0.002	<0.002	<0.002	<0.005	0.038	<0.005
BSBH046	<0.002	<0.010	<0.002	<0.005	<0.150	0.034	<0.005	<0.005	48.101	<0.002	<0.002	<0.002	<0.005	<0.025	<0.005
BSBH052	<0.002	<0.010	<0.002	<0.005	<0.150	0.015	<0.005	<0.005	19.197	<0.002	<0.002	<0.002	<0.005	<0.025	<0.005
BSBH053	<0.002	<0.010	<0.002	<0.005	<0.150	0.03	<0.005	<0.005	47.232	<0.002	<0.002	<0.002	0.008	<0.025	<0.005
BSBH054	<0.002	<0.010	<0.002	<0.005	<0.150	0.265	<0.005	<0.005	71.635	<0.002	<0.002	<0.002	<0.005	<0.025	<0.005
BSBH056	<0.002	<0.010	<0.002	<0.005	<0.150	0.072	<0.005	<0.005	44.62	<0.002	<0.002	<0.002	<0.005	<0.025	<0.005
BSBH063	<0.002	<0.010	<0.002	<0.005	<0.150	0.304	<0.005	<0.005	69.518	<0.002	<0.002	<0.002	<0.005	<0.025	<0.005
CBBH035	<0.002	<0.010	<0.002	<0.005	<0.150	0.083	<0.005	<0.005	82.946	<0.002	<0.002	<0.002	<0.005	<0.025	<0.005
CRBH008	0.004	<0.010	<0.002	<0.005	<0.150	0.146	<0.005	<0.005	30.921	<0.002	<0.002	<0.002	<0.005	0.026	<0.005
CRBH009	<0.002	<0.010	<0.002	<0.005	<0.150	0.297	<0.005	<0.005	62.969	<0.002	<0.002	<0.002	0.007	<0.025	<0.005
CRBH011	<0.002	<0.010	<0.002	<0.005	<0.150	0.372	<0.005	<0.005	79.433	<0.002	<0.002	<0.002	<0.005	<0.025	<0.005
EBBH034	<0.002	<0.010	<0.002	<0.005	<0.150	0.122	<0.005	<0.005	11.906	<0.002	<0.002	<0.002	<0.005	<0.025	<0.005
GFBH061	<0.002	<0.010	<0.002	<0.005	<0.150	0.005	<0.005	<0.005	68.789	<0.002	0.004	<0.002	0.03	<0.025	<0.005
GHBH001	<0.002	0.013	<0.002	<0.005	<0.150	0.048	<0.005	<0.005	18.372	<0.002	<0.002	<0.002	<0.005	<0.025	<0.005
GHBH002	<0.002	<0.010	<0.002	<0.005	<0.150	0.01	<0.005	<0.005	77.912	<0.002	<0.002	0.003	<0.005	<0.025	<0.005
GHBH004	<0.002	<0.010	<0.002	<0.005	<0.150	0.021	<0.005	<0.005	64.814	<0.002	<0.002	<0.002	<0.005	<0.025	<0.005
GHBH006	<0.002	<0.010	<0.002	<0.005	<0.150	0.147	<0.005	<0.005	79.334	<0.002	<0.002	<0.002	<0.005	<0.025	<0.005
GWBH067	<0.002	<0.010	<0.002	<0.005	<0.150	0.181	<0.005	<0.005	94.402	<0.002	<0.002	<0.002	<0.005	<0.025	<0.005
HKBH029	<0.002	<0.010	<0.002	<0.005	<0.150	0.159	<0.005	<0.005	27.864	<0.002	<0.002	<0.002	0.005	<0.025	<0.005
HSBH024	<0.002	<0.010	0.004	<0.005	<0.150	0.031	<0.005	<0.005	46.011	<0.002	<0.002	<0.002	<0.005	0.042	<0.005
HSBH036	<0.002	<0.010	<0.002	<0.005	<0.150	0.017	<0.005	<0.005	76.311	<0.002	<0.002	<0.002	<0.005	0.028	<0.005
KDBH023	<0.002	<0.010	<0.002	<0.005	<0.150	0.063	<0.005	<0.005	133.546	<0.002	<0.002	0.003	<0.005	<0.025	<0.005
KDBH024	<0.002	<0.010	<0.002	<0.005	<0.150	0.168	<0.005	<0.005	52.034	<0.002	<0.002	<0.002	0.009	<0.025	<0.005
KFBH079	<0.002	<0.010	<0.002	<0.005	<0.150	0.046	<0.005	<0.005	41.321	<0.002	<0.002	<0.002	0.009	<0.025	<0.005
KFBH080	<0.002	<0.010	<0.002	<0.005	<0.150	0.059	<0.005	<0.005	40.41	<0.002	<0.002	<0.002	<0.005	<0.025	<0.005
KFBH081	<0.002	<0.010	<0.002	<0.005	<0.150	0.047	<0.005	<0.005	53.316	<0.002	<0.002	<0.002	0.013	<0.025	<0.005
KFBH082	<0.002	<0.010	<0.002	<0.005	<0.150	0.018	<0.005	<0.005	40.32	<0.002	<0.002	<0.002	<0.005	<0.025	<0.005
KFBH083	<0.002	<0.010	<0.002	<0.005	<0.150	0.03	<0.005	<0.005	62.611	<0.002	<0.002	<0.002	<0.005	<0.025	<0.005
KFBH084	<0.002	0.014	0.002	<0.005	<0.150	0.03	<0.005	<0.005	59.028	<0.002	<0.002	0.002	0.009	0.125	<0.005
LBH044	<0.002	<0.010	<0.002	<0.005	<0.150	0.041	<0.005	<0.005	64.697	<0.002	<0.002	<0.002	<0.005	<0.025	<0.005
LESLIE BH004	<0.002	<0.010	<0.002	<0.005	<0.150	0.05	<0.005	<0.005	72.125	<0.002	0.004	<0.002	<0.005	<0.025	<0.005
LKBH030	<0.002	0.011	<0.002	<0.005	<0.150	0.032	<0.005	<0.005	5.152	<0.002	<0.002	<0.002	<0.005	<0.025	<0.005
LKBH031	<0.002	0.121	0.004	<0.005	<0.150	0.021	<0.005	<0.005	1.241	<0.002	<0.002	<0.002	<0.005	0.154	<0.005
LKBH032	<0.002	<0.010	<0.002	<0.005	<0.150	<0.005	<0.005	<0.005	50.787	<0.002	<0.002	<0.002	<0.005	0.066	<0.005
LKBH038	<0.002	<0.010	<0.002	<0.005	<0.150	0.131	<0.005	<0.005	45.762	<0.002	<0.002	<0.002	<0.005	<0.025	<0.005
LKS002	<0.002	<0.010	<0.002	<0.005	<0.150	0.015	<0.005	<0.005	116.063	<0.002	<0.002	0.003	<0.005	<0.025	<0.005
MB021	<0.002	<0.010	<0.002	<0.005	<0.150	0.075	<0.005	<0.005	13.995	<0.002	<0.002	<0.002	<0.005	0.261	<0.005
MB033	<0.002	0.033	<0.002	<0.005	<0.150	0.302	<0.005	<0.005	43.442	<0.002	<0.002	<0.002	<0.005	0.199	<0.005
MB053	<0.002	<0.010	<0.002	<0.005	0.187	<0.005	<0.005	<0.005	13.157	<0.002	<0.002	<0.002	<0.005	<0.025	<0.005
MC BH006M	<0.002	<0.010	<0.002	<0.005	<0.150	0.052	<0.005	<0.005	32.625	<0.002	<0.002	<0.002	<0.005	0.026	<0.005
MC BH009M	<0.002	<0.010	<0.002	<0.005	<0.150	0.011	<0.005	<0.005	4.328	<0.002	<0.002	<0.002	<0.005	<0.025	<0.005
MVBH007	<0.002	<0.010	<0.002	<0.005	<0.150	0.167	<0.005	<0.005	36.725	<0.002	<0.002	<0.002	<0.005	<0.025	<0.005
RANDWATER	<0.002	0.016	<0.002	<0.005	<0.150	0.044	<0.005	<0.005	18.638	<0.002	<0.002	<0.002	0.244	<0.025	<0.005
RFBH037	<0.002	<0.010	<0.002	<0.005	<0.150	0.031	<0.005	<0.005	32.368	<0.002	<0.002	<0.002	<0.005	<0.025	<0.005
SBLBH021	<0.002	<0.010	<0.002	<0.005	<0.150	0.096	<0.005	<0.005	124.853	<0.002	<0.002	<0.002	<0.005	<0.025	<0.005
SKBH047	<0.002	0.013	<0.002	<0.005	<0.150	0.045	<0.005	<0.005	19.045	<0.002	<0.002	<0.002	<0.005	<0.025	<0.005
SSBH026	<0.002	<0.010	<0.002	<0.005	<0.150	0.049	<0.005	<0.005	56.815	<0.002	<0.002	<0.002	<0.005	<0.025	<0.005

Borehole	Ag	Al	As	Au	B	Ba	Be	Bi	Ca	Cd	Co	Cr	Cu	Fe	Hg
SSBH027	<0.002	<0.010	<0.002	<0.005	<0.150	0.029	<0.005	<0.005	58.223	<0.002	<0.002	<0.002	<0.005	<0.025	<0.005
UMKBH048	<0.002	<0.010	<0.002	<0.005	<0.150	0.107	<0.005	<0.005	90.312	<0.002	<0.002	<0.002	0.095	<0.025	<0.005
UMKBH049	<0.002	<0.010	<0.002	<0.005	<0.150	0.066	<0.005	<0.005	81.1	<0.002	<0.002	<0.002	<0.005	<0.025	<0.005
UMKBH085	<0.002	<0.010	<0.002	<0.005	<0.150	0.007	<0.005	<0.005	106.087	<0.002	<0.002	<0.002	<0.005	<0.025	<0.005
VPBH071	<0.002	<0.010	<0.002	<0.005	<0.150	0.056	<0.005	<0.005	51.081	<0.002	<0.002	0.005	<0.005	<0.025	<0.005
VPBH072	<0.002	<0.010	<0.002	<0.005	<0.150	0.01	<0.005	<0.005	28.407	<0.002	<0.002	<0.002	<0.005	<0.025	<0.005
VPBH074	<0.002	<0.010	<0.002	<0.005	<0.150	0.014	<0.005	<0.005	95.111	<0.002	<0.002	<0.002	<0.005	<0.025	<0.005
VPBH076	<0.002	<0.010	<0.002	<0.005	<0.150	0.012	<0.005	<0.005	64.132	<0.002	<0.002	<0.002	<0.005	<0.025	<0.005
WBBH078	<0.002	<0.010	0.025	<0.005	<0.150	0.17	<0.005	<0.005	77.709	<0.002	<0.002	<0.002	<0.005	<0.025	<0.005
WHBH039	<0.002	<0.010	<0.002	<0.005	<0.150	0.045	<0.005	<0.005	166.351	<0.002	<0.002	<0.002	<0.005	<0.025	<0.005
WHBH040	<0.002	<0.010	<0.002	<0.005	<0.150	0.036	<0.005	<0.005	121.782	<0.002	<0.002	<0.002	<0.005	<0.025	<0.005
WHBH041	<0.002	<0.010	<0.002	<0.005	<0.150	0.013	<0.005	<0.005	65.647	<0.002	<0.002	<0.002	<0.005	<0.025	<0.005
WSBH058	<0.002	0.011	0.011	<0.005	<0.150	0.005	<0.005	<0.005	0.89	<0.002	<0.002	<0.002	<0.005	<0.025	<0.005
WSBH059	<0.002	<0.010	0.003	<0.005	<0.150	0.083	<0.005	<0.005	68.072	<0.002	<0.002	<0.002	0.01	<0.025	<0.005
WSBH060	<0.002	<0.010	<0.002	<0.005	<0.150	<0.005	<0.005	<0.005	<0.150	<0.002	<0.002	<0.002	0.007	<0.025	<0.005
WSBH065	<0.002	<0.010	<0.002	<0.005	<0.150	0.106	<0.005	<0.005	50.706	<0.002	<0.002	<0.002	<0.005	<0.025	<0.005
WSBH066	<0.002	<0.010	<0.002	<0.005	<0.150	0.128	<0.005	<0.005	59.731	<0.002	<0.002	<0.002	<0.005	<0.025	<0.005
WSBH073	<0.002	<0.010	<0.002	<0.005	<0.150	0.034	<0.005	<0.005	104.169	<0.002	<0.002	0.003	<0.005	<0.025	<0.005

Table 25. Various physical and hydrochemical results of groundwater samples collected from boreholes surrounding the proposed injection site. Dataset 3.

Borehole	Ir	K	La	Li	Mg	Mn	Mo	Na	Ni	P	Pb	Pd	Pt	Rh	Ru
BH005A	<0.005	35.45	<0.005	0.008	326.417	0.179	<0.002	243.202	0.006	<0.100	<0.002	<0.005	<0.005	<0.005	<0.005
BH011	<0.005	0.224	<0.005	0.006	374.946	<0.005	<0.002	470.146	0.005	<0.100	<0.002	<0.005	<0.005	<0.005	<0.005
BH012	<0.005	0.436	<0.005	0.011	151.113	<0.005	<0.002	362.876	0.003	<0.100	<0.002	<0.005	<0.005	<0.005	<0.005
BH017	<0.005	2.547	<0.005	0.006	51	<0.005	<0.002	57.191	0.007	0.208	<0.002	<0.005	<0.005	<0.005	<0.005
BKBH012	<0.005	2.359	<0.005	0.012	100.817	<0.005	0.003	99.998	0.003	<0.100	<0.002	<0.005	<0.005	<0.005	<0.005
BKBH013	<0.005	1.846	<0.005	0.034	40.851	<0.005	<0.002	129.106	<0.002	<0.100	<0.002	<0.005	<0.005	<0.005	<0.005
BKBH014	<0.005	0.897	<0.005	0.007	36.414	<0.005	<0.002	39.626	0.003	<0.100	<0.002	<0.005	<0.005	<0.005	<0.005
BKBH015	<0.005	1.263	<0.005	0.012	40.211	<0.005	<0.002	60.304	<0.002	<0.100	<0.002	<0.005	<0.005	<0.005	<0.005
BKBH017	<0.005	3.031	<0.005	0.037	71.364	0.007	0.017	61.981	0.003	<0.100	<0.002	<0.005	<0.005	<0.005	<0.005
BKBH018	<0.005	1.812	<0.005	0.036	12.742	<0.005	<0.002	121.216	<0.002	<0.100	<0.002	<0.005	<0.005	<0.005	<0.005
BKBH019	<0.005	2.326	<0.005	0.05	68.866	0.007	<0.002	51.911	<0.002	<0.100	<0.002	<0.005	<0.005	<0.005	<0.005
BKBH020	<0.005	3.902	<0.005	0.028	25.671	<0.005	<0.002	104.374	<0.002	<0.100	<0.002	<0.005	<0.005	<0.005	<0.005
BKBH022	<0.005	6.528	<0.005	0.026	20.551	0.008	0.002	17.539	<0.002	<0.100	<0.002	<0.005	<0.005	<0.005	<0.005
BKR001	<0.005	8.224	<0.005	<0.005	34.005	<0.005	<0.002	58.448	0.008	2.099	<0.002	<0.005	<0.005	<0.005	<0.005
BKS001	<0.005	0.284	<0.005	<0.005	47.686	0.02	<0.002	20.732	<0.002	<0.100	<0.002	<0.005	<0.005	<0.005	<0.005
BSBH006	<0.005	7.733	<0.005	0.01	16.558	<0.005	<0.002	39.476	<0.002	<0.100	<0.002	<0.005	<0.005	<0.005	<0.005
BSBH045	<0.005	2.38	<0.005	0.027	24.007	0.01	<0.002	61.649	<0.002	<0.100	<0.002	<0.005	<0.005	<0.005	<0.005
BSBH046	<0.005	5.704	<0.005	0.024	27.335	<0.005	<0.002	36.178	<0.002	<0.100	<0.002	<0.005	<0.005	<0.005	<0.005
BSBH052	<0.005	0.506	<0.005	0.011	31.654	<0.005	<0.002	55.998	<0.002	<0.100	<0.002	<0.005	<0.005	<0.005	<0.005
BSBH053	<0.005	0.183	<0.005	<0.005	33.334	<0.005	<0.002	23.172	<0.002	<0.100	<0.002	<0.005	<0.005	<0.005	<0.005
BSBH054	<0.005	2.179	<0.005	0.038	36.357	<0.005	<0.002	52.004	<0.002	<0.100	<0.002	<0.005	<0.005	<0.005	<0.005
BSBH056	<0.005	3.733	<0.005	0.013	23.483	<0.005	<0.002	42.834	0.003	0.17	<0.002	<0.005	<0.005	<0.005	<0.005
BSBH063	<0.005	9.594	<0.005	0.006	12.83	<0.005	<0.002	33.982	<0.002	<0.100	<0.002	<0.005	<0.005	<0.005	<0.005
CBBH035	<0.005	2.033	<0.005	0.016	56.085	<0.005	<0.002	53.494	<0.002	<0.100	<0.002	<0.005	<0.005	<0.005	<0.005
CRBH008	<0.005	2.238	<0.005	0.024	7.324	<0.005	<0.002	104.401	<0.002	<0.100	<0.002	<0.005	<0.005	<0.005	<0.005
CRBH009	<0.005	42.735	<0.005	0.019	21.823	<0.005	<0.002	27.384	0.002	0.262	<0.002	<0.005	<0.005	<0.005	<0.005
CRBH011	<0.005	4.314	<0.005	0.026	23.172	<0.005	<0.002	28.513	<0.002	<0.100	<0.002	<0.005	<0.005	<0.005	<0.005
EBBH034	<0.005	1.475	<0.005	0.021	5.093	<0.005	<0.002	139.887	<0.002	<0.100	<0.002	<0.005	<0.005	<0.005	<0.005
GFBH061	<0.005	0.392	<0.005	<0.005	46.246	<0.005	<0.002	15.771	0.015	<0.100	0.002	<0.005	<0.005	<0.005	<0.005
GHBH001	<0.005	3.909	<0.005	<0.005	6.69	<0.005	<0.002	12.253	0.002	<0.100	<0.002	<0.005	<0.005	<0.005	<0.005
GHBH002	<0.005	0.974	<0.005	<0.005	54.637	<0.005	<0.002	19.86	<0.002	<0.100	<0.002	<0.005	<0.005	<0.005	<0.005
GHBH004	<0.005	1.058	<0.005	0.012	34.107	<0.005	<0.002	19.544	<0.002	<0.100	<0.002	<0.005	<0.005	<0.005	<0.005
GHBH006	<0.005	6.389	<0.005	0.019	48.655	<0.005	0.005	102.496	<0.002	<0.100	<0.002	<0.005	<0.005	<0.005	<0.005
GWBH067	<0.005	<0.100	<0.005	<0.005	15.826	<0.005	<0.002	17.406	<0.002	<0.100	<0.002	<0.005	<0.005	<0.005	<0.005
HKBH029	<0.005	11.303	<0.005	0.03	9.603	<0.005	<0.002	17.238	<0.002	<0.100	<0.002	<0.005	<0.005	<0.005	<0.005
HSBH024	<0.005	8.007	<0.005	0.03	28.168	<0.005	0.002	31.988	<0.002	<0.100	<0.002	<0.005	<0.005	<0.005	<0.005
HSBH036	<0.005	3.745	<0.005	0.026	44.083	0.047	<0.002	31.444	<0.002	<0.100	<0.002	<0.005	<0.005	<0.005	<0.005
KDBH023	<0.005	203.344	<0.005	0.014	107.095	0.028	<0.002	79.786	0.008	<0.100	<0.002	<0.005	<0.005	<0.005	<0.005
KDBH024	<0.005	10.356	<0.005	0.04	17.42	<0.005	<0.002	23.744	<0.002	<0.100	<0.002	<0.005	<0.005	<0.005	<0.005
KFBH079	<0.005	10.742	<0.005	0.031	20.612	<0.005	<0.002	48.674	<0.002	<0.100	<0.002	<0.005	<0.005	<0.005	<0.005
KFBH080	<0.005	1.529	<0.005	0.025	15.271	<0.005	<0.002	51.077	<0.002	<0.100	<0.002	<0.005	<0.005	<0.005	<0.005
KFBH081	<0.005	4.02	<0.005	0.025	28.645	<0.005	<0.002	69.598	<0.002	<0.100	<0.002	<0.005	<0.005	<0.005	<0.005
KFBH082	<0.005	1.003	<0.005	0.008	18.667	0.006	<0.002	20.791	<0.002	<0.100	<0.002	<0.005	<0.005	<0.005	<0.005
KFBH083	<0.005	2.834	<0.005	0.017	30.317	<0.005	<0.002	31.461	<0.002	<0.100	<0.002	<0.005	<0.005	<0.005	<0.005
KFBH084	<0.005	2.621	<0.005	0.017	28.586	<0.005	<0.002	33.501	0.004	<0.100	<0.002	<0.005	<0.005	<0.005	<0.005
LBH044	<0.005	1.207	<0.005	<0.005	46.995	0.018	<0.002	33.246	<0.002	<0.100	<0.002	<0.005	<0.005	<0.005	<0.005
LESLIE BH004	<0.005	9.93	<0.005	0.015	24.77	<0.005	<0.002	36.997	0.003	<0.100	<0.002	<0.005	<0.005	<0.005	<0.005
LKBH030	<0.005	0.917	<0.005	0.032	0.535	<0.005	<0.002	143.933	<0.002	<0.100	<0.002	<0.005	<0.005	<0.005	<0.005
LKBH031	<0.005	0.821	<0.005	0.03	0.445	<0.005	<0.002	194.041	<0.002	<0.100	<0.002	<0.005	<0.005	<0.005	<0.005
LKBH032	<0.005	0.524	<0.005	<0.005	56.763	<0.005	<0.002	25.438	<0.002	<0.100	<0.002	<0.005	<0.005	<0.005	<0.005
LKBH038	<0.005	3.38	<0.005	0.047	28.138	0.008	0.005	226.221	<0.002	<0.100	<0.002	<0.005	<0.005	<0.005	<0.005
LKS002	<0.005	0.553	<0.005	<0.005	80.876	<0.005	<0.002	40.509	<0.002	<0.100	<0.002	<0.005	<0.005	<0.005	<0.005
MB021	<0.005	3.031	<0.005	0.022	5.669	<0.005	<0.002	33.884	<0.002	<0.100	<0.002	<0.005	<0.005	<0.005	<0.005
MB033	<0.005	4.115	<0.005	0.06	9.322	<0.005	<0.002	36.078	<0.002	<0.100	<0.002	<0.005	<0.005	<0.005	<0.005
MB053	<0.005	6.782	<0.005	0.099	89.782	<0.005	<0.002	286.092	<0.002	<0.100	<0.002	<0.005	<0.005	<0.005	<0.005
MC BH006M	<0.005	7.159	<0.005	<0.005	18.666	<0.005	<0.002	18.979	<0.002	<0.100	<0.002	<0.005	<0.005	<0.005	<0.005
MC BH009M	<0.005	8.254	<0.005	<0.005	7.234	<0.005	<0.002	13.863	<0.002	<0.100	<0.002	<0.005	<0.005	<0.005	<0.005
MVBH007	<0.005	3.093	<0.005	0.028	21.211	<0.005	<0.002	72.616	<0.002	<0.100	<0.002	<0.005	<0.005	<0.005	<0.005
RANDWATER	<0.005	3.679	<0.005	<0.005	7.42	<0.005	<0.002	12.444	0.038	<0.100	<0.002	<0.005	<0.005	<0.005	<0.005
RFBH037	<0.005	5.046	<0.005	0.052	11.69	<0.005	<0.002	155.867	<0.002	<0.100	<0.002	<0.005	<0.005	<0.005	<0.005
SBLBH021	<0.005	11.749	<0.005	0.025	23.031	<0.005	<0.002	29.613	<0.002	<0.100	<0.002	<0.005	<0.005	<0.005	<0.005
SKBH047	<0.005	3.782	<0.005	<0.005	7.536	<0.005	<0.002	12.575	0.004	<0.100	<0.002	<0.005	<0.005	<0.005	<0.005
SSBH026	<0.005	3.024	<0.005	0.057	34.243	<0.005	<0.002	54.966	<0.002	<0.100	<0.002	<0.005	<0.005	<0.005	<0.005

Borehole	Ir	K	La	Li	Mg	Mn	Mo	Na	Ni	P	Pb	Pd	Pt	Rh	Ru
SSBH027	<0.005	2.59	<0.005	0.009	22.753	<0.005	<0.002	14.207	<0.002	<0.100	<0.002	<0.005	<0.005	<0.005	<0.005
UMKBH048	<0.005	2.397	<0.005	0.02	53.247	0.016	<0.002	52.292	0.002	<0.100	<0.002	<0.005	<0.005	<0.005	<0.005
UMKBH049	<0.005	0.678	<0.005	0.011	50.996	<0.005	<0.002	27.989	<0.002	<0.100	<0.002	<0.005	<0.005	<0.005	<0.005
UMKBH085	<0.005	0.883	<0.005	<0.005	58.102	<0.005	<0.002	53.882	<0.002	<0.100	<0.002	<0.005	<0.005	<0.005	<0.005
VPBH071	<0.005	0.653	<0.005	<0.005	23.161	<0.005	<0.002	41.812	<0.002	<0.100	<0.002	<0.005	<0.005	<0.005	<0.005
VPBH072	<0.005	0.825	<0.005	0.019	12.836	<0.005	0.004	92.766	<0.002	<0.100	<0.002	<0.005	<0.005	<0.005	<0.005
VPBH074	<0.005	0.807	<0.005	0.012	44.106	<0.005	<0.002	69.352	<0.002	<0.100	<0.002	<0.005	<0.005	<0.005	<0.005
VPBH076	<0.005	2.315	<0.005	<0.005	93.998	<0.005	<0.002	88.612	<0.002	<0.100	<0.002	<0.005	<0.005	<0.005	<0.005
WBBH078	<0.005	1.888	<0.005	0.043	35.333	<0.005	0.003	77.546	0.005	<0.100	<0.002	<0.005	<0.005	<0.005	<0.005
WHBH039	<0.005	0.846	<0.005	<0.005	141.843	<0.005	<0.002	25.792	0.002	<0.100	<0.002	<0.005	<0.005	<0.005	<0.005
WHBH040	<0.005	0.859	<0.005	0.016	71.811	<0.005	<0.002	31.614	<0.002	<0.100	<0.002	<0.005	<0.005	<0.005	<0.005
WHBH041	<0.005	0.961	<0.005	0.012	46.844	<0.005	<0.002	20.671	<0.002	<0.100	<0.002	<0.005	<0.005	<0.005	<0.005
WSBH058	<0.005	0.567	<0.005	0.03	0.309	<0.005	0.011	281.335	<0.002	<0.100	<0.002	<0.005	<0.005	<0.005	<0.005
WSBH059	<0.005	3.007	<0.005	0.02	29.052	<0.005	0.002	60.061	<0.002	<0.100	<0.002	<0.005	<0.005	<0.005	<0.005
WSBH060	<0.005	0.431	<0.005	<0.005	<0.020	<0.005	0.003	258.335	<0.002	<0.100	<0.002	<0.005	<0.005	<0.005	<0.005
WSBH065	<0.005	1.58	<0.005	0.042	17.378	<0.005	0.003	92.914	<0.002	<0.100	<0.002	<0.005	<0.005	<0.005	<0.005
WSBH066	<0.005	1.487	<0.005	0.046	22.194	0.009	0.061	128.432	<0.002	<0.100	<0.002	<0.005	<0.005	<0.005	<0.005
WSBH073	<0.005	0.986	<0.005	<0.005	66.638	<0.005	<0.002	57.557	<0.002	<0.100	<0.002	<0.005	<0.005	<0.005	<0.005

Table 26. Various physical and hydrochemical results of groundwater samples collected from boreholes surrounding the proposed injection site. Dataset 4.

Borehole	S	Sb	Se	Sn	Sr	Te	Th	Ti	Tl	U	V	W	Zn	Zr
BH005A	486.681	<0.005	<0.005	<0.005	3.6	<0.005	<0.005	0.008	<0.005	<0.005	0.007	<0.020	0.03	<0.005
BH011	238.351	<0.005	<0.005	<0.005	2.769	<0.005	<0.005	<0.005	<0.005	0.085	0.082	<0.020	0.016	<0.005
BH012	81.232	<0.005	<0.005	<0.005	0.713	<0.005	<0.005	<0.005	<0.005	0.013	0.094	<0.020	<0.005	<0.005
BH017	44.662	<0.005	<0.005	<0.005	0.479	<0.005	<0.005	<0.005	<0.005	<0.005	<0.005	<0.020	0.019	<0.005
BKBH012	132.639	<0.005	<0.005	<0.005	0.592	<0.005	<0.005	<0.005	<0.005	<0.005	<0.005	<0.020	0.014	<0.005
BKBH013	24.498	<0.005	<0.005	<0.005	0.724	<0.005	<0.005	<0.005	<0.005	<0.005	<0.005	<0.020	<0.005	<0.005
BKBH014	11.058	<0.005	<0.005	<0.005	0.315	<0.005	<0.005	<0.005	<0.005	<0.005	<0.005	<0.020	<0.005	<0.005
BKBH015	15.94	<0.005	<0.005	<0.005	0.374	<0.005	<0.005	<0.005	<0.005	<0.005	<0.005	<0.020	0.015	<0.005
BKBH017	63.943	<0.005	<0.005	<0.005	0.697	<0.005	<0.005	<0.005	<0.005	0.008	<0.005	<0.020	0.008	<0.005
BKBH018	3.244	<0.005	<0.005	<0.005	0.365	<0.005	<0.005	<0.005	<0.005	<0.005	<0.005	<0.020	0.056	<0.005
BKBH019	35.886	<0.005	<0.005	<0.005	0.959	<0.005	<0.005	<0.005	<0.005	<0.005	<0.005	<0.020	0.007	<0.005
BKBH020	27.803	<0.005	<0.005	<0.005	0.678	<0.005	<0.005	<0.005	<0.005	<0.005	<0.005	<0.020	0.012	<0.005
BKBH022	15.535	<0.005	<0.005	<0.005	0.53	<0.005	<0.005	<0.005	<0.005	<0.005	<0.005	<0.020	<0.005	<0.005
BKR001	29.7	<0.005	<0.005	<0.005	0.242	<0.005	<0.005	<0.005	<0.005	<0.005	0.011	<0.020	0.019	<0.005
BKS001	38.075	<0.005	<0.005	<0.005	0.296	<0.005	<0.005	<0.005	<0.005	<0.005	0.007	<0.020	0.014	<0.005
BSBH006	8.335	<0.005	<0.005	<0.005	0.235	<0.005	<0.005	<0.005	<0.005	<0.005	0.015	<0.020	0.088	<0.005
BSBH045	15.362	<0.005	<0.005	<0.005	0.731	<0.005	<0.005	<0.005	<0.005	<0.005	<0.005	<0.020	0.017	<0.005
BSBH046	16.941	<0.005	<0.005	<0.005	0.259	<0.005	<0.005	<0.005	<0.005	<0.005	0.007	<0.020	0.006	<0.005
BSBH052	7.318	<0.005	<0.005	<0.005	0.097	<0.005	<0.005	<0.005	<0.005	<0.005	0.023	<0.020	0.008	<0.005
BSBH053	4.643	<0.005	<0.005	<0.005	0.257	<0.005	<0.005	<0.005	<0.005	<0.005	0.029	<0.020	0.045	<0.005
BSBH054	20.57	<0.005	<0.005	<0.005	2.136	<0.005	<0.005	<0.005	<0.005	<0.005	<0.005	<0.020	0.011	<0.005
BSBH056	6.559	<0.005	<0.005	<0.005	0.263	<0.005	<0.005	<0.005	<0.005	<0.005	0.015	<0.020	0.01	<0.005
BSBH063	8.429	<0.005	<0.005	<0.005	0.22	<0.005	<0.005	<0.005	<0.005	<0.005	0.016	<0.020	0.02	<0.005
CBBH035	35.015	<0.005	<0.005	<0.005	0.514	<0.005	<0.005	<0.005	<0.005	<0.005	0.015	<0.020	0.007	<0.005
CRBH008	3.708	<0.005	<0.005	<0.005	0.212	<0.005	<0.005	<0.005	<0.005	<0.005	<0.005	<0.020	0.006	<0.005
CRBH009	18.318	<0.005	<0.005	<0.005	0.325	<0.005	<0.005	<0.005	<0.005	<0.005	<0.005	<0.020	0.019	<0.005
CRBH011	7.225	<0.005	<0.005	<0.005	0.409	<0.005	<0.005	<0.005	<0.005	<0.005	<0.005	<0.020	0.011	<0.005
EBBH034	6.098	<0.005	<0.005	<0.005	0.29	<0.005	<0.005	<0.005	<0.005	<0.005	<0.005	<0.020	0.005	<0.005
GFBH061	17.773	<0.005	<0.005	<0.005	0.156	<0.005	<0.005	<0.005	<0.005	<0.005	0.055	<0.020	0.036	<0.005
GHBH001	5.718	<0.005	<0.005	<0.005	0.095	<0.005	<0.005	<0.005	<0.005	<0.005	<0.005	<0.020	0.011	<0.005
GHBH002	62.448	<0.005	<0.005	<0.005	0.227	<0.005	<0.005	<0.005	<0.005	<0.005	0.05	<0.020	0.008	<0.005
GHBH004	22.495	<0.005	<0.005	<0.005	0.29	<0.005	<0.005	<0.005	<0.005	<0.005	0.01	<0.020	0.005	<0.005
GHBH006	31.051	<0.005	<0.005	<0.005	0.61	<0.005	<0.005	<0.005	<0.005	<0.005	0.006	<0.020	0.011	<0.005
GWBH067	7.717	<0.005	<0.005	<0.005	0.208	<0.005	<0.005	<0.005	<0.005	<0.005	0.032	<0.020	0.047	<0.005
HKBH029	1.538	<0.005	<0.005	<0.005	0.137	<0.005	<0.005	<0.005	<0.005	<0.005	<0.005	<0.020	0.115	<0.005
HSBH024	23.126	<0.005	<0.005	<0.005	0.212	<0.005	<0.005	<0.005	<0.005	<0.005	0.009	<0.020	<0.005	<0.005
HSBH036	26.698	<0.005	<0.005	<0.005	0.257	<0.005	<0.005	<0.005	<0.005	<0.005	<0.005	<0.020	0.573	<0.005
KDBH023	76.357	<0.005	<0.005	<0.005	0.947	<0.005	<0.005	<0.005	<0.005	<0.005	<0.005	<0.020	0.012	<0.005
KDBH024	8.95	<0.005	<0.005	<0.005	0.301	<0.005	<0.005	<0.005	<0.005	<0.005	<0.005	<0.020	0.012	<0.005
KFBH079	7.177	<0.005	<0.005	<0.005	0.299	<0.005	<0.005	<0.005	<0.005	<0.005	<0.005	<0.020	0.009	<0.005
KFBH080	13.199	<0.005	<0.005	<0.005	0.371	<0.005	<0.005	<0.005	<0.005	<0.005	<0.005	<0.020	0.012	<0.005
KFBH081	7.453	<0.005	<0.005	<0.005	0.292	<0.005	<0.005	<0.005	<0.005	<0.005	0.013	<0.020	0.023	<0.005
KFBH082	10.421	<0.005	<0.005	<0.005	0.217	<0.005	<0.005	<0.005	<0.005	<0.005	0.007	<0.020	<0.005	<0.005
KFBH083	15.19	<0.005	<0.005	<0.005	0.3	<0.005	<0.005	<0.005	<0.005	<0.005	0.012	<0.020	0.023	<0.005
KFBH084	15.407	<0.005	<0.005	<0.005	0.271	<0.005	<0.005	0.006	<0.005	<0.005	0.069	<0.020	0.008	<0.005
LBH044	9.569	<0.005	<0.005	<0.005	0.267	<0.005	<0.005	<0.005	<0.005	<0.005	<0.005	<0.020	<0.005	<0.005
LESLIE BH004	57.579	<0.005	<0.005	<0.005	0.346	<0.005	<0.005	<0.005	<0.005	<0.005	<0.005	<0.020	<0.005	<0.005
LKBH030	15.671	<0.005	<0.005	<0.005	0.077	<0.005	<0.005	<0.005	<0.005	<0.005	<0.005	<0.020	0.012	<0.005
LKBH031	8.302	<0.005	<0.005	<0.005	0.041	<0.005	<0.005	<0.005	<0.005	<0.005	<0.005	<0.020	0.046	<0.005
LKBH032	30.066	<0.005	<0.005	<0.005	0.156	<0.005	<0.005	<0.005	<0.005	<0.005	<0.005	<0.020	<0.005	<0.005
LKBH038	40.103	<0.005	<0.005	<0.005	0.822	<0.005	<0.005	<0.005	<0.005	<0.005	<0.005	<0.020	0.007	<0.005
LKS002	99.625	<0.005	<0.005	<0.005	0.307	<0.005	<0.005	<0.005	<0.005	<0.005	0.048	<0.020	0.092	<0.005
MB021	<1.250	<0.005	<0.005	<0.005	0.11	<0.005	<0.005	<0.005	<0.005	<0.005	<0.005	<0.020	<0.005	<0.005
MB033	5.442	<0.005	<0.005	<0.005	0.741	<0.005	<0.005	<0.005	<0.005	<0.005	<0.005	<0.020	0.01	<0.005
MB053	188.302	<0.005	<0.005	<0.005	0.481	<0.005	<0.005	<0.005	<0.005	<0.005	<0.005	<0.020	<0.005	<0.005
MC BH006M	<1.250	<0.005	<0.005	<0.005	0.148	<0.005	<0.005	<0.005	<0.005	<0.005	<0.005	<0.020	0.005	<0.005
MC BH009M	<1.250	<0.005	<0.005	<0.005	0.024	<0.005	<0.005	<0.005	<0.005	<0.005	<0.005	<0.020	<0.005	<0.005
MVBH007	8.595	<0.005	<0.005	<0.005	0.61	<0.005	<0.005	<0.005	<0.005	<0.005	<0.005	<0.020	0.007	<0.005
RANDWATER	6.193	<0.005	<0.005	<0.005	0.088	<0.005	<0.005	<0.005	<0.005	<0.005	<0.005	<0.020	0.09	<0.005
RFBH037	13.697	<0.005	<0.005	<0.005	0.336	<0.005	<0.005	<0.005	<0.005	<0.005	<0.005	<0.020	0.125	<0.005
SBLBH021	25.642	<0.005	<0.005	<0.005	0.428	<0.005	<0.005	<0.005	<0.005	<0.005	<0.005	<0.020	0.011	<0.005
SKBH047	6.306	<0.005	<0.005	<0.005	0.089	<0.005	<0.005	<0.005	<0.005	<0.005	<0.005	<0.020	0.022	<0.005
SSBH026	13.315	<0.005	<0.005	<0.005	0.291	<0.005	<0.005	<0.005	<0.005	0.006	<0.005	<0.020	0.017	<0.005

Borehole	S	Sb	Se	Sn	Sr	Te	Th	Ti	Tl	U	V	W	Zn	Zr
SSBH027	31.725	<0.005	<0.005	<0.005	0.238	<0.005	<0.005	<0.005	<0.005	<0.005	0.007	<0.020	0.079	<0.005
UMKBH048	57.127	<0.005	<0.005	<0.005	0.603	<0.005	<0.005	<0.005	<0.005	<0.005	<0.005	<0.020	0.099	<0.005
UMKBH049	43.023	<0.005	<0.005	<0.005	0.355	<0.005	<0.005	<0.005	<0.005	<0.005	0.018	<0.020	0.006	<0.005
UMKBH085	32.401	<0.005	<0.005	<0.005	0.32	<0.005	<0.005	<0.005	<0.005	<0.005	0.044	<0.020	0.289	<0.005
VPBH071	24.602	<0.005	<0.005	<0.005	0.163	<0.005	<0.005	<0.005	<0.005	<0.005	0.042	<0.020	0.113	<0.005
VPBH072	19.553	<0.005	<0.005	<0.005	0.226	<0.005	<0.005	<0.005	<0.005	<0.005	0.006	<0.020	0.217	<0.005
VPBH074	33.358	<0.005	<0.005	<0.005	0.351	<0.005	<0.005	<0.005	<0.005	<0.005	0.023	<0.020	0.068	<0.005
VPBH076	75.416	<0.005	<0.005	<0.005	0.204	<0.005	<0.005	<0.005	<0.005	<0.005	0.021	<0.020	0.01	<0.005
WBBH078	9.138	<0.005	<0.005	<0.005	0.568	<0.005	<0.005	<0.005	<0.005	<0.005	<0.005	<0.020	0.046	<0.005
WHBH039	99.688	<0.005	<0.005	<0.005	0.376	<0.005	<0.005	<0.005	<0.005	<0.005	0.024	<0.020	<0.005	<0.005
WHBH040	54.331	<0.005	<0.005	<0.005	0.384	<0.005	<0.005	<0.005	<0.005	<0.005	0.027	<0.020	0.009	<0.005
WHBH041	32.875	<0.005	<0.005	<0.005	0.202	<0.005	<0.005	<0.005	<0.005	<0.005	0.022	<0.020	0.007	<0.005
WSBH058	3.925	<0.005	<0.005	<0.005	0.032	<0.005	<0.005	<0.005	<0.005	<0.005	<0.005	<0.020	0.01	<0.005
WSBH059	6.906	<0.005	<0.005	<0.005	0.322	<0.005	<0.005	<0.005	<0.005	<0.005	0.009	<0.020	0.35	<0.005
WSBH060	9.348	<0.005	<0.005	<0.005	<0.005	<0.005	<0.005	<0.005	<0.005	<0.005	<0.005	<0.020	0.015	<0.005
WSBH065	30.267	<0.005	<0.005	<0.005	0.515	<0.005	<0.005	<0.005	<0.005	<0.005	<0.005	<0.020	0.178	<0.005
WSBH066	34.565	<0.005	<0.005	<0.005	0.478	<0.005	<0.005	<0.005	<0.005	<0.005	<0.005	<0.020	0.109	<0.005
WSBH073	86.505	<0.005	<0.005	<0.005	0.256	<0.005	<0.005	<0.005	<0.005	<0.005	0.051	<0.020	0.036	<0.005

Council for Geoscience

280 Pretoria Street
Silverton, Pretoria
South Africa
www.geoscience.org.za

ISBN 978-1-990942-24-2